DISS. ETH NO. 22383

EXTENDED SOURCE APPORTIONMENT OF ORGANIC AEROSOLS

A thesis submitted to attain the degree of

DOCTOR OF SCIENCES of ETH ZURICH

(Dr. sc. ETH Zurich)

presented by

ROBERT WOLF

Dipl.-Chem, TU Bergakademie Freiberg

born on 09.06.1986

citizen of Germany

accepted on the recommendation of

Prof. Dr. Urs Baltensperger (examiner)
Prof. Dr. Alexander Wokaun (co-examiner)
Prof. Dr. Yinon Rudich (co-examiner)
Dr. André S.H. Prévôt (co-examiner)

2015

Contents

Summary

The development of aerosol mass spectrometers has revolutionized atmospheric aerosol research. Our scientific understanding of aerosol composition, conversion processes and sources has improved significantly in the last two decades by deploying them at various field sites worldwide and in laboratory studies. The time-resolved analysis of non-refractory aerosols with particle diameters up to one micrometer has almost become a routine. However, less attention has been paid to aerosol particles with diameters above one micrometer by means of on-line aerosol mass spectrometry.

In this work, a novel $PM_{2.5}$ inlet for the widely-used Aerodyne aerosol mass spectrometer has been tested in the laboratory and under ambient conditions. This modified inlet extends the upper limit of detectable aerosol particles to about 2.5 micrometers. Since an increased fraction of airborne bacteria may be present in this size range and since they might constitute a source of aerosol mass, this thesis focuses on the quantification of airborne bacteria.

Laboratory experiments at the AIDA cloud chamber facility in Karlsruhe were conducted to determine the mass spectral features of viable bacteria when sampled with an Aerodyne high-resolution time-of-flight aerosol mass spectrometer (HR-ToF-AMS). Signals from bacteria and from the agar nutritive medium, in which the bacteria were cultivated, were successfully distinguished by applying positive matrix factorization (PMF) and multilinear engine (ME-2) statistical analysis. Nitrogen-containing ions were the most salient feature of the bacteria mass spectra and $C_4H_8N^+$ (mass-to-charge ratio, m/z 70) as well as $C_5H_{12}N^+$ (m/z 86) may serve as potential markers for the detection of bacteria aerosol particles when using electron impact ionization.

Field measurements with two HR-ToF-AMS equipped with a standard (PM_1) and a $PM_{2.5}$ inlet were performed at an urban background site in Zurich (Switzerland) in spring 2011. The previously obtained mass spectra of pure bacteria were used as an input in ME-2 calculations to distinguish airborne particles with a bacteria-like mass spectrum from other constituents of ambient aerosol. Bacteria-like particles represented a minor source of non-refractory aerosol mass with estimated average organic mass fractions of 0.5% (PM_1) and 1.7% ($PM_{2.5}$). Single particle analysis using an integrated light-scattering module for the aerosol mass spectrometer during measurements at a rural site in Payerne (Switzerland) in summer 2012 yielded number concentrations of bacteria-like particles up to $4.7 \times 10^5\, m^{-3}$ supporting the concentration estimates by the ME-2 technique. Short-term concentration peaks up to approximately $2\,\mu g/m^3$ were observed during time periods of rainfall.

A spatially-resolved source assessment of non-refractory $PM_{2.5}$ aerosol was performed by deploying the PSI mobile laboratory in the south-east Po Valley within the framework of the PEGASOS project in summer 2012. Essential changes in both aerosol composition and concentration were induced by the ventilation of the valley and the recirculation of air masses in east-west direction (land/sea breeze system) and via the Apennines mountain range (mountain/valley wind system). Hydrocarbon-like and cooking organic aerosol were identified as major components of primary aerosol. The organic aerosol mass was governed by secondary aerosol comprising semi-volatile and low volatility as well as regionally influenced oxygenated organic aerosol components. An urban increment of aerosol pollution in Bologna of $1.6 - 2.3$ $\mu g/m^3$ was determined which can be explained by the sum of local contributions from cooking activities and traffic.

Zusammenfassung

Die Entwicklung von Aerosolmassenspektrometern hat die Forschung auf dem Gebiet der atmosphärischen Aerosole revolutioniert. Durch die Verwendung dieser Instrumente an verschiedenen Orten weltweit hat sich das Verständnis der Zusammensetzung der Aerosole und deren atmosphärische Umwandlungsprozesse in den letzten zwei Dekaden signifikant verbessert. Die zeitaufgelöste Analyse von nicht-refraktionären Aerosolen mit Partikeldurchmessern bis zu einem Mikrometer ist beinahe zu einer Routine geworden. Jedoch wurde bisher weniger Aufmerksamkeit den Teilchen mit Durchmessern über einem Mikrometer mit Hilfe der on-line Aerosolmassenspektrometrie beigemessen.

In dieser Arbeit wurde ein neues $PM_{2.5}$-Einlasssystem für das inzwischen weit verbreitete Aerodyne Aerosolmassenspektrometer unter Labor- und Aussenbedingungen getestet. Dieses modifizierte Einlasssystem erweitert die obere Grenze für detektierbare Aerosolteilchen auf ungefähr 2.5 Mikrometer. Da ein erhöhter Anteil an luftgetragenen Bakterien in diesem Grössenbereich vorliegen mag und damit als eine Quelle zum Aerosol beitragen könnte, wurde diese Arbeit der Quantifizierung der sich in der Luft befindenden Bakterien gewidmet.

Laborexperimente an der AIDA-Wolkenkammer-Einrichtung in Karlsruhe wurden durchgeführt, um die Eigenschaften der Massenspektren lebender Bakterien mit Hilfe eines hochauflösenden Flugzeit-Aerosolmassenspektrometers (HR-ToF-AMS) der Firma Aerodyne zu bestimmen. Signale der Bakterien und des Agar-Nährmediums, in dem die Bakterien gezüchtet wurden, konnten erfolgreich durch die Anwendung der statistischen Analyse der nichtnegativen Matrixfaktorisierung (PMF) und des Multilinear engine-Algorithmus (ME-2) voneinander unterschieden werden. Stickstoffhaltige Ionen stellten ein besonders charakteristisches Merkmal der Bakterienmassenspektren dar. $C_4H_8N^+$ (Masse-Ladungsverhältnis, m/z 70) sowie $C_5H_{12}N^+$ (m/z 86) wurden als potenzielle Marker für die Detektion von Bakterien-Aerosolpartikeln unter Benutzung der Elektronenstoss-Ionisation identifiziert.

Aussenmessungen mit zwei HR-ToF-AMS, die mit einem konventionellen (PM_1) und einem $PM_{2.5}$ Einlasssystem bestückt waren, wurden an einem urbanen Hintergrund-Messort in Zürich (Schweiz) im Frühling 2011 durchgeführt. Die vorher erhaltenen, reinen Bakterien-Massenspektren wurden als Eingabe in ME-2-Berechnungen benutzt, um in der Luft enthaltene Bakterien von anderen Aerosolkomponenten in der Umwelt abzugrenzen. Partikel mit einem Bakterien-ähnlichen Massenspektrum stellten nur eine untergeordnete Quelle der nichtrefraktionären Aerosolmasse mit einem mittleren, organischen Massenanteil von 0.5% (PM_1) und 1.7% ($PM_{2.5}$) dar. Einzelpartikelanalysen unter Benutzung eines integrierten Lichtstreu-Moduls für das Aerosolmassenspektrometer während Messungen an einem ländlichen Messort in Payerne (Schweiz) im Sommer 2012 ergaben Anzahlkonzentrationen für Partikel, die Bakterien ähnlich sind, von bis zu $4.7 \times 10^5\, m^{-3}$, womit die Abschätzung der Konzentration mit der

ME-2-Methode weiter bekräftigt wurde. Kurzzeitige Konzentrationshöchstwerte von ungefähr $2\,\mu g/m^3$ wurden während Niederschlagsperioden beobachtet.

Eine räumlich-aufgelöste Beurteilung der Zusammensetzung und der Quellen der nicht-refraktionären $PM_{2.5}$-Fraktion wurde mit dem mobilen Laboratorium des PSI in der südöstlichen Po-Ebene im Rahmen des EU-PEGASOS Projekts im Sommer 2012 durchgeführt. Die Resultate deuten darauf hin, dass wesentliche Veränderungen der Aerosolzusammensetzung und -konzentration durch die Belüftung des Tals und die Rezirkulation von Luftmassen in Ost-West-Richtung (Land-See-Windsystem) und über die Apenninen (Berg-Tal-Windsystem) veranlasst werden. Kohlenwasserstoff-ähnliches und von Kochprozessen beeinflusstes, organisches Aerosol wurden als Hauptkomponenten der aus primären Emissionen stammenden Aerosolpartikel identifiziert. Die organische Aerosolmasse wurde durch Sekundäraerosol, gebildet aus der Oxidation gasförmiger Vorläuferstoffe, bestimmt. Dieses umfasste semi-flüchtige, geringflüchtige sowie regional-beeinflusste, organische Aerosolkomponenten. Ein urbanes Inkrement der Aerosolverschmutzung in Bologna von $1.6 - 2.3\ \mu g/m^3$ wurde quantifiziert, welches sich durch die Summe der lokalen Beiträge der Emissionen durch das Kochen und durch den Verkehr erklären lässt.

1

Introduction

1.1. Aerosols

An aerosol is a heterogeneous mixture of liquid or solid particles in a gas. In the atmosphere, aerosols affect climate, health, visibility and may cause damage to buildings. In clean room facilities, for example for the production of microchips, aerosols need to be monitored and filtered continuously. Various natural and anthropogenic sources contribute to the total aerosol burden and influence the composition and size properties of aerosol particles. Aerosols that are directly emitted into the atmosphere are also referred to as primary aerosols. The formation of particulate mass following chemical transformation processes of gaseous precursors results in secondary aerosol. The level of scientific understanding of interactions between the components of atmospheric aerosols and climate as well as their impact on health is still modest.

Aerosols are classified according to their size which strongly influences tropospheric lifetime and physical behavior. Ultrafine (particle diameter (D_p) $< 100\,nm$), fine ($D_p < 2.5\,\mu m$) and coarse ($2.5\,\mu m < D_p < 10\,\mu m$) particles are distinguished. Furthermore, certain size ranges are categorized as nucleation mode ($\approx 5\,nm < D_p < 20\,nm$), Aitken mode ($20\,nm < D_p < 100\,nm$), accumulation mode ($100\,nm < D_p < 2.5\,\mu m$) and coarse mode ($D_p > 2.5\,\mu m$). Characteristic fractions of ambient aerosol mass concentrations (in $\mu g\,m^{-3}$) are PM_1 (aerodynamic particle diameter[1] $D_a < 1\,\mu m$), $PM_{2.5}$ ($D_a < 2.5\,\mu m$) and PM_{10} ($D_a < 10\,\mu m$). These fractions are also used to set target and legally binding limit values for air quality. For

1 Diameter of a spherical particle with a density of $1\,g\,cm^{-3}$ and the same settling velocity as the particle of interest (Hinds, 1999).

instance, in Europe a maximum of 35 exceedances of $50\,\mu g\,m^{-3}$ in PM_{10} ($24\,h$ average) is allowed.

Particle shapes can vary from nearly spherical to highly asymmetric and particulate matter may include internal voids. Thus, different definitions of their diameters exist. Common definitions, which originate from the type of analysis method, are the mobility diameter (D_m), the aerodynamic diameter (D_a) and the optical diameter (D_o). It should be noted that the sampling conditions may influence the diameter, for example values of the aerodynamic diameter differ when sampled at ambient pressure or in high vacuum.

In order to detect and mitigate high aerosol concentrations, a detailed knowledge about their origins and their evolution in the atmosphere is essential. For this purpose, aerosols are investigated in various ways using *in situ* measurements which are carried out either at a stationary site or using mobile platforms for the instrumentation such as cars, ships or planes. To investigate the evolution of aerosols in a controlled environment, chamber (environmental or "smog chamber") and laboratory experiments are conducted, for instance to estimate the potential aerosol mass produced by secondary aerosol formation or to study new particle formation events. A more global view on aerosol concentrations can be obtained by remote sensing techniques, e.g. to determine the aerosol optical depth, with the help of satellites. Additionally, experiments which deal with the impact of aerosols on ecosystems are conducted as well.

1.1.1. Climate effects

Aerosols have a key role in the assessment and prediction of climate change (Stocker et al., 2014). Figure 1.1 from the fifth Assessment Report (AR5) of the Intergovernmental Panel on Climate Change (IPCC) depicts contributions of the most important gases, aerosols and precursors of the Earths atmosphere to the change in radiative forcing since pre-industrial times. Gases such as CO_2, CH_4, N_2O or halo-carbons which are also referred to as greenhouse gases (GHG) clearly show a net warming effect. Long-wavelength radiation from the surface of the Earth is absorbed by these gases and can be radiated back. The Earth's radiation budget is influenced by aerosols through a net cooling effect. Figure 1.2 shows the terminology for the interactions used in AR5. Two main causes for changes in irradiance due to the presence of aerosols can be distinguished. Aerosol-radiation interactions (formerly "direct aerosol effect") are based on the absorption and the scattering of aerosol particles. Incoming short wavelength solar radiation can be directly scattered back depending, for example, on the single scattering albedo (scattering coefficient/extinction coefficient) and the upscatter fraction (fraction of light scattered into the upward hemisphere) of the particles. Aerosol particles with low single scattering albedo such as soot particles can absorb solar radiation to a larger extent and thus contribute to the warming of the atmosphere. Aerosol-cloud interactions (formerly "indirect aerosol effect") describe the influence of aerosol on the cloud clover and other properties of clouds such as their reflectance and their lifetime. An elevated concentration of aerosol particles that act as cloud condensation nuclei (CCN) leads to clouds with a smaller average droplet size and a higher reflectivity. Therefore, solar radiation is scattered more efficiently back into space ("Twomey effect"). Furthermore, the total cloud lifetime is increased because smaller droplets have a longer lifetime inside the clouds and thus prevent them from precipitating. The new terminology of the fifth IPCC assessment report

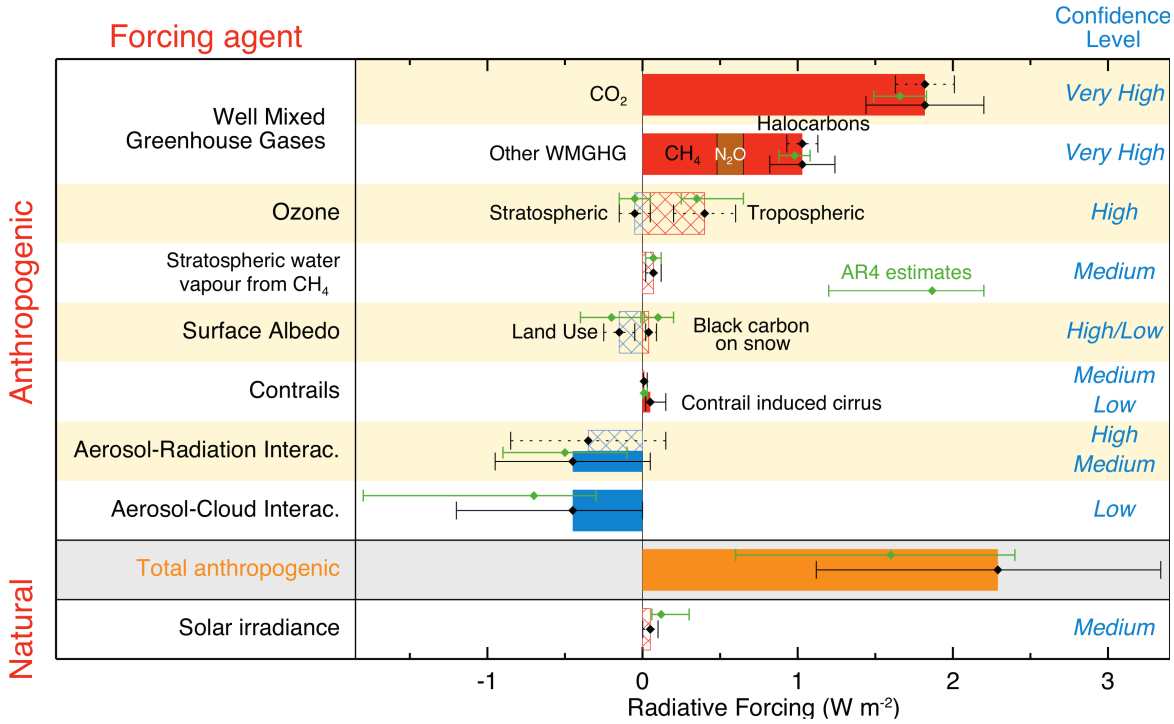

Figure 1.1.: Global average radiative forcing with respect to pre-industrial times (1750) (Stocker et al., 2014).

takes into account effects that come into play at shorter timescales. For example, aerosols that absorb solar radiation can locally increase the temperature of a tropospheric layer but decrease the temperature in the layer below. The same local cooling effect might lead to the extension of cloud lifetime or the formation of clouds if absorbing aerosols are present above the clouds. Additionally, clouds might evaporate if absorbing aerosols are present within the cloud leading to a local enhancement of the temperature above the point of saturation. These effects are summarized as "rapid adjustments" and are taken into account in the effective radiative forcing values. Until now, the level of confidence of these combined effects is still rather low.

1.1.2. Impact on health

Depending on their size, morphology and chemical composition, atmospheric aerosols can have adverse effects on human, animal and plant health. Particles enter the respiratory tract and can be deposited in different regions (figure 1.3). Especially particles with sizes around a few hundred nanometers can penetrate deep into the lungs. Smaller particles with diameters of a few nanometers mostly deposit in the lower respiratory tract at low air velocity (e.g. bronchia) as a consequence of the prevalent diffusion deposition mechanism. Larger particles with diameters of several micrometers rather deposit in the upper tract at higher air velocities and more abrupt direction change as a result of impaction on the surrounding tissue. A series of epidemiological studies have found a correlation between aerosol pollution and increased acute and chronic mortality (Pope et al., 2006). Furthermore, reduced $PM_{2.5}$

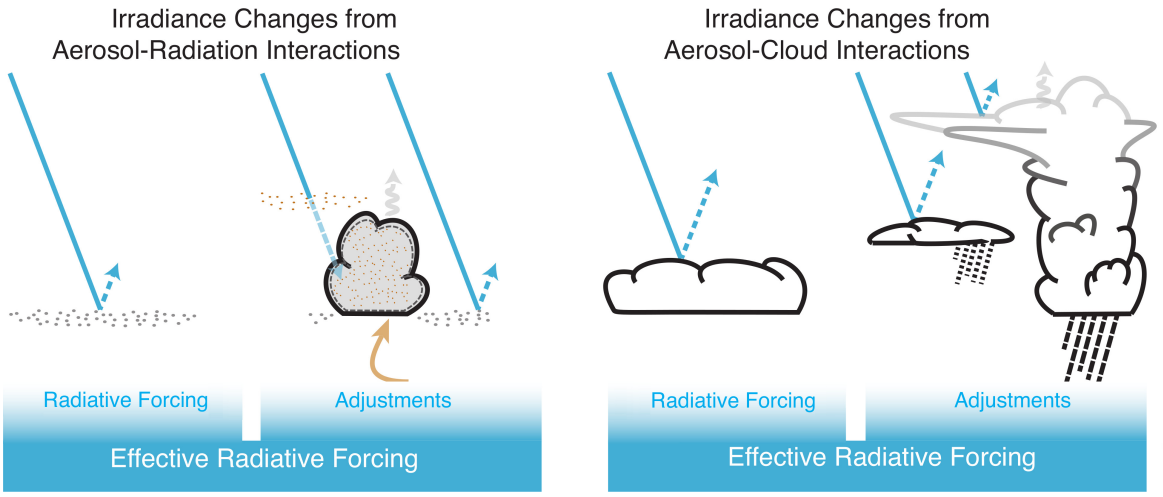

Figure 1.2.: Classification of aerosol-radiation and aerosol-cloud interactions (adapted from AR5 Stocker et al., 2014). Grey arrows symbolize terrestrial radiation and blue arrows depict solar radiation.

levels are associated with a reduced mortality risk (Laden et al., 2006). Modeling studies for different $PM_{2.5}$ exposure scenarios suggest a reduction of average life expectancy in Europe up to 36 months (Amann et al., 2005).

The chemical composition of aerosol particles influences the degree of adverse effects significantly ranging from practically nonhazardous species such as sea salt to potentially carcinogenic and mutagenic components such as polycyclic aromatic hydrocarbons (Ramírez et al., 2011). Inorganic, non-degradable components may induce lung cancer through their morphological properties, e.g. asbestos which can release needle-like particles that may reside in the alveolar region once entrained.

Especially bioaerosols often pose a threat to human, animal and crop health. Their effects on the host or target organism can be very specific and potentially more severe than other organic aerosols components. For example, ice-nucleation active bacteria can destroy their hosting plants by catalyzing the formation of ice on the leaf surfaces at low temperatures (Hirano and Upper, 2000; Szyrmer and Zawadzki, 1997). The opened leaf surfaces give those bacteria strains access to nutritive compounds from the plants metabolism. As a second example, the evolution and termination of large-scale algae blooms can be influenced by viruses (Suttle, 2005) which may have an effect on the global particulate organic carbon cycles. However, the depth of understanding of the natural reservoirs and the transfer ways (e.g. airborne dissemination) of microorganisms both in the marine milieu and the phyllosphere is very limited.

Further phenomena exist which are potentially related to health effects of bioaerosols but are still lacking a detailed explanation. For instance, an increased number of hospitalizations due to severe asthma during thunderstorms has been ascribed to increased concentrations of pollen and fungal spores (Celenza et al., 1996; Wardman et al., 2002). Another observation which is not understood is the apparent discrepancy in the prevalence of asthma, atopies and rhinitis in the ”western world” compared with former socialist countries (Bjorksten et al., 1998). As allergies can be linked with the abundance of bioaerosols, they could be a possible cause

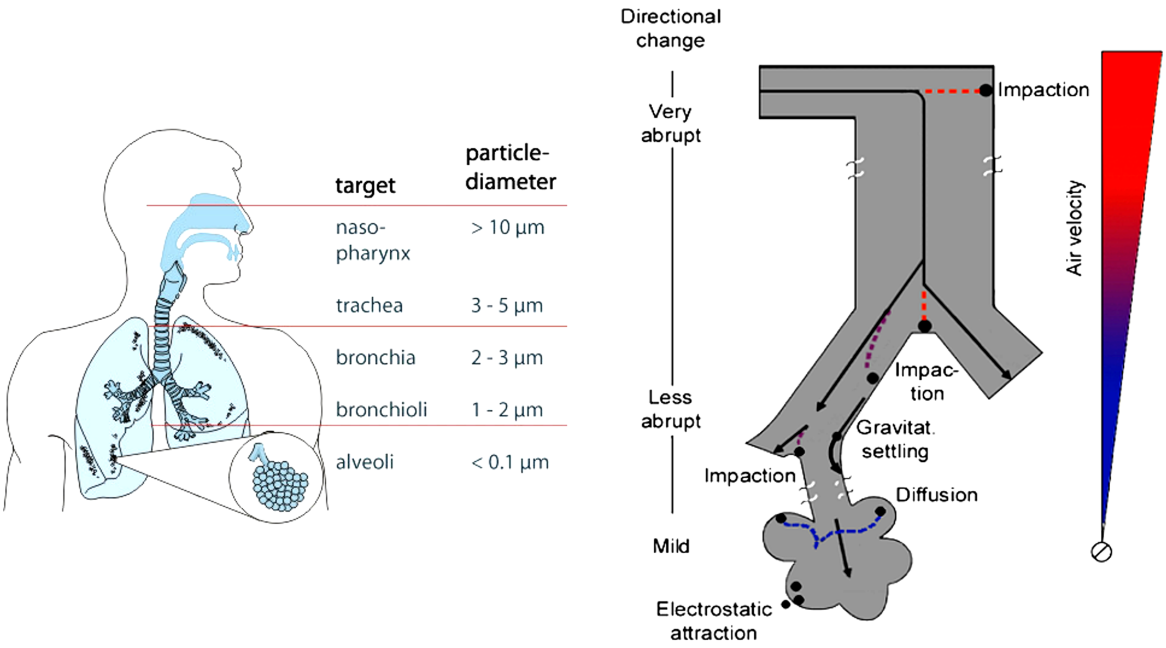

Figure 1.3.: Sketch of the human respiratory tract and major particle deposition mechanisms (adapted from Hussain et al., 2011 and P. Straehl, Swiss Federal Office for the Environment).

for this phenomenon amongst other environmental factors. Another mystery is the so-called Kawasaki disease that is the leading cause for acquired heart disease for children worldwide. Evidence exists that it may be caused by the large-scale distribution of wind-borne *Candida* fungal species as a recent study has claimed (Rodó et al., 2014).

1.1.3. Size-segregated chemical composition

Ambient aerosol mass concentrations can show characteristic modes as a function of the particle diameter. As an example, figure 1.4 illustrates the size-resolved aerosol composition in Marseille, France. Typically, most of the aerosol mass is concentrated in the accumulation mode and the coarse particle mode whereas the number concentration of particles is highest in the nucleation mode. Particles in the accumulation range are formed by the coagulation of smaller particles and the condensation of low-volatility gas phase compounds on pre-existing particles. Coarse mode particles can be generated mechanically, e.g. via aerosolization/resuspension by wind or traffic. Bubble-burst mechanisms on the oceans or volcanic eruptions can also lead to the natural formation of particles with diameters larger than 2.5 micrometers. As a consequence of their formation mechanism, fine and coarse mode aerosols often have quite distinct chemical compositions. Fine mode particles are dominated by elementary carbon, organic matter and secondary inorganic species such as nitrate, sulfate and ammonium. Coarse mode particles are commonly governed by primary inorganic species, e.g. mineral dust and sea salt as well as primary organic matter, e.g. from particles of biogenic origin.

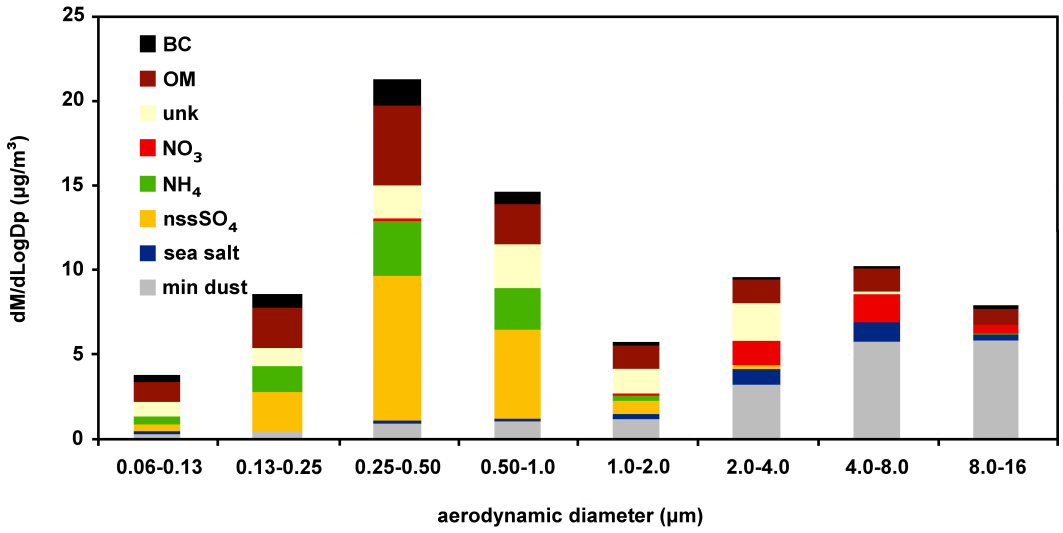

Figure 1.4.: Median size segregated aerosol chemical composition observed in a suburb in Marseille, France (adapted from Putaud et al., 2004).

Commonly-used samplers for the collection of both coarse and fine mode aerosol include high-volume filter samplers or cascade impactors such as the Berner impactor, the micro-orifice uniform deposition impactor (MOUDI) or the rotating drum impactor (RDI). A subsequent analysis of the chemical composition of the collected material can be conducted with a growing number of techniques. Typical methods are: X-ray induced fluorescence, high-pressure liquid chromatography (HPLC), nuclear-magnetic resonance (NMR), Fourier-transform infrared spectroscopy (FT-IR), ion chromatography (IC), secondary ion mass spectrometry (SIMS), scanning electron microscopy (SEM) and off-line aerosol mass spectrometric analysis.

Few near-real time instruments and prototypes exist for the chemical analysis for particles larger than one micrometer, e.g. the aerosol mass time-of-flight spectrometer, the bioaerosol mass spectrometer or the laser ablation time-of-flight aerosol mass spectrometer. Commercial Aerodyne AMS instruments possess an upper size cutoff (50% transmission) slightly below one micrometer. However, it is shown in figure 1.4 that significant aerosol mass is concentrated in a range from $1 - 2.5$ micrometers which currently can not be detected with the conventional AMS inlet. This size range is particularly of importance as particles up to 2.5 micrometers can also penetrate deep into the gas exchange regions of the human lung and at the same time have average, atmospheric residence times in the order of weeks. It may be possible to cover this size range in future measurements with the AMS when it is equipped with the novel inlet (discussed below) for the sampling of $PM_{2.5}$ aerosol (Williams et al., 2013).

1.2. Bioaerosols

The investigation of airborne particles of biological origin reaches back into the 19th century (Ehrenberg, 1847; Pasteur, 1862). Miquel, 1883 has shown that apparent correlations exist between human mortality and the concentration of airborne bacteria in Paris.

Bioaerosols are typically defined as suspension of airborne particles that contain living organisms or were released from living organisms (Cox and Wathes, 1995). Major classes of frequently studied bioaerosols comprise bacteria, fungal spores, viruses and pollen. Further classes of bioaerosols are for example airborne lichen, plant debris, fur fibers, skin fragments and algae. Little is known about the contribution of biological particles to particulate matter concentrations because analysis methods are time-consuming, often not standardized or not specific to a certain class of bioaerosols. Especially fragmented biological material with diameters smaller than one micrometer may be hard to identify by means of light microscopy or flow cytometry, for instance.

Due to the heterogeneity of all classes of bioaerosols, a suite of different measurement methods in different size ranges is necessary for a comprehensive quantification. Therefore, the total concentration of bioaerosols in ambient air is largely unknown although previously estimated mass concentrations indicate a substantial influence. Past studies which employed microscopic analysis of protein-stained samples claim that primary biological aerosol particles may contribute up to about 20% of the number of ambient particles in different environments throughout the whole year (Jaenicke, 2005). $55 - 95\%$ of the particles over the Amazonian rainforest are claimed to be of biogenic origin such as pollen grains, fungi, algae and leaf fragments (Artaxo et al., 1990). Interestingly, bioaerosols where not even mentioned in the previous Assessment Report (AR4) of the Intergovernmental Panel on Climate Change (IPCC). However, the recent assessment report (AR5) estimates the annual global emission flux of terrestrial primary biological aerosol particles of $50 - 1000\ Tg$/year compared against a SOA production from biogenic volatile organic compounds of $20 - 380\ Tg$/year, for example.

Impacts of bioaerosols, which can act as cloud condensation nuclei or ice-nucleating particles, on the global climate remain essentially unknown. Modeling studies suggest that global climate effects of airborne biological particles may be minor compared to other aerosol components (Sesartic et al., 2012; Hoose et al., 2010). Bioaerosols are sources of atmospheric nitrogen and are believed to be important for the global nitrogen budget (Milne and Zika, 1993). Artifacts on gravimetric filter analysis of aerosols might also occur due to the presence of deposited microorganisms as they can reproduce within the filtered material at favorable conditions such as high relative humidity (Forthomme et al., 2014).

The most common collection-based sampling methods are based on the following principles: impaction, impingement, centrifugation as well as gravitational settling and electrostatic precipitation (Agranovski, 2012). A summary of methods for the further analysis of the collected material is given in table 1.1.

Besides the analysis of filters, near-real time methods exist for the detection of primary biological aerosol particles. These include prototypes based on mass-spectrometric methods such as the bioaerosol mass spectrometer (BAMS) or the commercial aerosol time-of-flight mass spectrometer (ATOFMS), optical methods such as the ultraviolet aerosol particle sizer (UVAPS) and flame tomography.

Table 1.1.: Analysis methods for collected bioaerosols. A more detailed review of methods can also be found in Cox and Wathes, 1995; Agranovski, 2012.

Method	**Principle**	**Detection limit**
Microscopy (optical, fluorescence, atomic force)	Enumeration of single microorganisms or cell cultures	> 1 cell
Analysis of genetic material	Investigation of genetic material of various microorganisms, e.g. using quantitative polymerase chain reaction	several copies of genetic material
Chromatography	Quantification based on defined tracer compounds	$> 1\,\mathrm{ng/sample}$
Immunochemical methods	Identification by certain epitopes (sites) of macromolecules	several microorganisms
Spectroscopic methods (Raman, Fourier, X-ray)	Study of the surface layers of different biol. molecules	$> 1\,\mathrm{ng/sample}$
Cytometry	Counting and characterization of cells, e.g. via suspension in a stream of fluid and optical detection	10^2 cells/ml
Mass spectrometry	Characterization of the chem. composition of microorganisms down to the strain level	$10^{-15}\,g$

To the $PM_{2.5}$ aerosol fraction, bacteria are believed to have the biggest mass contribution among other classes of bioaerosols since fungal spores tend to have larger sizes (Huffman et al., 2012; Toprak and Schnaiter, 2013) and viruses likely contribute only little to the aerosol mass as a consequence of their small size. Other classes of bioaerosol, e.g. pollen, plant debris or fur fibers rather have sizes of tens of micrometers.

2

Methodology

2.1. Aerosol mass spectrometry

2.1.1. Aerodyne aerosol mass spectrometer

On-line aerosol mass spectrometry is an established measurement technique that has been developed first around 1975 by Myers and Fite for the near-real time analysis of alkaline metals by using a critical orifice, a heated tungsten wire and a quadrupole mass spectrometer. Further advances of this technique include the simultaneous analysis of the aerosol size (Davis, 1973), the application of laser ablation and ionization (Van Vaeck et al., 1990) and the possibility of single particle analysis (McKeown et al., 1991). For more than a decade, the only commercial single-particle instrument has been the ATOFMS (Hock, 2005) which originated from a device used by Prather et al., 1994. Other instruments for single particle analysis that are currently used in aerosol research are the compact single-particle mass spectrometer (LAMPAS 3, University Giessen; Hinz et al., 2011) or the laser ablation time-of-flight aerosol mass spectrometer (LAAPToF, AeroMegt GmbH). Instruments that are more robust and that have been developed for routine measurements are the Aerodyne (Aerodyne Research Inc., Billerica, MA, USA) aerosol chemical speciation mass spectrometer ACSM (Ng et al., 2011; rough estimate > 300 instruments) and its time-of-flight version (ToF-ACSM, Fröhlich et al., 2013). A commercial instrument which has recently been spread worldwide (rough estimate > 100 instruments) is the Aerodyne aerosol mass spectrometer (AMS) which uses thermal evaporation on a heated surface and electron impact ionization (EI) and a quadrupole or a time-of-flight mass spectrometer (Jayne et al., 2000).

The Aerodyne aerosol mass spectrometer provides near real-time, semi-quantitative mass spectral information and size of non-refractory aerosol particles. In this context, particles that evaporate completely in a few milliseconds on a heated tungsten surface at 600 °C and 10^{-7} $Torr$ are referred to as non-refractory. The instrument consists of three differentially pumped chambers dedicated to sampling, sizing and detection. Aerosol particles are drawn through a 100 μm critical orifice into an aerodynamic lens in which several apertures form a focused, narrow beam. This particle beam passes through a first chamber held at 10^{-3} $Torr$ in which the principal part of the gas phase molecules are removed. After that, the beam passes a rotating chopper wheel and hits a resistively-heated tungsten surface on which the particles flash vaporize. Non-refractory particles such as elemental carbon, sea salt, several oxides or phosphates evaporate too slowly or bounce off the vaporizer surface. When operated in particle time-of-flight mode the particle beam will be chopped into discrete parcels of particles on the chopper wheel (150 Hz) which has two slits with a slit width of about $1 - 2\%$ of the perimeter of the wheel. The chopper can also alternately be moved in "open" and "blocked" position in which all particles or no particles can pass the chopper wheel, respectively.

The total collection efficiency (CE) of the AMS is given by the empiric relationship

$$CE(D_{va}) = E_S(D_{va}) * E_L(D_{va}) * E_B(D_{va}) \tag{2.1}$$

which combines three terms for the efficiency of the particle transmission due to particle bounce at the vaporizer surface (E_B), particle losses during transmission of the beam inside the aerodynamic lens (E_L) and particle losses due to the particle shape (E_S). Since a proper assessment of the collection efficiency is essential for a quantitative sampling, extensive characterizations have been carried out in the past in order to investigate the effects of particle phase, asymmetry, particle acidity and relative humidity. Beam width probes have shown that a wide range of particles that are relevant in ambient conditions are focused well on the vaporizer surface (Huffman et al., 2005). Comparisons using ambient data show that liquid particles tend to have higher collection efficiencies than solid particles. Similarly, acidic particles or particles exposed to high relative humidity (RH) show higher CE than nominally neutral particles or particles sampled at lower RH. Above a certain fraction of ammonium nitrate, which vaporizes rapidly, particles have higher CE as well. As a result of this, a composition-dependent collection efficiency has been proposed by Middlebrook et al., 2012. As a further consequence, sampling of ambient aerosol should always be carried out using an aerosol dryer, e.g. with a Nafion®-membran or silica diffusion dryer system to avoid an influence on the CE by a changing relative humidity.

The evaporated analytes are ionized via electron-impact (EI) ionization causing extensive fragmentation. Further ionization techniques for the Aerodyne AMS that are currently being developed include a 1064 nm Nd:YAG laser for the ionization of soot particles and a vacuum ultraviolet photoionization system. Produced ions are subsequently transferred into a Quadrupole or a high-resolution time-of-flight spectrometer using an ion optics system. Defined parcels of ions from the cloud of ionized atoms and molecules are extracted at intervals of about 30 ns and detected at the microchannel plate (MCP) with a maximum acquisition rate of 10000 raw scans per second. Depending on the mode of operation the ions follow a V-shaped path or a W-shaped path using two reflectrons upon detection by the MCP. The resolution power in V-mode is, depending on the quality of the tuning of the instrument, about 4000 in W-mode and 2000 in V-mode. Reasonable sampling times can be down to a few seconds.

Recent modifications of the AMS include a cyro-trap for the measurement of more volatile species, a soot-particle unit for the detection of black carbon and a coupling to a thermal desorption gas chromatograph system (TAG). A recently developed single-particle module allows for the detection of single aerosol particles larger than $\approx 180\,nm$ in optical diameter (Cross et al., 2009). Optical detection is realized with a diode-pumped $405\,nm$ continuous wave $50\,mW$ laser (figure 2.1). Scattered light of crossing single particles is detected by a photomultiplier tube (PMT) which also triggers the acquisition of a mass spectrum of the incident single particle.

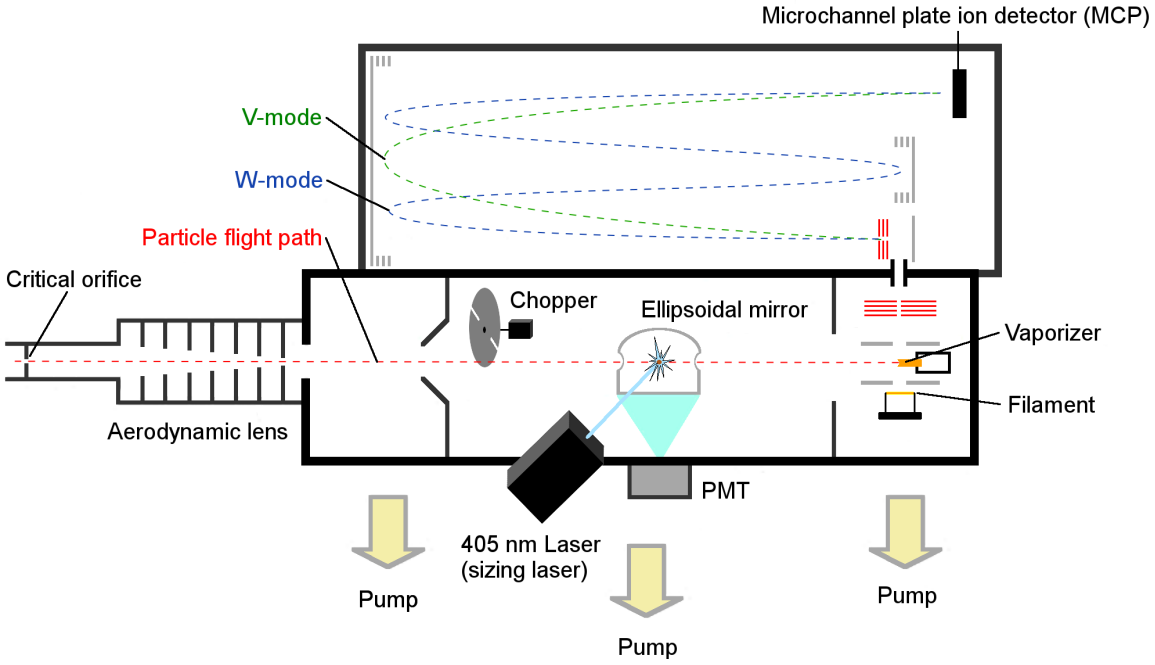

Figure 2.1.: Sketch of the light-scattering single particle high-resolution time-of-flight aerosol mass spectrometer (LSSP-HR-ToF-AMS) for the improved sizing and the detection of single particles with diameters larger than $\approx 180\,nm$.

Calibrations and data treatment

For a proper operation of the aerosol mass spectrometer a series of calibrations is necessary. The aerodynamic lens has to be aligned in order to collect particles of all transmitted sizes on the vaporizer surface. This is carried out by scanning different lens positions in horizontal and vertical direction for different sizes of NH_4NO_3 particles.

An accurately controlled vaporizer (heater) temperature is essential for the comparison of data obtained from different AMS instruments. Differences in this temperature may affect mass spectral features and frequently used metrics, for example the fraction of the organic signal at mass-to-charge ratio (m/z) 44: f_{44} (Williams, 2010). The standard vaporizer temperature of the AMS is 600 °C which has been chosen as a compromise according to the following criteria:

1. Sufficient number of ions resulting from the ionization of NH_4NO_3 aerosol particles. The higher the temperature, the more ions per particles can be produced.

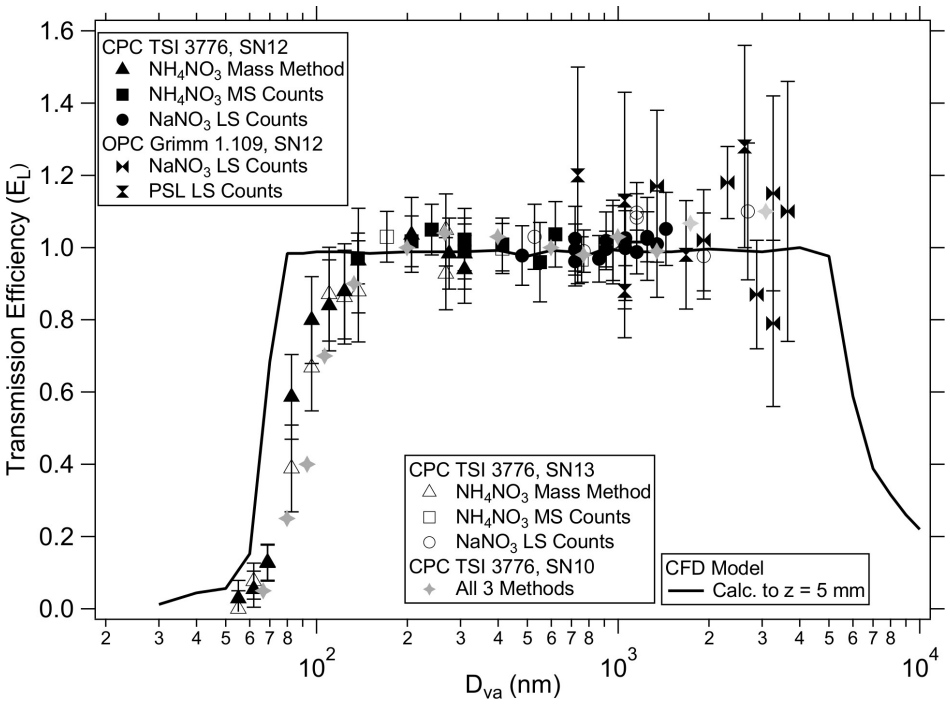

Figure 2.2.: Experimentally determined transmission efficiency (E_L) as a function of particle size for three prototypes of the $PM_{2.5}$ lens with serial numbers SN10, SN12 and SN13 (adapted from Williams et al., 2013). In this thesis, aerodynamic lenses with serial numbers SN13 and SN6 (not shown) were used. Supplementary continuous flow dynamics (CFD) calculations are shown in solid lines.

2. Reasonably low temperature to prevent deterioration of the tungsten surface and other attached ceramic elements which would lead to increased background signals, e.g. for tungsten W^+, potassium K^+ or sodium Na^+.

3. Fast vaporization from the heater surface to enable measurements of particle size. The time needed for evaporation of a particle adds to the particle time-of-flight in the sizing chamber and the ion time-of-flight prior to detection at the microchannel plate ion detector. For a majority of atmospherically relevant particles the time span for the flash vaporization is in the order of a few micro seconds and thus negligible compared the particle time-of-flight of a few milliseconds.

4. Maintain a constant temperature within AMS measurements to be able to compare mass spectra, e.g. in a database (Ulbrich et al., 2009). Temperature changes can, in addition to poorly tuned ion optics voltages, lead to altered mass spectra as a result of surface-type ionization reactions that may lead to an artificial abundance of amine-derived ions (Hildebrandt et al., 2011) or ions that are present in vaporizer assembly materials such as K^+, Na^+ and rubidium Rb^+.

The heater temperature can be determined and adjusted by a calibration with $300\,nm$ $NaNO_3$ aerosol particles. According to the recommendations by L.R. Williams (Aerodyne), the particle time-of-flight signal at mass-to-charge ratio m/z 30 is acquired at different vaporizer feed currents. The exponential fitting of the falling edge of the signal of m/z 30 depending

on the particle time-of-flight is then used to set a temperature of 600 °C.

In the AMS, particle sizes are determined using an empiric relationship between the particle size and the particle flight velocity in the vacuum. Polystyrene latex (PSL) solutions with defined particle diameters are sampled at an increased vaporizer temperature of about 800 °C. Figure 2.3 shows the relationship between the particle time-of-flight and the particle diameter. Please note that due to the density of the PSLs ($1.03\,g\,cm^{-3}$) the geometric diameter and the vacuum aerodynamic diameter are almost equal (DeCarlo et al., 2004). The empiric relationship between the vacuum aerodynamic diameter D_{va} and the particle velocity v that is used for the size determinations is as follows:

$$v = v_l + \frac{v_g - v_l}{(1 + \left(\frac{D_{va}}{D^*}\right)^b)} \tag{2.2}$$

where v_l is the gas velocity in the lens, v_g is the gas velocity at the lens exit, and D^* and b are fitting parameters.

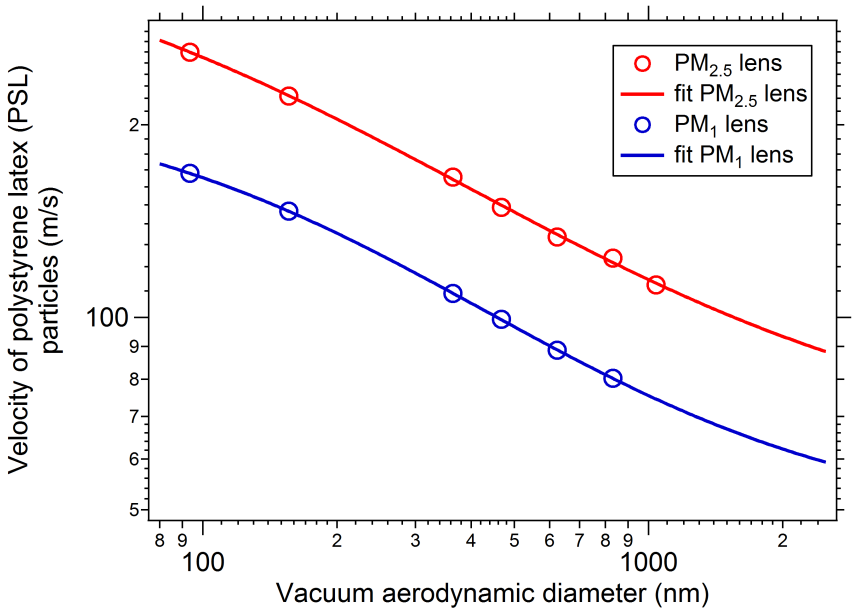

Figure 2.3.: Size calibration comparison between the conventional PM_1 lens and the $PM_{2.5}$ lens (second generation lens provided by L.R. Williams, Aerodyne).

For the quantification of the measured aerosol concentration a mass calibration with NH_4NO_3 particles of $400\,nm$ in mobility diameter is carried out. Mass calculations are based on the detection of NO^+ and NO_2^+ ions in the mass spectrometer which are assigned relative ionization efficiencies of one. Here, the ionization efficiency is defined as the average number of ions per number of molecules in the particles. Relative ionization efficiencies of other ions have been determined empirically using laboratory standard compounds or accompanying measurements. The equation to calculate the total aerosol mass concentration C_s according to Jimenez et al., 2003 is:

$$C_s = R_t \frac{\sum_f I_{sf}}{N_A Q X_{sf}} \frac{MW_{NO_3}}{IE_{NO_3}} \tag{2.3}$$

where R_t is a response factor of a certain type of molecules relative to the AMS species NO_3, N_A is the Avogadro constant, Q is the volumetric sample flow, X_{sf} is the fraction of the ions of species s that are detected at its f_{th} fragment, I_{sf} is the number of detected ions per unit time at the f_{th} fragment, MW_{NO_3} is the molecular weight of NO_3 and IE_{NO_3} is the ionization efficiency of NO_3. NH_4NO_3 particles with $400\,nm$ in mobility diameter (D_m) are used in the calibrations of the ionization efficiency since their shape and density are well-known; they are focused well by the aerodynamic lens and NH_4NO_3 evaporates/sublimes completely and sufficiently fast at the vaporizer surface. Additionally, it is also a relevant constituent of atmospheric aerosol.

A common practice for the quantification of the inorganic aerosol fraction is a separate calculation of the relative ionization efficiencies for the AMS species: sulfate (SO_4), nitrate (NH_4) and their derived ions, respectively. This is particularly necessary for an accurate investigation of the acidic and basic properties of the aerosol particles. Separate water solutions containing $(NH_4)_2SO_4$ and NH_4NO_3 are aerosolized, dryed and sampled by the AMS. The relative ionization efficiencies referred to the NO_3 species are determined by implying a mass balance calculation between the cations and anions.

2.1.2. $PM_{2.5}$ inlet

The aerodynamic diameter of aerosol particles that can be sampled with an AMS employing the standard Liu-type aerodynamic lens ranges between roughly $80\,nm$ to $800\,nm$ at 50% transmission (Liu et al., 2007). To extent this range, a novel inlet has been developed to minimize losses of aerosol particles due to diffusion and impaction on the inlet walls. A modified orifice holder, custom-built main valve (bigger borehole) and a relaxation tube prevent from sharp changes in the flow pattern and thus optimize laminar flow conditions inside the inlet. A detailed description of this inlet is given by Williams et al., 2013. This inlet allows for a near-real time detection of non-refractory $PM_{2.5}$ aerosol. Since the particle flight velocity is

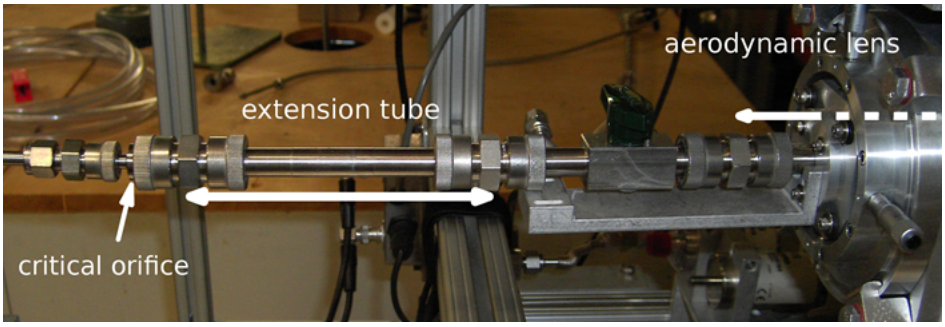

Figure 2.4.: $PM_{2.5}$ inlet (second generation) mounted on a HR-ToF-AMS in the laboratory.

higher when using this inlet, it can be assumed that asymmetric particles, which may diffuse away from the center of the particle beam, are better focused on the middle of the vaporizer surface. Additionally, due to the larger pressure drop between the inlet of the aerodynamic lens and the first AMS chamber (from 13 $Torr$ to 10^{-3} $Torr$) a cooling of the aerosol particles might occur as a result of a near supersonic expansion into vacuum. Possible changes of the phase of the particles from fluid to solid could affect the collection efficiency and need further

studies. The higher velocity of the aerosol beam leads to a partial overlap with the beam or air molecules in particle time-of-flight mode. This can lead to a slight left-side onset on the organics size distribution which originates from CO_2^+ ions for a particular lens (especially serial number SN6) that has been tested. The chopper slit of the mechanical chopper is finite and as a consequence of the faster transmission of the particles, the parcels of aerosol particles might be less well defined resulting in a higher uncertainty in the size measurement. To assess the influence of the chopper and its rotation frequency, model calculations on a generic size distribution were performed (figure 2.5). At a frequency of $120\,Hz$ the change in the size distribution appears to be negligible whereas at $50\,Hz$ a significant broadening exists. As typical chopper frequencies are in a range between $120\,Hz$ and $150\,Hz$ it can be concluded that a changed transmission function due to the chopper does not severely change the size distribution characteristics.

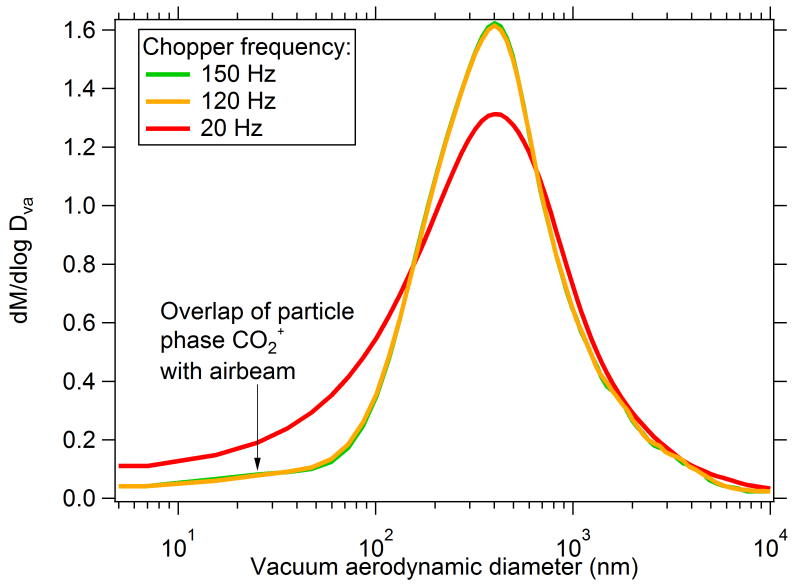

Figure 2.5.: Influence of the chopper rotating frequency on a generic size distribution (at $150\,Hz$). The lowest rotation frequency ($120\,Hz$) that is typically used in experiments has only negligible effects on the size distribution shape. A larger discrepancy on the left onset of the peak is a consequence of a lower number of sampling points in logarithmic D_{va} space compared to equal intervals of sampling points in particle time-of-flight space.

2.1.3. Measurement uncertainties

Various measurement uncertainties arise from the sampling process, the instrument itself and the data analysis process. For this reason, sampling lines, sample flow velocities and residence times for gas and particle phase instruments need to be optimized to prevent the loss of analytes prior to the detection with the instrument. A particularly challenging task is to maintain isokinetic sampling conditions on mobile platforms in order not to discriminate particles with different sizes in the inlet due to the velocity of the platform. Accumulation

mode aerosol particles generally tend to be less affected because particle loss by diffusion and sedimentation or impaction are less important.

A calculation of the AMS measurement uncertainties is necessary for further data interpretation, for example when using positive matrix factorization (discussed below). Uncertainties for the measurement of the ion rate I (in Hz) in the AMS comprise:

- Electronic noise $\Delta I_{Elec.}$ which resembles the uncertainty from electronic instrument noise and possible scattered ion signals that are presumed to contribute to every measured ion signal.
- 1-ion minimum error ΔI_{1-ion}. It is equal to the signal measured from one ion during one time step.
- Ion counting error ΔI_{IC} which is the precision from Poisson ion-counting statistics. $\Delta I_{IC} = \alpha\sqrt{\frac{I}{t_s}}$ where t_s is the amount of time (s) that is spent sampling at a particular m/z. α is a factor to account for the fact that a single ion signal is not constant but arises from a Gaussian distribution of pulse areas of finite width. This factor has been determined to be 1.2 (Allan et al., 2003a).

The uncertainty for the final ion rate I_D, which is the arithmetic difference between "open" and "blocked" chopper cycles, is $\Delta I_D = \sqrt{\Delta I_o^2 + \Delta I_b^2} = \alpha\frac{\sqrt{\Delta I_o + \Delta I_b}}{\sqrt{t_s}}$.

2.2. Source apportionment

Source apportionment describes a methodological approach for the identification of sources of atmospheric particulate matter as well as the estimation of their contribution to the aerosol mass concentration. Herein, a source is any process that releases aerosol particles or their precursor compounds into the atmosphere.

Two main source apportionment strategies can be classified. In a bottom-up approach, emissions of know sources, e.g. various vehicles, are measured. The temporal evolution of gaseous and particulate emissions can be further determined in environmental chambers. The derived information about the emission factors of primary aerosol and the potential secondary aerosol can be integrated in emission maps or used in models to evaluate source contributions up to a global scale.

In a top-down approach, ambient measurements are conducted at particular sites. The quantitative attribution of sources is realized with a statistical analysis of the measurement data. Statistical methods which reconstruct the sources of atmospheric aerosol from measurement data obtained at a particular ("receptor") site are also termed as receptor models. A fundamental assumption of these models is the conservation of mass and the number of measured species between the emission source and the receptor site in mass balance calculations. Various receptor models have been developed in the last years (Belis et al., 2014).

2.2.1. Positive matrix factorization and multilinear engine (ME-2)

Positive matrix factorization (PMF) is a widely used (Viana et al., 2008) model for receptor modeling. This factor analysis variant is based on the bilinear model

$$X = GF + E \tag{2.4}$$

in which X denotes the measured matrix, G describes the factors (sources) and F is the factor (source) contribution as represented in figure 2.6. PMF does not require any *a priori*

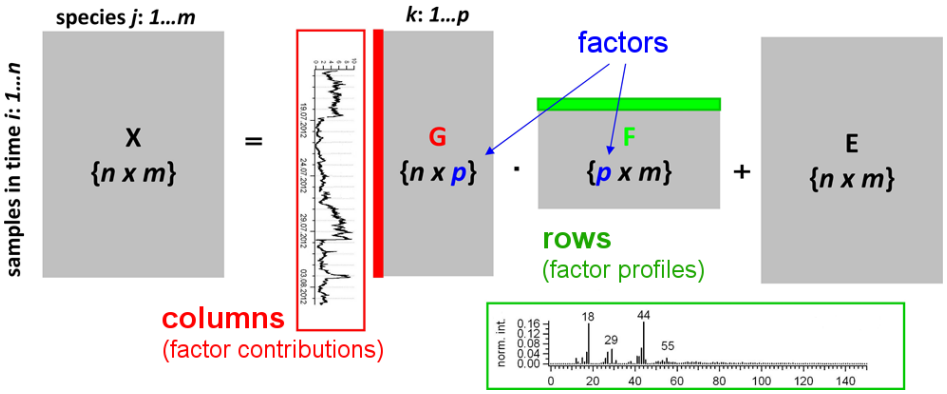

Figure 2.6.: Schematic working principle of the positive matrix factorization (PMF) model. Adapted from Ulbrich et al., 2009.

information about the sources which separates it from other receptor models, e.g. the chemical mass balance technique (CMB). As the solutions of this model are non-negative it is better suited for environmental applications than for example principal component analysis (PCA). It should be noted that PMF assumes static source profiles (e.g. mass spectra) and thus does not account for the evolution of the aerosol chemical composition from its emission to the detection at the receptor site. Consequently, sources that are very similar in chemical composition may not be resolved as different factors.

The entity Q:

$$Q = \sum_i \sum_j \left(\frac{e_{i,j}}{s_{i,j}} \right)^2 \tag{2.5}$$

is a parameter for the quality of fit of the model. The PMF algorithm minimizes this value using the conjugate-gradient method towards a local/global minimum. The minimum of the obtained solution can be explored using mathematically equally valid solutions with pseudo-rotations (discussed below). Q also decreases with the an increasing number of factors because the underlying linear combination will explain variability in a given data set better. The actual value of Q or its decrease may not be used for the identification of environmentally reasonable PMF solutions (Paatero et al., 2014).

PMF solutions possess rotational ambiguity, i.e. an arbitrary matrix T with the same dimensions as matrix G and its inverse T^{-1} also satisfy the condition:

$$X = GTT^{-1}F + E = G'F' + E \tag{2.6}$$

and are equally valid solutions of the model. Although PMF calculations have been validated by using a generic data set with known contributions of different sources (Zhang et al., 2005), the possible model solutions are sensitive to user interpretation. A possible standardized protocol for a source assessment with AMS data sets within Europe has been discussed by Crippa et al., 2014. In brief, after an unconstrained PMF evaluation, calculations with a constrained hydrocarbon-like organic aerosol (HOA) mass spectrum are performed. A thorough analysis of the residuals as well as of the diurnal structures of markers for biomass burning and cooking organic aerosol will give evidence if these sources need to be possibly constrained for a clear separation from each other.

As a further support, the results should ideally be accompanied by measurements on filter samples such as ion chromatography (IC), organic carbon/elemental carbon (OC/EC), proton-induced X-ray emission (PIXE), gas phase analysis (GC-MS, PTR-MS), black carbon analysis or inductively coupled plasma atomic emission spectroscopy (ICP-AES). Meteorological data, e.g. boundary layer height, temperature, wind direction and speed or air mass back trajectory analysis have been proven to be helpful tools in the source apportionment.

Advanced factor analysis models can be used since positive matrix factorization is not well suited for a separation of sources with similar chemical composition, during stagnant meteorological conditions which lead to a build-up of pollutants, and for the identification of minor sources. One recent development is an improved model that additionally employs the particle size information from the AMS particle time-of-flight mode (Ulbrich et al., 2012). In another approach, the input for PMF calculations can be directly extended with data from co-located instruments (e.g. proton transfer reaction mass spectrometer data) which can be useful for a simultaneous source apportionment of particulate phase and gas phase compounds (Slowik et al., 2010) and may allow for a better distinctions of primary and secondary aerosol components (Crippa et al., 2013a). Another possibility is the application of the multilinear engine (ME-2) source apportionment (Paatero, 1999) technique.

In ME-2 calculations an *a priori* information about one or more sources can be used as an input of the model. ME-2 source apportionment thus can be classified as a source apportionment technique that ranges between techniques without any *a priori* input information about the source composition (e.g. PMF) and techniques in which information about the composition of all sources is necessary (e.g. CMB). The constraining of the source composition can be accomplished via the so-called a-value approach or using so-called pulling equations (Canonaco et al., 2013). In the a-value approach the factor mass spectrum is allowed to vary within predefined limits given by the a-value parameter. The pulling method applies a more "soft" constraint by parabola-like penalty functions when a factor profiles deviates from its original input. Parameter sensitivity tests on the tightness of constraints by the a-value or the pulling equations are essential tools in the interpretation of environmentally reasonable model solutions.

3

Characterization of ice-nucleating bacteria using on-line electron impact ionization aerosol mass spectrometry

R. Wolf[1], J. G. Slowik[1], C. Schaupp[2], P. Amato[3], H. Saathoff[2], O. Möhler[2], A.S.H Prévôt[1] and U. Baltensperger[1]

[1] *Laboratory of Atmospheric Chemistry, Paul Scherrer Institute, 5232, Villigen PSI, Switzerland*

[2] *Institute for Meteorology and Climate Research, Karlsruhe Institute of Technology, 76021, Karlsruhe, Germany*

[3] *National Center for Scientific Research, Institute of Chemistry of Clermont-Ferrand, 63000, Clermont-Ferrand, France*

Published in Journal of Mass Spectrometry, 50, 662–671, 2015

Abstract

The mass spectral signatures of airborne bacteria were measured and analyzed in cloud simulation experiments at the AIDA (Aerosol Interaction and Dynamics in the Atmosphere) facility. Suspensions of cultured cells in pure water were sprayed into the aerosol and cloud chambers forming an aerosol which consisted of intact cells, cell fragments and residual particles from the agar medium in which the bacteria were cultured. The aerosol particles were analyzed with a high-resolution time-of-flight aerosol mass spectrometer equipped with a newly developed $PM_{2.5}$ aerodynamic lens. Positive matrix factorization (PMF) using the multilinear engine (ME-2) source apportionment was applied to deconvolve the bacteria and agar mass spectral signatures. The bacteria mass fraction contributed between 75 and 95% depending on the aerosol generation, with the remaining mass attributed to agar. We present mass spectra of *Pseudomonas syringae* and *Pseudomonas fluorescens* bacteria typical for ice-nucleation active bacteria in the atmosphere to facilitate the distinction of airborne bacteria from other constituents in ambient aerosol, e.g. by PMF/ME-2 source apportionment analyses. Nitrogen-containing ions were the most salient feature of the bacteria mass spectra, and a combination of $C_4H_8N^+$ (m/z 70) and $C_5H_{12}N^+$ (m/z 86) may be used as marker ions.

3.1. Introduction

Airborne bacteria have been identified in various parts of the atmosphere including remote locations such as desert regions (Marafie and Ashkanani, 1991; Griffin et al., 2007; Maki et al., 2010) and as high as 50 km in the stratosphere (Imshenetsky et al., 1978). They have been found in cloud water (Sattler et al., 2001; Bauer et al., 2002), ice-crystals and snow (Pratt et al., 2009; Christner et al., 2008) as well as fog droplets (Fuzzi et al., 1997). In the upper troposphere, viable bacteria appear to be the prevailing microorganisms and can represent up to around 20% of the total number of particles between 0.25 and 1 μm in diameter (DeLeon-Rodriguez et al., 2013). Bacterial cells contribute not only to the total organic aerosol burden, but may also serve as cloud condensation nuclei (Möhler et al., 2007; Bauer et al., 2003). Certain ice-nucleation active strains are among the most efficient ice-nuclei known (Möhler et al., 2008b). It has been hypothesized that these ice-nucleating particles influence climatic conditions and may play a role in the local hydrological cycle of the pristine rainforest (Pöschl et al., 2010) . Since they can act as pathogens to humans, animals and plants they are also of great interest for indoor and outdoor air quality even at low number concentrations (Burge and Rogers, 2000; Frieden et al., 2011). Bacterial emissions from surfaces strongly depend on the location as well as meteorological and seasonal parameters (Jones and Harrison, 2004), and little is known about anthropogenic influences such as harvesting or soil treatment activities on the emission source strength.

Reported estimates of airborne bacteria concentrations in ambient air are highly variable due to different quantification methods and a lack of standardization (Kuske, 2006; Peccia and Hernandez, 2006). For example, the prevalent analysis of colony forming units (CFU), still largely employed in atmospheric studies, only quantifies cultivable cells and therefore neglects cell fragments, non-viable cells and those that are viable but unable to multiply under the culture conditions at which they are exposed. The fraction of cultivable cells in different habitats ranges between < 0.1 and 2% (Bussmann et al., 2001), and thus the total number

concentration of bacteria can be more than 100 times higher than the reported number of CFUs. In the atmosphere, bacteria may exist as individual cells (Pösfai et al., 2003), clusters, attached to other particles (e.g. pollen, soil particles, fungal spores, plant and animal debris) (Bovallius et al., 1978; Lighthart, 1997) or as cell fragments, making their quantification even more challenging.

Traditional methods to determine ambient concentrations of bacteria make use of aerosol collection (e.g. filtration, liquid impingers, agar plate impaction) with subsequent analysis of the collected material either by enumeration of bacteria colonies after cultivation on a growth medium or by using light microscopy in combination with different staining procedures (Després et al., 2012). Flow cytometry with specific fluorescent stains is an established technique for microbial enumeration but it remains rarely employed in atmospheric studies yet (Christner et al., 2008). Further advances in bioaerosol detection include quantitative polymerase chain reaction analysis (qPCR) (Hospodsky et al., 2010), biosensors based on nanowires (García-Aljaro et al., 2010) and potentiometric tomography in flames (Sarantaridis et al., 2012).

In recent years, mass spectrometric and optical techniques have evolved to detect bacteria in near real-time, e.g. aerosol time-of-flight mass spectrometry (Noble and Prather, 1996), bioaerosol mass spectrometry (Fergenson et al., 2004), online matrix-assisted laser desorption time-of-flight mass spectrometry (Kleefsman et al., 2007), ion trap mass spectrometry (Gieray et al., 1997) or methods based on the emission of fluorescent light by aerosols (Agranovski and Ristovski, 2005; Toprak and Schnaiter, 2013; Pinnick et al., 1995). However, these techniques are not all specific to bacteria and are subject to interferences from other species, yielding uncertain or ambiguous results. For example, fluorescence methods are subject to cross-interferences with other fluorophores containing NADH, NADPH or riboflavin. Laser-based mass spectrometers suffer from variability in desorption, ionization and fragmentation processes (Silva and Prather, 2000) for instance as a result of varying laser power (Steele et al., 2003). Thus, in the absence of well-defined markers, the source assessment is compromised because variations in mass spectral patterns are difficult to ascribe to compositional differences. Even though a number-based quantification of bacteria by these techniques is feasible, the mass-based apportionment of bacteria is subject to a higher degree of uncertainties (Sullivan and Prather, 2005).

In this study, we employ the widely-used Aerodyne aerosol mass spectrometer (AMS) (Jayne et al., 2000) which uses defined thermal vaporization and electron impact ionization in combination with a newly developed aerodynamic lens for the detection of super-micron aerosol directly from the aerosol phase. We present the size distributions and characteristic mass spectra of two ice-nucleation active strains of *Pseudomonas* bacteria. The mass fraction of the partially aerosolized agar nutrient medium is quantified using both AMS particle time-of-flight (pToF) data and positive matrix factorization source apportionment analysis.

Table 3.1.: Summary of all experiments with bacteria cells (I – IV) and blank experiments.

Experiment	**I**	**II**	**III**	**IV**	**Blank**	
					Agar	**Centrifuged solution**
Species	*P.syr.*	*P.syr.*	*P.flu.*	*P.flu.*	King's B Agar	Supernatant of *P.flu.*
AMS vaporizer temperature (T_{vap})	600 °C	730 °C	600 °C	730 °C	600 °C/730 °C	600 °C/730 °C
Chamber	APC	APC	APC	APC	Custom[a]	APC
Relative humidity	30%	30%	30%	30%	[a]	30%
Temperature	≈ 25°C	≈ 25°C	≈ 25°C	≈ 25°C	≈ 20°C	≈ 25°C

[a] Aerosol was generated with a custom-built nebulizer, dried with a silica gel diffusion dryer and directly sampled with a HR-ToF-AMS.

3.2. Materials and methods

3.2.1. Experiments

Two strains of Gram-negative Gammaproteobacteria were investigated in the AIDA (Aerosol Interaction and Dynamics in the Atmosphere) cloud chamber at the Karlsruhe Institute of Technology (KIT). *Pseudomonas syringae* (*P. syringae*) strain 32b-74 (Attard et al., 2012; Vaïtilingom et al., 2012; Joly et al., 2013) isolated from cloud water collected from the Puy de Dôme Mountain in November 2009 and *Pseudomonas fluorescens* (*P. fluorescens*) strain CGina-01 (originally provided by C. Foreman, Montana State University (Attard et al., 2012)) from Antarctic glacier melt water were cultivated on sterile King's B agar nutrient medium (King et al., 1954). Viable cells of either *P. syringae* or *P. fluorescens* were scratched from the agar surface, resuspended into sterile, distilled water and dispersed directly into the Aerosol Preparation Chamber (APC) (Möhler et al., 2008a) with a two component spray nozzle from Schlick (model 970) operated with particle-free synthetic air at a pressure of $0.2\,MPa$. An overview of all experiments is given in table 3.1. An additional blank (denoted as "Centrifuged solution") consisted of the supernatant of a centrifuged suspension ($5000 \times g$, $20\,min$, 4 °C) of *P. fluorescens* cells. A different blank experiment (denoted as "Agar") was carried out by scratching the surface of a sterile agar medium in the same way used to immerse the bacteria cells into water and by aerosolizing the obtained suspension with a custom-built, collision-type nebulizer. Aerosol was sampled from the chamber, dried using a silica-gel diffusion dryer and continuously analyzed by an Aerodyne high-resolution time-of-flight aerosol mass spectrometer (HR-ToF-AMS) (DeCarlo et al., 2006) through a 6-mm stainless steel sampling line with a total flow of about $1\,L\,min^{-1}$. Here, the term high resolution refers to an advanced version of the Aerodyne AMS which is equipped with a time-of-flight mass analyzer instead of a quadrupole analyzer. This mass analyzer can be operated in two modes, i.e. different

ion flight distances. In this study, we used the mode with higher sensitivity in which mass resolutions ($\frac{m}{\Delta m}$) of 2100 up to m/z 200 have been demonstrated. The AMS was equipped with a newly developed inlet and aerodynamic lens which transmits particles up to about $3\,\mu m$ in aerodynamic diameter (Williams et al., 2013), allowing direct detection of bacteria aerosol.

The strategy employed herein to distinguish bacteria and agar mass spectra requires adequately resolved size measurements. Preliminary experiments indicated that slow vaporization of the measured particles (decreasing the size resolution) could compromise these efforts. The vaporization process can be sped up by increasing the AMS vaporizer temperature (T_{vap}); however, this may increase the extent of thermal decomposition, perturbing the measured mass spectra with respect to typical ambient AMS operating conditions. To attain both a well-resolved size measurement and a mass spectrum relevant to typical AMS operation, measurements were conducted with T_{vap} set to both 600 °C (standard temperature for reported AMS mass spectra, see Ulbrich et al., 2009) and 730 °C (faster evaporation from the vaporizer surface). Sampling alternated between mass spectrum (MS) mode in V-mode configuration and particle time-of-flight mode with $30\,s$ sampling time for each mode. High-resolution AMS data were processed with SQUIRREL (SeQUential Igor data RetRiEvaL) v1.52F and PIKA (Peak Integration by Key Analysis) v1.11G within the IGOR Pro software package (Wavemetrics, Inc., Portland, OR, USA). O/C, H/C and N/C elemental ratios were calculated as described by Aiken et al., 2007.

3.2.2. Distinction of mass spectra of bacteria and residual particles

Positive matrix factorization (PMF) is a bilinear factor analytical model which has been described in detail by Paatero, 1999. The multilinear engine (ME-2) is an implementation of the PMF algorithm that additionally allows for the inclusion of known factor profiles in the model. Calculations with the ME-2 algorithm offer several advantages over conventional PMF analyses and have been recently used in the source apportionment of organic aerosols (Lanz et al., 2008; Crippa et al., 2013a). In brief, a measured matrix X can be approximated as a linear combination of static source profiles (e.g. mass spectra) described by the matrix F, and the temporal variability of these sources (e.g. the contribution of each mass spectrum to the total modeled mass), described by the matrix G. The algorithm minimizes the squared model residual (E) weighted by the AMS measurement uncertainties.

$$X = GF + E \tag{3.1}$$

All PMF solutions have some degree of rotational ambiguity, which can be fully explored in the ME-2 implementation. To optimize exploration of the complex, multidimensional solution space, we constrain elements of the source profiles f_i (mass-to-charge ratios, m/z) to direct the solution towards environmentally reasonable rotations. Here these constraints are implemented using the a-value approach providing a fixed range within which the output factor profile is allowed to vary. For a single f_i, this is expressed as:

$$f_i(solution) = f_i \pm a \times f_i \tag{3.2}$$

In order to distinguish bacterial mass spectra from those of the residual components in the chamber aerosol we used SoFi (Source Finder) v4.5 (Canonaco et al., 2013), a user frontend

for the configuration of the ME-2 algorithm (Paatero, 1999) input matrices and visualization of the results.

The measured matrix X of ions ranging from m/z 12 to m/z 100 and the corresponding AMS measurement uncertainties were calculated following the recommendations as described by Ulbrich et al., 2009, described briefly as follows. A minimum error corresponding to measurement of a single ion was applied, ions with a signal-to-noise ratio (SNR) between $0.2 < SNR < 2$ were downweighted by a factor of 2 and ions with a $SNR < 0.2$ were downweighted by a factor of 10. In cases where multiple isotopes of an ion were detected, only the dominant isotope was included. Ions calculated as a constant fraction of the CO_2^+ signal (Allan et al., 2004) were downweighted such that they exert the correct weight on the ME-2 solution.

To estimate the relative agar mass fraction, the pure agar mass spectrum which was measured in the blank experiment was constrained by using the ions that were identified in both agar and bacteria experiments. ME-2 calculations with one to four factors and five different pseudo random starting points were performed. We tested a range of a-values from 0.01 to 0.5 to examine the sensitivity of the results on the magnitude of the a-value.

Furthermore, the ME-2 source apportionment solution was compared with an alternative method using AMS pToF data. For a size distribution that is a convolution of two distinguishable modes one can calculate the mass fraction of the residual particles in the first mode (m_{res}) as the ratio of the integrated mass of the first mode to the total integrated mass. This calculation assumes that agar particles are detectably smaller and do not coagulate with particles originating from the bacteria during these experiments. Taking into account a possible fragmentation of the bacteria cells by rupture of the cell membrane which could yield particles of similar size to the agar particles, we derive an equation to calculate a true agar mass fraction (m_{agar}) for this binary mixture:

$$m_{agar} = m_{res} \times m_{agar}^{1stmode} \tag{3.3}$$

$$m_{agar}^{1stmode} = 1 - \frac{f_{marker}^{1stmode} - f_{marker}^{agar}}{f_{marker}^{2ndmode} - f_{marker}^{agar}} \tag{3.4}$$

Here, $m_{agar}^{1stmode}$ represents the mass fraction of agar in the first size mode, which obeys the condition $0 \leq m_{agar}^{1stmode} \leq 1$ as a result of the presence of bacteria fragments in this mode. $f_{marker}^{1stmode}$ and $f_{marker}^{2ndmode}$ are the organic mass fractions of the identified bacteria marker m/z ($f_{marker} = \frac{m/z_{marker}}{Organics}$) in the first size mode and the second size mode. f_{marker}^{agar} is the corresponding fraction for the agar blank experiment.

3.3. Results and discussion

3.3.1. Distinction of mass spectra of bacteria and residual particles

A representative mass size distribution of an aerosolized suspension of *Pseudomonas* bacteria shows two distinct modes. In figure 3.1, the larger mode ("bacteria") can be attributed to single, non-spherical bacteria cells having sizes around $0.9\,\mu m$ in vacuum aerodynamic diameter (D_{va}) consistent with previous studies (Möhler et al., 2008b; Johnson, 1999). The

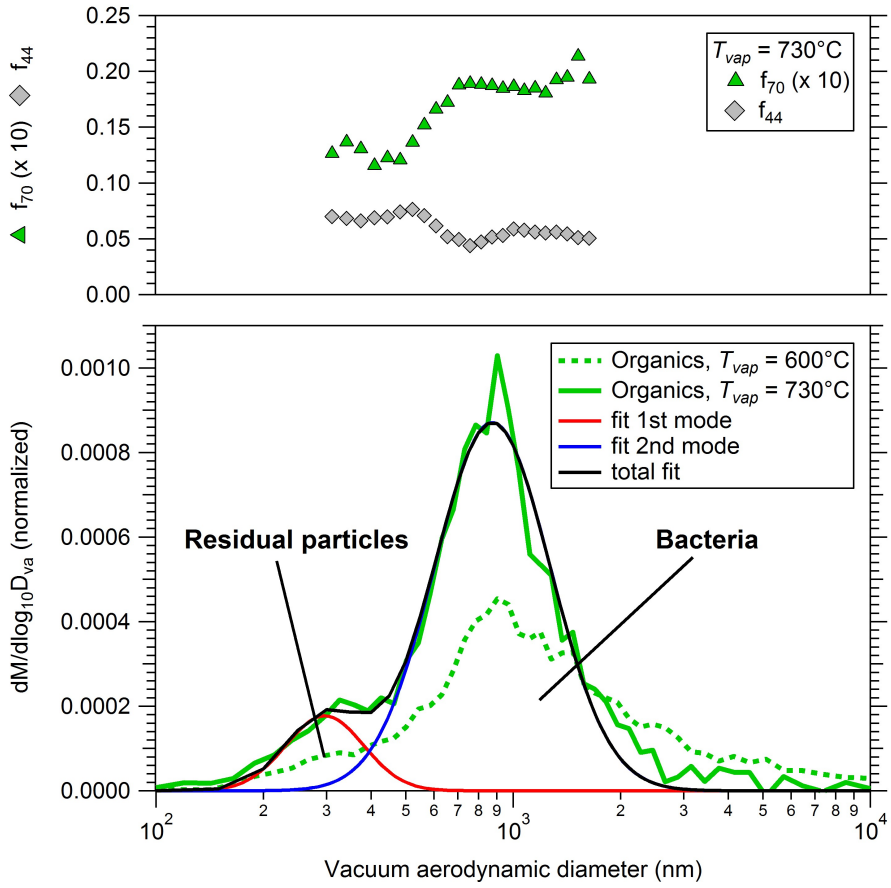

Figure 3.1.: Organic mass size distribution of combined *P. fluorescens* and *P. syringae* experiments obtained at AMS vaporizer temperatures $T_{vap} = 730\,°C$ (Exp. II, Exp. IV) and $T_{vap} = 600\,°C$ (Exp. I, Exp. III) including organic mass fractions characteristic for bacteria (m/z 70) and agar (m/z 44). The residual particle mass fraction (m_{res}) is calculated by fitting the size distributions as the sum of two log-normal functions (solid black line). The individual log-normal distributions are shown as red and blue lines.

smaller mode ("residual particles") at about $200 - 400\,nm$ contains particles that originate from the agar medium, evidenced by agar and centrifuged blank experiments which show a mass mode size of approximately 200 and $300\,nm$, respectively (figure A.1). Furthermore, identified organic marker fractions for agar (f_{44}) and bacteria (f_{70}) (discussed below) are strongly size-dependent, with higher f_{44} in the smaller and higher f_{70} in the larger size mode.

In all experiments, the chemical composition of agar and bacteria aerosol as measured by the AMS in unit mass resolution (UMR) is very similar, complicating their distinction. For example, size-selected UMR mass spectra integrated from 100 to 300 nm (residual particles) and 1000 to 2000 nm (bacteria) show a coefficient of determination of $R^2 = 0.895$ (Pearson) in a linear orthogonal regression (figure A.2). Similarly, the size-selected mass spectra of the agar blank experiment (integrated from 100 to 300 nm) and bacteria (integrated from 1000 to 2000 nm) also exhibit significant correlation ($R^2 = 0.869$). The correlation is even stronger ($R^2 = 0.925$) when comparing the integrated mass spectra between the centrifuged solution (integrated from 100 to 300 nm) with the bacteria. This indicates that the sample obtained after centrifugation and filtration may contain an increased fraction of cell fragments.

To quantify the bacteria fragments in the first size mode and the true agar mass fraction, ME-2 calculations were successfully performed on four combined experiments (Exp. I – Exp. IV, figure 3.2) to separate one factor originating from agar-containing particles and one combined *Pseudomonas* bacteria factor. Because electron impact ionization (70 eV) causes major ana-

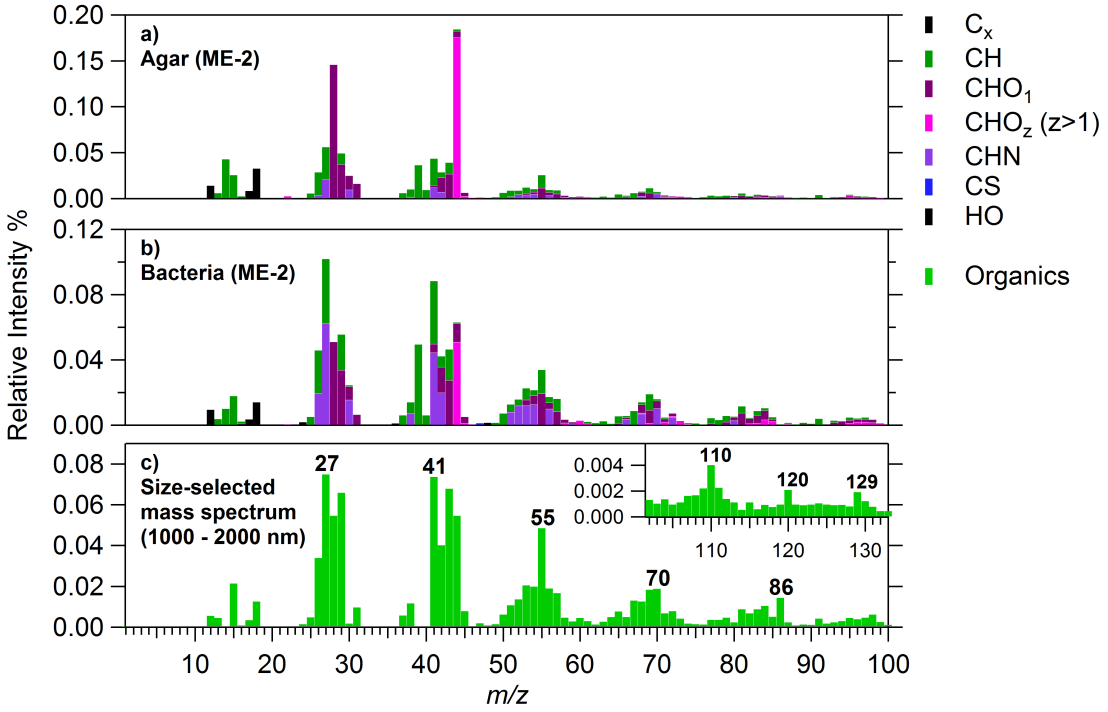

Figure 3.2.: Distinction between **a)** agar nutrient medium and **b)** bacteria using the ME-2 algorithm with constrained agar mass spectrum (average result of ME-2 calculations with $a = 0.01$, $a = 0.05$ and $a = 0.1$) and comparison with **c)** a size-selected spectrum of *P. fluorescens* (Exp. III). Spectral similarity is higher between the size-selected bacteria spectrum and the bacteria factor ($R^2 = 0.97$) than between the agar factor and the size-selected spectrum ($R^2 = 0.72$). Differences between mass spectra **c)** and **b)** are a result of different fragmentation tables (Allan et al., 2004) in unit mass resolution and high-resolution as well as a consequence of a lower number of fitted nitrogen-containing ions that are used in the constrained agar factor in the ME-2 calculations.

lyte fragmentation, reducing the ability to detect small differences in molecular composition we do not expect this method to quantitatively separate the different *Pseudomonas* strains. In general, a differentiation between various bacteria strains appears to be not feasible with an AMS instrument when electron impact ionization is applied. We present averaged results for $a = 0.01$, $a = 0.05$ and $a = 0.1$ because differences in the calculated agar contribution in this range were negligible (figure A.3).The presence of these two different components in the mixture is supported by principal component analysis (PCA) on size-resolved pToF mass spectra data. Using an eigenvalue (λ) criterion of $\lambda = 1$ we separated two components (figure A.4 and figure A.5). At low vacuum aerodynamic diameter ($200 - 300\,nm$) PCA scores in the biplot originate from the residual particles whereas at higher D_{va} ($1000 - 1600\,nm$) PCA scores originate from bacteria particles. Mass-to-charge ratios m/z 70, 110, 120 and 129 appear to be rather correlated with bacteria as confirmed by the size-selected UMR spectrum (figure 3.2c) whereas m/z 86 has contributions in both bacteria and residual particles (discussed below).

In addition to ME-2 calculations, f_{70} was used as a marker to calculate the agar mass fraction (m_{agar}) using equation 3.4. Since the particle signal at m/z 44 partially overlaps with gas phase CO_2 at low aerodynamic diameters around $100\,nm$ when using this particular high-pressure lens and since m/z 44 is also influenced by changes in neutral fragmentation processes when changing from 600 °C to 730 °C it has not been used as a marker in the calculations. Figure 3.3 summarizes the agar mass fraction and the fraction of bacteria fragments in the residual particle size mode for four experiments with *P. syringae* and *P. fluorescens* strains at vaporizer temperatures $T_{vap} = 600\,°C$ and $T_{vap} = 730\,°C$.

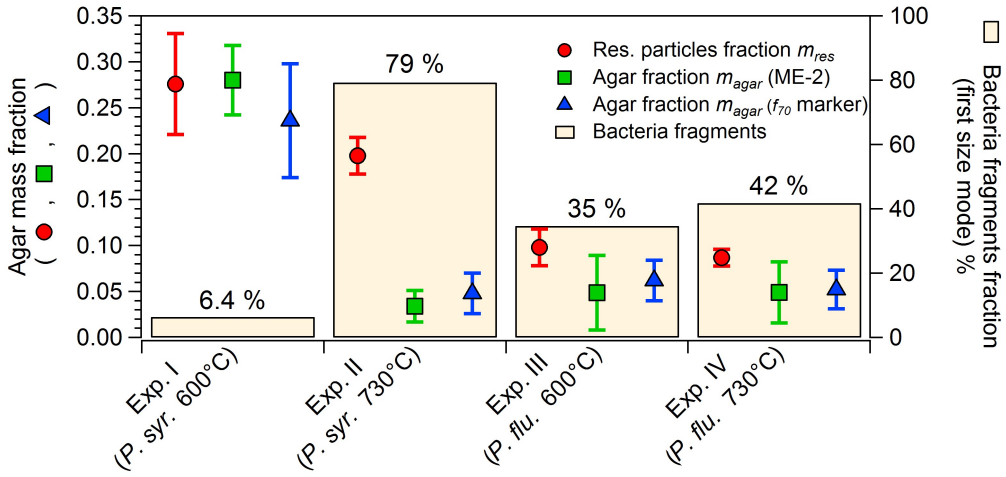

Figure 3.3.: Summary of the residual particle mass fraction (m_{res}) which does not take into account bacteria fragments and the agar mass fraction (m_{agar}, 3σ error bars) using both the ME-2 method and the f_{70} marker calculations. The mass fraction of bacteria fragments (see table A.1) in the first size mode is shown in orange. 10% uncertainty for absolute values of m_{res} at $T_{vap} = 730\,°C$ (more accurate size measurements) and 30% uncertainty at $T_{vap} = 600\,°C$ are assumed.

It can be concluded that a significant mass fraction of residual particles is present in the experiments, ranging between 5 and 25%. Differences between the fraction of residual particles (m_{res}) and the average agar mass fraction can be attributed to bacteria fragments (table A.1). Variations in the relative quantities of agar or bacteria fragments likely depend on the preparation procedure of the bacteria aerosol. Scraping of bacteria from the agar-containing petri dishes may yield different fractions of agar products in the resulting aerosol and shear forces on the bacteria cells during the nebulization process can cause rupture of the cell membrane creating smaller fragments (Peterson et al., 2012; Stewart et al., 1995). It can be speculated that the immersion of bacteria into distilled water may also lead to the burst of single cells due to hypo-osmotic shock (Booth and Louis, 1999).

3.3.2. Characterization of bacteria mass spectra

All high-resolution mass spectra of *Pseudomonas* bacteria obtained at a vaporizer temperature of 600 °C reveal a considerable abundance of nitrogen-containing ions (figure 3.4).

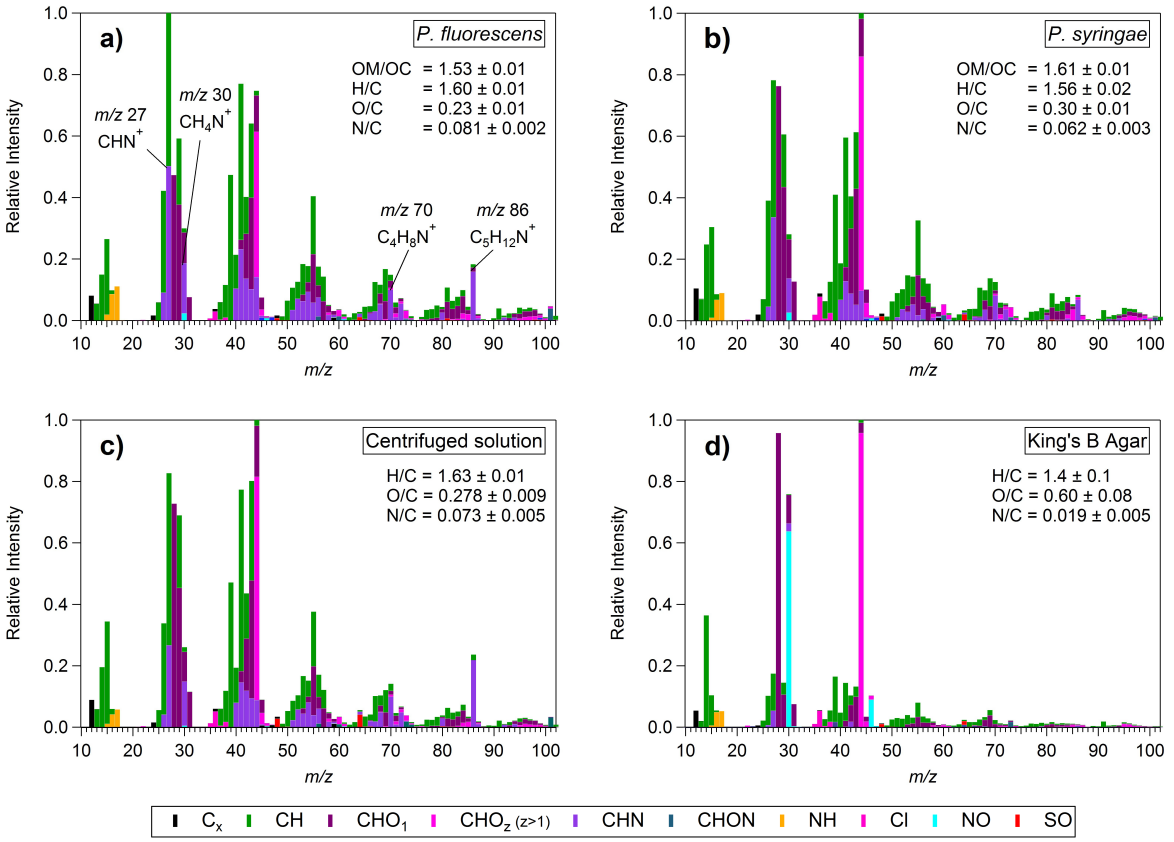

Figure 3.4.: High-resolution mass spectra of **a)** *Pseudomonas fluorescens*, **b)** *Pseudomonas syringae* and **c)** centrifuged *Pseudomonas fluorescens* dispersion at $T_{vap} = 600\,°C$. **d)** shows the high-resolution mass spectrum of the agar blank experiments at $T_{vap} = 600\,°C$.

Figure 3.5 provides the high-resolution peak fitting for the most important species. Particularly prominent ions are $C_4H_8N^+$ (m/z 70) and $C_5H_{12}N^+$ (m/z 86). These ions are the

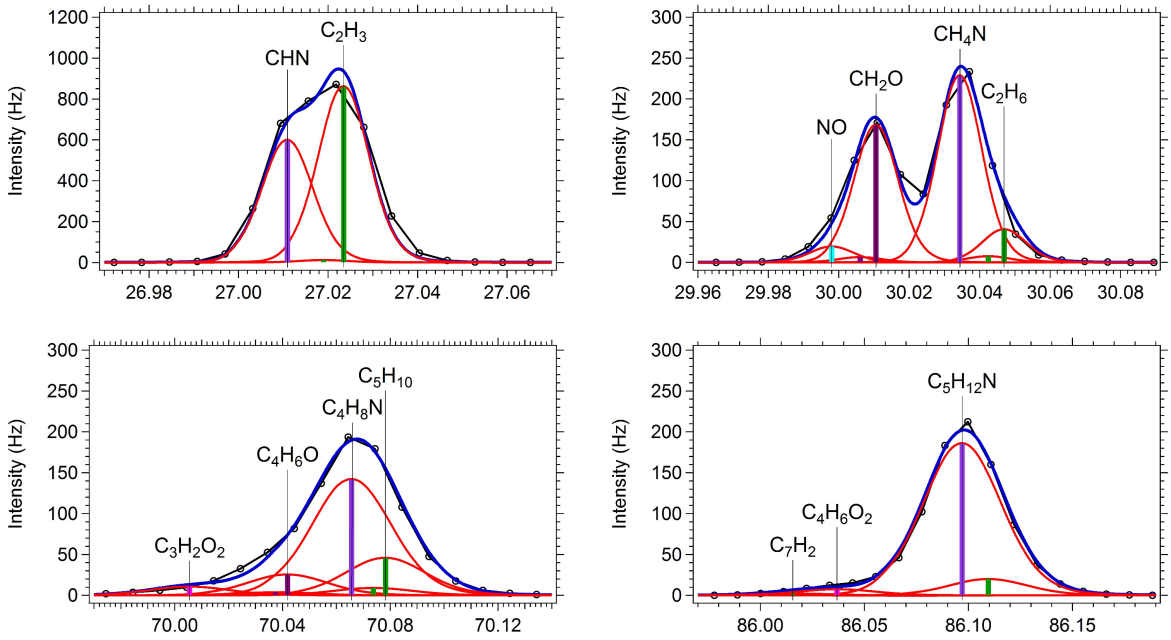

Figure 3.5.: Examples for the high-resolution peak fitting of m/z values with significant contribution from nitrogen-containing ions at low agar contribution ($\overline{m}_{agar} = 6\%$) for *P. fluorescens* (Exp. III) at $T_{vap} = 600\,°C$.

fragmentation products of the corresponding amino acids. Isoleucine and leucine directly decarboxylate into $C_5H_{12}N^+$ and decomposition pathways of asparagine, lysine, arginine and proline can yield the detected $C_4H_8N^+$ ion (Falick et al., 1993). Elevated signals at nominal masses 70 and 86 have also been reported in positive ion mass spectra of different bacteria species e.g. *Clostridium acetobulyticum* by Fergenson et al., 2004, vegetative cells of *Bacillus athrophaeous* by Czerwieniec et al., 2005 and *Enterobacter* by Gieray et al., 1997. AMS mass spectra of selected amino acids and proteins (Schneider et al., 2011) as well as mass spectra of ethyl ester amino acids (Biemann et al., 1961) also show distinct contributions by these N-containing ions. Possible interferences with triethylammonium salts and related species at m/z 86 may emerge in ambient aerosols (Murphy et al., 2007). Since amines and their oxidation products probably are prevailing at particle diameters below one micrometer in the atmosphere (Facchini et al., 2008), these species can be distinguished from bacteria by means of particle size data from the HR-ToF-AMS, for example by using a three dimensional source apportionment technique (Ulbrich et al., 2012).

As proteins and amino acids make up about 55% of the total bacteria dry mass (Watson et al., 2007) a combination of these two ions is suggested as potential marker ions for bacteria cells when using an AMS instrument with electron impact ionization. Signals at m/z 110, m/z 120 and m/z 129 (discussed above) are also characteristic for amino acids (Falick et al., 1993) and likely result from the decomposition of histidine (yielding $C_5H_7N_3^+$, m/z 110), phenanthroline (yielding $C_8H_{10}N^+$, m/z 120) and arginine, glutamine as well as lysine (ambiguous peak fit, m/z 129). Since these m/z have low signal-to-noise and cannot be fit unambiguously in the HR analysis of ambient data they are not recommended as markers. Variations in the high-

resolution mass spectra of *P. syringae* (Exp. I, $m_{agar} = 25 \pm 4\%$) and *P. fluorescens* (Exp. III, $m_{agar} = 6 \pm 3\%$) (figure 3.4a and figure 3.4b) are mainly a consequence of different agar mass concentrations. The agar mass spectrum (figure 3.4d) is dominated by oxygen-containing ions (O/C elemental ratio = 0.60 ± 0.08) and high m/z 44 caused by oxidized functional groups (Ng et al., 2010) of the agarobiose polymer fragments and its enzymatic digestion products (Wahl et al., 2010). Carbon-hydrogen-nitrogen (CHN) containing compounds in the agar blank aerosol are probably a result of the peptone constituent which has a total nitrogen content of about 12% (Conda, 2014). Furthermore, NO_2^+ and NO^+ ions appear to be typical features of the agar blank which have also been identified by aerosol time-of-flight mass spectrometer (ATOFMS) measurements using the same blank sample (B. Sierau, personal communication, 2012). The centrifuged solution is rich in nitrogen-containing compounds (N/C = 0.073 ± 0.005) (figure 3.4c) and the mass spectrum is generally similar to the bacteria mass spectra which supports the finding that this sample contained a significant fraction of bacteria fragments since the corresponding size distribution (figure A.1) rather resembles the residual particle mode at about 350 nm.

3.3.3. N/C and O/C elemental ratios

High-resolution aerosol mass spectrometer data can be used to retrieve the elemental ratio of non-refractory aerosol (Aiken et al., 2007). N/C and O/C elemental ratios for bacteria without agar influence were derived by extrapolating N/C and O/C ratios to zero agar mass fraction for four bacteria experiments and the agar blank experiment. High correlation (R^2 = 0.98) for N/C and (R^2 = 0.97) for O/C (figure 3.6) in a linear orthogonal regression indicates that elemental ratio variations are primarily explained by different agar mass fractions. Extrapolated values for an average agar mass fraction of zero ($\overline{m}_{agar} = 0$) are N/C = 0.086

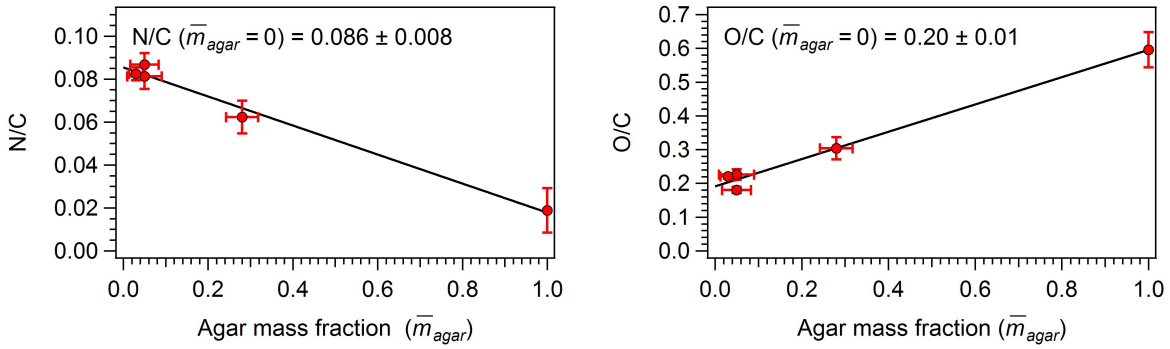

Figure 3.6.: N/C and O/C as a function of the average agar mass fraction ($\overline{m}_{agar}$) for different experiments with *P. fluorescens*, *P. syringae* and agar nutritive medium ($\overline{m}_{agar}$ = 1). $\overline{m}_{agar}$ is an arithmetic average of the ME-2 and the marker calculations. Linear extrapolation to an agar mass fraction of zero ($\overline{m}_{agar} = 0$) yields elemental ratios for the pure bacteria of N/C= 0.086 ± 0.008 and O/C= 0.20 ± 0.01. N/C and O/C ratios include 3σ error bars.

± 0.008 and O/C = 0.20 ± 0.01. This N/C ratio is at the lower end of reported values for *P. fluorescens* bacteria (8 to 13%) (Chrzanowski and Kyle, 1996). It should be noted that elemental ratios of bacteria in general can be highly variable depending on culturing and living

conditions (Vrede, 1998). Although evident in the high-resolution peak fits of the bacteria samples (figure 3.7), phosphorus was not fully quantified by the AMS since proper relative ionization efficiency estimations for the phosphorous species and parametrization with laboratory standards are currently lacking. In addition, fractions of f_{PO^+} and $f_{PO_2^+}$ (figure 3.8)

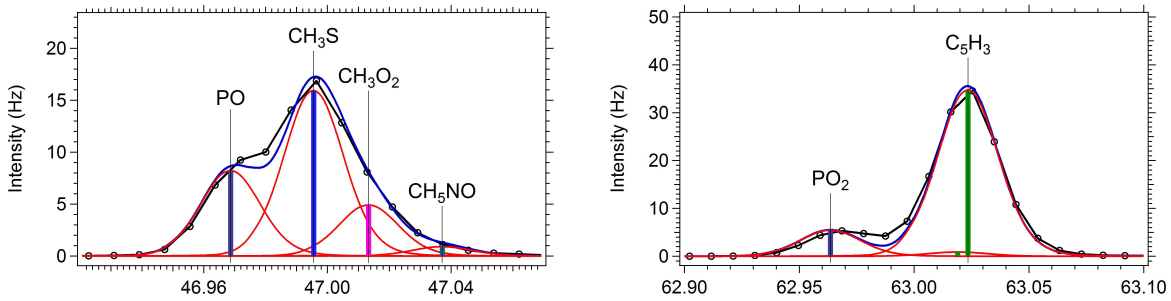

Figure 3.7.: Examples for the high-resolution peak fitting of m/z with significant contribution from phosphorous-containing ions at low agar contribution ($m_{agar} = 6\%$) for *P. fluorescens* (Exp. III) at $T_{vap} = 600\,°C$.

appear to be influenced by the AMS vaporizer temperature with higher f_{PO^+} and $f_{PO_2^+}$ at $T_{vap} = 730\,°C$. Similarly, potassium (K^+) ion signals were observed at m/z 39 and m/z 41. However, an accurate quantification of potassium is compromised as a consequence of lacking relative ionization efficiencies and more importantly due to competing electron ionization and surface ionization pathways. The fraction of the total potassium signal likely depends on the vaporizer temperature with highest values at 730 °C compared to the standard temperature of 600 °C (figure A.6). Furthermore, the sole use of potassium as a tracer for biological particles in ambient air may be limited by interferences with slowly evaporating potassium containing salts, e.g. from biomass burning emissions.

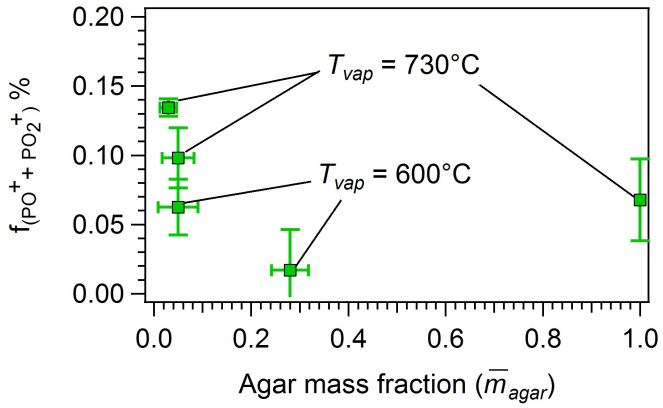

Figure 3.8.: Fraction of phosphorous-containing ions f_{PO^+} and $f_{PO_2^+}$ as function of the agar mass fraction ($\overline{m}_{agar}$) for different experiments with *P. fluorescens*, *P. syringae* and agar nutritive medium ($\overline{m}_{agar} = 0$).

To our knowledge, the estimated bacteria N/C and their mass spectral features do not resemble any of the reported organic mass spectra with elevated nitrogen content as measured by an AMS equipped with the standard inlet (Sun et al., 2011; Saarikoski et al., 2012; Docherty

et al., 2011; He et al., 2010; Aiken et al., 2009; Hayes et al., 2013). A comparison of a bacteria mass spectrum at low agar contribution (Exp. III) with other reported spectra from positive matrix factorization is given in table 3.2. It is evident that the bacteria mass spectra are

Table 3.2.: Similarity of the bacteria mass spectrum with factorized mass spectra of selected ambient studies in high-resolution (HR) and unit mass resolution (UMR).

Bacteria HR mass spectrum (Exp. III, $T_{vap} = 600\,°C$) *versus*	**R^2 (HR) m/z 20 − 100**	**R^2 (UMR) summed from HR**
COA[a], Paris (Crippa et al., 2013c)	0.675	0.787
HOA[b], Barcelona (Mohr et al., 2012)	0.374	0.529
BBOA[c], Barcelona (Mohr et al., 2012)	0.704	0.834
SVOOA[d], Paris (Crippa et al., 2013c)	0.740	0.857

Bacteria UMR mass spectrum (Exp. III, $T_{vap} = 600\,°C$) *versus*	**R^2 (UMR)**
COA[a], Paris (Crippa et al., 2013b)	0.841
HOA[b], Paris (Crippa et al., 2013b)	0.681
BBOA[c], Paris (Crippa et al., 2013b)	0.879
SVOOA[d], Los Angeles (Hersey et al., 2011)	0.797

[a] Cooking organic aerosol, [b] Hydrocarbon-like organic aerosol, [c] Biomass burning organic aerosol, [d] Semi-volatile organic aerosol

distinguishable from other factorized components of primary and secondary organic aerosol. Consequently, the total bacterial mass spectra could be used as input in a positive matrix factorization (PMF/ME-2) source apportionment approach for ambient, high-resolution AMS data sets to differentiate bacteria from other aerosol components. In these techniques, compositional discrepancies between bacteria mass spectra in the laboratory and in ambient are taken into account by predefined limits in which they can vary (Canonaco et al., 2013).

Fungal spores might show mass spectra that contain ions typical for amino acids and proteins as well. Sugar alcohols such as mannitol that are abundant in spores (Bauer et al., 2008) yield significantly elevated signals at m/z 60, m/z 61 and m/z 73 (Schneider et al., 2011). However, the corresponding carbon-hydrogen-oxygen (CHO) containing ions at these m/z have only marginal signals in the mass spectra of the investigated bacteria. Moreover, considering the average diameters of fungal spores ($\approx 2 - 10\,\mu m$, Glikson et al., 1995) or those of other bioaerosols such as pollen ($\approx 10 - 100\,\mu m$, Reponen et al., 2001), we expect that they can be distinguished from single bacterial cells ($\approx 1\,\mu m$) when using a $PM_{2.5}$ inlet. The identified

potential marker ions together with the typical diameter of the bacteria particles could help to validate the results of the PMF/ME-2 technique when using a high-resolution AMS instrument for single-particle measurements with an integrated light-scattering single-particle module (Cross et al., 2009).

3.4. Conclusions

We have investigated the chemical composition and the size of bacteria cells in the aerosol phase using an HR-ToF-AMS equipped with a $PM_{2.5}$ inlet. The measurements indicate that the AMS, which is an established and wide-spread instrument for on-line measurements of non-refractory aerosol, is capable of detecting airborne bacteria. Aerosolized water suspensions of cultured cells showed a bacteria size mode at a vacuum aerodynamic diameter of about $0.9\,\mu m$. Mass spectra of selected *Pseudomonas* bacteria contain a wide range of nitrogen-containing ions of which $C_4H_8N^+$ (m/z 70) and $C_5H_{12}N^+$ (m/z 86) are particularly prominent. These identified ions may serve as potential markers for a real-time, reagentless quantification of airborne bacteria in general when the AMS is operated in single particle mode. The mass spectra as described here could be applied to high-resolution AMS datasets, especially for instruments equipped with a $PM_{2.5}$ lens, using positive matrix factorization to distinguish bacteria from other constituents of ambient aerosol. With this statistical method the detection limit for bacteria would depend on the temporal variation of the bacteria mass concentration and the dissimilarity between bacteria mass spectra and those of other aerosol components. However, a differentiation between various bacteria strains does not seem to be feasible if electron impact ionization is employed.

Acknowledgement

The authors would like to thank the excellent laboratory support of the KIT AIDA chamber facility as well as Pierre Amato and Muriel Mourguy for preparing the bacteria cell samples. Support by Thomas Schwartz from the KIT Institute of Functional Interfaces (IFG) in preparing the bacteria cultures is gratefully acknowledged. We also thank Aerodyne Research especially Leah Williams for providing the 2nd generation prototype of the $PM_{2.5}$ lens. We acknowledge the support of Francesco Canonaco for assistance in the analysis with the SoFi ME-2 toolkit. We acknowledge funding from the joint DFG-CNRS project BIOCLOUDS for C. S. and O. M. (under MO 668/2-1) and the EU FP7 program EUROCHAMP2. J. G. S. acknowledges support from the Swiss National Science Foundation (SNF) through the AMBIZIONE program.

4

Contribution of bacteria-like particles to $PM_{2.5}$ aerosol in urban and rural environments

R. Wolf[1], I. El Haddad[1], J. G. Slowik[1], K.R. Dällenbach[1], E. Bruns[1], U. Baltensperger[1] and A.S.H. Prévôt[1]

[1] *Laboratory of Atmospheric Chemistry, Paul Scherrer Institute, 5232, Villigen PSI, Switzerland*

In preparation for Atmospheric Environment

Abstract

We report time-resolved estimates of airborne bacteria concentrations in ambient aerosol using an Aerodyne aerosol mass spectrometer (AMS). AMS measurements with a newly developed $PM_{2.5}$ and the standard PM_1 inlet were performed at an urban background site (Zurich) and at a rural site (Payerne). Positive matrix factorization modeling calculations using the multilinear engine (ME-2) implementation were conducted to estimate the contribution of bacteria-like particles as a component of non-refractory organic aerosol. The success of the method was evaluated by a size-resolved analysis of the organic mass and the analysis of single particle mass spectra which were detected with a light scattering system integrated into the AMS. At each measurement site, the bacteria-like component resulting from the ME-2 technique indicates that airborne bacteria likely constitute a minor fraction of non-refractory organic aerosol mass when sampled with a $PM_{2.5}$ inlet. Estimated average mass concentrations were lower than $0.1\,\mu g\,m^{-3}$ and relative contributions were lower than 2% at both sites. During rainfall, concentrations of the bacteria-like component increased considerably reaching a short-time maximum of approximately $2\,\mu g\,m^{-3}$ at the Payerne site in summer 2012.

4.1. Introduction

Bioaerosols are typically defined as suspensions of airborne particles that contain living organisms or were released from living organisms (Cox and Wathes, 1995). Primary biological aerosol particles (PBAP) comprise various species such as viruses, bacteria, fungal spores, pollen as well as fragments of lichen, skin, algae, plant debris or fur fibers. PBAP span a wide range of aerodynamic diameters (D_a) from viruses being the smallest ($D_a \approx 20 - 300\,nm$) to pollen which, among other species, can have diameters up to $100\,\mu m$. Other frequently investigated classes of bioaerosols are bacteria having typical D_a of about $1-3\,\mu m$ and fungal spores ($D_a \approx 1.5 - 30\,\mu m$) (Grinshpun, 2010).

Particles of biological origin are still poorly quantified regarding their contribution to the global aerosol burden (Spracklen and Heald, 2014) as a consequence of a limited number of available measurement data and a lack of standardization between the quantification techniques (Kuske, 2006; Peccia and Hernandez, 2006). Recent estimations of the global annual PBAP emission vary substantially between 50 to 1000 Tg/year (Stocker et al., 2014). Thus, PBAP appear to be significant contributors to the global aerosol mass in comparison, for example, to an upper estimate for the production of secondary organic aerosol (SOA) of $140 - 910\ TgC$/year (Goldstein and Galbally, 2007; Hallquist et al., 2009) or the estimated production of SOA from biogenic volatile organic compounds ranging from 20 to 380 Tg/year (Stocker et al., 2014). Global emissions of fungal spores are estimated from 8 to 186 Tg/year (Spracklen and Heald, 2014). Bacteria emissions are even less constrained and cover two orders of magnitude from 0.4 to 41.4 Tg/year (Burrows et al., 2009; Jacobson and Streets, 2009). Relative PBAP contributions greater than 10% have been reported using various analytical techniques in the last decades. Table 4.1 presents a selected literature review on the estimated concentrations of both PBAP and airborne bacteria. For a more complete literature synthesis on PBAP and airborne bacteria, the reader may refer to Després et al., 2012 and Spracklen and Heald, 2014.

A rapid detection of bacteria is of special interest for civil protection (Demirev and Fenselau, 2008) because individual strains such as *Bacillus anthracis* can be highly hazardous for humans (Meselson et al., 1994). Furthermore, bacteria can act as cloud condensation nuclei (CCN) (Möhler et al., 2007) and particular strains are among the most efficient ice-nucleating particles known so far (Möhler et al., 2008b). It has been hypothesized that bacteria in addition to other biological aerosol particles might influence atmospheric ice nucleation (Christner et al., 2008) and local hydrological cycles especially in pristine areas such as the Amazonian rainforest (Pöschl et al., 2010; Phillips et al., 2009; Pöhlker et al., 2012). Modeling studies have shown a change in reflection of shortwave radiation of clouds by up to 14% and altered cloud lifetime with the inclusion of bacteria as ice-nucleating particles in the modeled domain (Costa et al., 2014). However, other studies reveal a minor impact on global precipitation patterns and cloud formation under recently estimated microbial concentrations (Hoose et al., 2010; Sesartic et al., 2012).

Table 4.1.: Summary of selected studies with significant ($>$ 10%) PBAP and bacteria concentrations.

Contribution	**Site**	**Method**	**Reference**
PBAP			
$5-55\%$ (number) diameter $> 0.2\,\mu m$	Mainz, Germany (urban)	protein staining	Jaenicke (2005)
$4-11\%$ (mass) in $PM_{2.5}$	Toronto, Canada (urban)	liquid chromatography/mass spectrometry	Womiloju et al. (2003)
33% (number) of ice residuals	Wyoming, US (altitude: $\approx 8\,km$)	aerosol time-of-flight mass spectrometer (ATOFMS)	Pratt et al. (2009)
up to 20% (mass) in PM_1	Amazonian rainforest	aerosol mass spectrometry (AMS)	Schneider et al. (2011)
Bacteria			
20% (number) diameter: $0.25-1\,\mu m$	Caribbean Sea (altitude: $8-15\,km$)	quantitative polymerase chain reaction (qPCR)	DeLeon-Rodriguez et al. (2013)
$10^5-10^6\,cm^{-3}$	Colorado, USA (different land types)	qPCR	Bowers et al. (2011)

Few methods facilitate a selective determination of the total bacteria number concentration in ambient air among other constituents of primary biological aerosol. An elaborate method is the deposition on aerosol filters and the subsequent counting of selectively stained cells under the light or fluorescence microscope. The analysis of smaller or fragmented cells can be carried out by a scanning-electron-microscope (SEM) equipped with an energy dispersive X-ray spectrometer (EDX) (Matthias-Maser et al., 1997). Uncertainties related to this method arise from the selectivity of the staining and the ambiguity of the manual classification of the microorganisms under the microscope. The quantitative polymerase chain reaction method, which recently finds increasing use in the field of aerosol science, is capable of both quantifying and identifying broad microbial populations. Nevertheless, method detection limits of about 2000 bacterial cells, e.g. for a *Bacillus atropheus* test organism (Hospodsky et al., 2010) are significantly higher than for microscopic analysis techniques. Current laser-based, real-time mass spectrometric methods may allow for a distinction of different bacterial strains at concentrations higher than 10^4 cells per liter of air in the laboratory. However, mass spectral patterns are affected by changes in laser power during the vaporization/ionization process (Steele et al., 2003). They also depend on the culturing conditions of the microorganisms and can change with atmospheric processing of the particles. Schneider et al., 2011 estimated the contribution of bioaerosols in the Amazonian rain forest using an Aerodyne high-resolution time-of-flight aerosol mass spectrometer (HR-ToF-AMS) (Jayne et al., 2000; DeCarlo et al., 2006) which uses thermal vaporization and electron impact ionization in combination with a new aerodynamic lens prototype for the detection of super-micron aerosol. Their method is based on a bottom-up scaling of single markers obtained from a calibration with amino acids, proteins and carbohydrates. Since these single markers are not very specific for bioaerosols, this approach likely is not applicable to non-pristine regions where interferences with other compounds can not be excluded.

In this study, we employed an Aerodyne HR-ToF-AMS equipped with a newly developed aerodynamic lens (second generation) for the detection of aerosol particles with aerodynamic diameters up to about $3\,\mu m$ (Williams et al., 2013). The estimated contribution of bacteria to non-refractory organic aerosol was determined by constraining an anchor profile that represents bacteria-like particles using the multilinear engine (ME-2) algorithm (Paatero, 1999). Therefore, the presented methodology employs the mass spectral information as identified in pure bacteria from previous laboratory experiments (Wolf et al., 2015). A first validation of this method by an analysis of marker size distributions and single particle mass spectra is presented.

4.2. Methods

4.2.1. Sampling sites

Stationary measurements were performed at Zurich Kaserne (Switzerland) in April 2011 and in Payerne (Switzerland) from June to August 2012. Zurich Kaserne is an urban background site (N 47°22'39.295", E 8°31'49.648") hosted by the Swiss NABEL ("Nationales Beobachtungsnetz für Luftfremdstoffe") network. The instruments were located in a dedicated, air-conditioned trailer in which a constant air temperature of about 20 °C was maintained. The same trailer was deployed at the rural measurement site in Payerne (N 46°48'46.829", E 6°56'40.167") in close vicinity both to the local Meteoswiss and the local NABEL site.

4.2.2. Instrumentation

An Aerodyne high-resolution time-of-flight aerosol mass spectrometer equipped with a novel $PM_{2.5}$ inlet was deployed at each site. During the measurements in Zurich, a second HR-ToF-AMS instrument equipped with a standard PM_1 inlet was used on the same sampling line for comparison. In Payerne, the $PM_{2.5}$-HR-ToF-AMS was additionally equipped with a light scattering module for an accurate detection of single particles diameters and their corresponding mass spectra (Cross et al., 2009, 2007). The AMS sampling modes were alternated between mass spectrum (MS) mode in V-mode configuration (30 s), particle time-of-flight mode (pToF, 30 s) and light scattering single particle mode (LSSP, 30 s). V-mode and pToF mode data were analyzed using the Squirrel (v1.52F) and PiKa (v1.11G) programming codes within the IGOR Pro software (Wavemetrics, Inc., USA). LSSP mode data was analyzed with an own version adapted from the Sparrow package v1.04D. A composition-dependent collection efficiency as parametrized by Middlebrook et al., 2012 was applied.

4.2.3. Quantification of the bacteria component

Three independent analysis strategies using the AMS were employed: (1) factor analysis of the ensemble mass spectral data, (2) size distribution analysis of the tracer at mass-to-charge ratio (m/z) 70 and (3) the classification of size-resolved single particle mass spectra. The validation of the analysis relies on the agreement between these three methods. Limitations of the single methods are described in the dedicated sections. Results are presented sequentially for measurements in Zurich and in Payerne.

Positive matrix factorization (PMF) and multilinear engine (ME-2)

Positive matrix factorization (PMF) is a factor analytical technique used in receptor modeling that allows for the deconvolution of bulk aerosol composition data into a selected number of factors (Paatero and Tapper, 1994). These factors can be ascribed to sources or components of organic aerosol without any information about the source composition. This technique has become a standard in the source apportionment of aerosol mass spectrometer data with a maximum temporal resolution down to about one minute (Zhang et al., 2011; Viana et al.,

2008; Crippa et al., 2014). It is commonly applied to two-dimensional data consisting of time-dependent mass-to-charge ratios as provided by the mass spectrometer. The bilinear (two-dimensional) PMF model is based on the following equation:

$$x_{ij} = \sum_{k=1}^{p} g_{ik} f_{kj} + e_{ij} \tag{4.1}$$

in which x_{ij} is an element of the matrix of measured ion mass-to-charge ratios (index i) as a function of time (index j). f and g are the matrices of the identified factors and their contributions, respectively. e_{ij} denotes an element of the matrix of residuals. The PMF model solves equation 4.1 by minimizing the objective function Q which is expressed as:

$$Q = \sum_{i=1}^{m} \sum_{j=1}^{n} \left(\frac{x_{ij} - g_{ik} f_{kj}}{\sigma_{ij}} \right)^2 \tag{4.2}$$

The multilinear engine (ME-2) is an implementation of the PMF algorithm in which known information about the aerosol component composition can be used as an *a priori* input in the calculations. This facilitates the identification of sources which have a minor contribution to the organic aerosol mass because major aerosol sources tend to split in artificial components at a higher number of factors in PMF calculations.

The quantification of airborne bacteria was conducted with a commonly-used source apportionment methodology presented as follows:

1. Positive matrix factorization calculations were performed using the SoFi (Source Finder, v4.6) software package (Canonaco et al., 2013) as a user front-end for the preparation of the calculation input, the analysis and the visualization of the results. Solutions from two to eight factors were investigated to choose the optimal representation of aerosol components using established evaluation criteria such as characteristic factor mass spectra, diurnal cycles and the correlation with particulate nitrate and sulfate (Lanz et al., 2007; Crippa et al., 2014).

2. In the next step, one factor profile representing bacteria that has been identified in previous laboratory experiments (Wolf et al., 2015) was constrained. The selected mass spectrum of *Pseudomonas* bacteria cells was chosen from an experiment with negligible contamination ($< 5\,\mathrm{mass\,\%}$) from agar nutritive medium which was used to cultivate the bacteria. Survival rate tests during the experiment provide evidence that about 50% of the bacteria were viable one hour after injection into the chamber (P. Amato, unpublished data). Since precedent experiments with non-viable bacteria cells from Snomax® powder showed very similar mass spectra (J. Schneider, unpublished data) we assume that this anchor mass spectrum may serve as a proxy for a larger ensemble of viable and non-viable bacteria species. To account for differences in bacterial cell composition in ambient, the so-called a-value approach was applied which allows the input mas spectrum to vary within predefined limits. For a detailed explanation of the a-value approach the reader is referred to Canonaco et al., 2013; Lanz et al., 2008 and Paatero, 1999. A sensitivity test on the parameter a ranging from a very tight constraint ($a = 0.0001$) to a loose constraint ($a = 0.4$) was conducted. Each calculation at a given a-value was repeated at five different pseudo random starting points of the least-squares minimization algorithm to explore potentially different local minimums in the solution space.

The relative mass fraction of airborne bacteria is expected to be low compared to other components of non-refractory particulate matter. In order to test whether the relative fraction of the bacteria component is limited by the factor analytical method, an artificial factor profile was constrained. Additional calculations using this artificial profile were performed for the same a-values as used for the bacteria input mass spectrum. The artificial factor profile was generated from the bacteria input mass spectrum in which the signal intensity at nominal masses m/z 70 and m/z 86, which are typical for bacteria, were multiplied by a factor of 10. The two resulting signal intensities were added to ions that are the nearest neighbors of the mass-to-charge ratios of the potential nitrogen marker ions, i.e. $C_4H_6O^+$ at m/z 70 and $C_5H_{10}O^+$ at m/z 86. This procedure was chosen because the relevant nitrogen marker ions at these two mass-to-charge ratios could not be fitted unambiguously in the ambient data set and thus could be constrained in the bacteria anchor profile. As the generated artificial profile does not resemble any reported component of ambient aerosol, a very low contribution from this factor is expected. Therefore, the mass fraction of this artificial factor may serve as an estimation of the ME-2 method detection limit in a first approximation. Figure B.2 shows that the relative fraction of such an artificial factor is well below ($\approx 14\%$) the relative fraction of the calculated bacteria factor in the a-value range from 0.01 to 0.2. It can be concluded that the calculated mass fraction of bacteria-like particles is not limited by the method detection limit for this data set.

The AMS detection limit for bacteria-like particles was estimated using three times the standard deviation of the entire group of carbon, hydrogen and nitrogen-containing ($C_xH_yN_1$) ions during time periods in which aerosol particles were removed from the sampled air using an aerosol filter (HEPA) in front of the inlet. This estimation based on the family of nitrogen-containing ions was chosen since these ions are particularly abundant in bacteria mass spectra. The calculated detection limit of $0.024\,\mu g\,m^{-3}$ for the $PM_{2.5}$ inlet is comparable to other reported limits for the detection for organics ($0.022\,\mu g\,m^{-3}$) for the HR-ToF-AMS with an averaging time of one minute in V-mode (Fröhlich et al., 2013).

Not all ions that were identified in mass spectra of pure *Pseudomonas* bacteria cells can be fitted unambiguously in the ambient data set. Since this concerns also several of nitrogen-containing ions of low intensity, e.g. the tracer ion at m/z 70, the bacteria component anchor profile has a decreased specificity. For this reason and because compositional-differences in the solution mass spectrum are allowed when using the a-value approach, the factor representing bacteria is also referred to as "bacteria-like".

Size-resolved marker analysis

Size distributions of the organic mass fragment $f_{70} = Org_{70}/Org$ and the organic signal Org_{70} at m/z 70 were analyzed. This fragment has been proposed as a potential bacteria marker because of a significant contribution from decarboxylation products of amino acids to the $C_4H_8N^+$ ion (Wolf et al., 2015). It can be assumed that this fragment shows a higher contribution at larger diameters as single bacteria cells have typical aerodynamic diameters of about one micrometer. Among other sources, traffic emissions may also contribute to the f_{70} fragment as factorized mass spectra and laboratory studies suggest (Lanz et al., 2007; Canagaratna et al., 2004). It should be noted that interferences by other sources of biogenic material can not be excluded as the signal at m/z 70 can result from the decomposition

of protein- or amino acid-containing matter in general. Furthermore, the analysis of size distribution data may suffer from a slow evaporation of organic matter on the heated surface of the tungsten vaporizer in the AMS. This may artificially increase the apparent organic signal at larger aerodynamic diameter for aerosol components with high boiling points or for particles with high masses.

Single particle analysis

Single particle measurements were used to screen for particles which have a similar contribution of the characteristic f_{70} fragment in their single particle mass spectra. Particles were classified as bacteria-like when the following three conditions were satisfied. (1) The total organic signal must be greater than $300\,Hz$ to exclude interferences from instrument noise. (2) The characteristic fragment f_{70} must be greater than 0.01. This value is deduced from the f_{70} value that has been quantified in pure *Pseudomonas* bacteria ($f_{70} = 0.018$) (Wolf et al., 2015). In ambient air, bacteria cells may be fractured, partially decomposed or attached to other particles. To account for such differences in bacteria cell composition of the unit resolution mass spectrum, a lower value of 0.01 was chosen. (3) The fragment f_{57} has to be smaller than 0.02 to avoid interferences with hydrocarbon-like particles. A sensitivity analysis on these two parameters is provided in figure B.9. It can be concluded that changes in the selection criteria (f_{57} and f_{70}) for bacteria-like particles have a minor impact on the number of particles classified as bacteria-like. Another characteristic fragment, f_{86}, which has been identified in pure bacteria particles was not included as a constraint since it can also be abundant in amines and their derivatives such as triethylammonium-containing particles (Murphy et al., 2007). The standard unit mass fragmentation table (Allan et al., 2003b) was applied to the mass spectrum. For this reason and as a consequence of the low number of signals in the single mass spectra, the assignment of the raw signals to the AMS species such as organics, nitrate or sulfate may be erroneous in a few cases. For example, the signal at m/z 30 might be rather related to the CH_4N^+ ion than to a inorganic nitrate fragment. The possibly erroneous assignment of the raw signals to the AMS species only has an implication for the displayed colors of the single particle mass spectra.

The number concentration $C_{number,\,BAC}$ of particles classified as bacteria-like was calculated following the recommendations by Freutel et al., 2013 using equation 4.3:

$$C_{number,\,BAC} = \frac{n(MS)_{BAC}}{Q \times t \times DC \times S_{eff} \times f(MS)_{BAC}} \tag{4.3}$$

in which $n(MS)_{BAC}$ represents the total number of bacteria-like mass spectra in the averaged time period, t is the averaging time ($3600\,s$), DC is the sampling duty cycle which is a combination of the chopper duty cycle and the fraction of the sampling time in LSSP mode (0.02×0.5). Q is the average sampling flow rate ($1.4\,cm^3\,s^{-1}$). The saving efficiency S_{eff} describes the fraction of particles that are both detected by the light scattering system and that are subsequently saved to the file. This value varies with the particle number concentration in the detectable size range. At the rural site in Payerne, the standard deviation of S_{eff} throughout the campaign is below 10% and thus an average value of 0.58 was applied. $f(MS)_{BAC}$ is the ratio between all particles that yield a mass spectrum and all particles that are detected by the light scattering system within the ensemble of particles classified as bacteria. Since this time-dependent ratio can not be retrieved directly, it can be approximated

by the ratio between the total number of mass spectra and the total number of light scattering counts. This approximation assumes a similar particle bouncing behavior at the vaporizer surface for bacteria-like particles with respect to all other particles. As particle losses between the detection by the laser beam and the mass spectrometer result from the asymmetry of the particle beam and the bouncing off at the vaporizer surface, $f(MS)_{BAC}$ is generally smaller than one. The campaign average has been estimated to be $f(MS)_{BAC} = 0.19 \pm 0.02$ which is close to a previously reported value of 0.22 for hydrocarbon-like particles (Freutel et al., 2013). The discrepancy between $f(MS)_{BAC}$ and a typical collection efficiency of 0.5 for AMS instruments results from a threshold of 300 ion counts per second that was set to distinguish real single particle mass spectra from instrument noise.

Number concentrations derived from light-scattering data were converted into mass concentrations using:

$$C_{mass,\,BAC} = \frac{\pi}{6} \times \rho_{eff} \times D_{va}^3 \times C_{number,\,BAC} \tag{4.4}$$

in which ρ_{eff} describes the effective particle density and D_{va} is the particle vacuum aerodynamic diameter as measured by the sizing laser of the light-scattering system. The method for the calculation of the particle aerodynamic diameter by the sizing laser was calibrated using aerosolized solutions of polystyrene latex particles of different diameters ($450\,nm$, $600\,nm$ and $1\,\mu m$) as well as $400\,nm$ (D_m) ammonium nitrate aerosol particles. In a first order approximation, a spherical particle shape and an average particle density of $\rho_{eff} = 1.4\,g\,cm^{-3}$ for all bacteria-like particles was applied. The particle density was calculated from the average bacteria ensemble mass spectrum with the following density increments (in $g\,cm^{-3}$): Org = 1.27, SO_4 = 1.78, NO_3 = 1.72, NH_4 = 1.75 and Chl = 1.4 (Duplissy et al., 2011). The assumed density is within the limit of reported values for microorganisms from $1.1-1.5\,g\,cm^{-3}$ (Bakken and Olsen, 1983).

4.3. Results and discussion

4.3.1. Zurich, Switzerland

During a time period of uninterrupted sampling from 07.04.2011 until 19.04.2011, the total non-refractory mass concentrations were on average 35.4% higher in the $PM_{2.5}$ size range than in PM_1 (figure B.1). The organic mass concentrations were increased by 30.4% whereas sulfate concentrations were comparable with marginally less sulfate in $PM_{2.5}$ (4.1%).

The unconstrained source apportionment using positive matrix factorization yielded four distinct components for the non-refractory organic mass fraction in both $PM_{2.5}$ and PM_1. The factors comprise hydrocarbon-like organic aerosol (HOA), cooking-influenced organic aerosol (COA) as well as semi-volatile and low volatility oxygenated organic aerosol (SVOOA, LVOOA) which is consistent with results from Canonaco et al. (in prep.) who identified the same factors with a co-located aerosol chemical speciation monitor (ACSM) in PM_1 at the Zurich Kaserne site. The inclusion of an additional bacteria factor profile with the ME-2 approach has a negligible ($< 2\%$) impact on the relative fractions of the remaining factors in comparison to the unconstrained PMF calculations. Therefore, only results from the ME-2 calculations with the constrained bacteria factor profile are presented. All calculation results

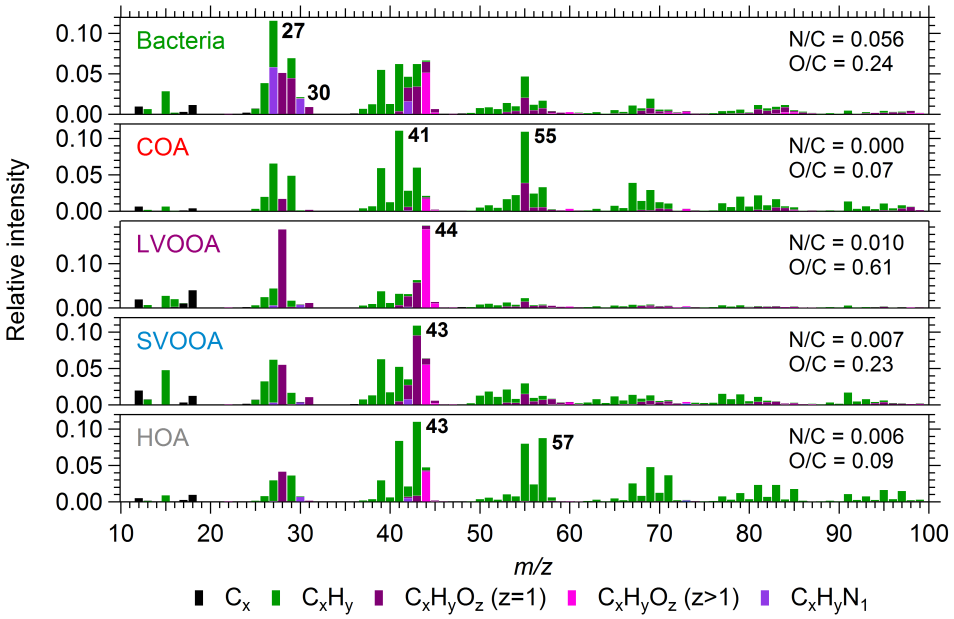

Figure 4.1.: Mass spectra of the identified factors in $PM_{2.5}$ at the Zurich Kaserne site from 07.04.2011 until 19.04.2011. The bacteria component was constrained by the a-value approach whereas the other components were unconstrained.

were averaged for four selected a-values: 0.01, 0.05, 0.1 and 0.2 because a parameter sensitivity test indicates only a minor variation (standard deviation, $\sigma < 9\%$) of the estimated bacteria fraction in this range (figure B.2). Lower a-values were not included in the average as different convergence criteria in the ME-2 calculations were used. At a-values above this range the constrained solution mass spectrum shows features of an HOA component.

Mass spectra of the aerosol components, their corresponding diurnal cycles and their time series are given in figure 4.1, figure 4.2 and figure B.3. The presented factors, except the bacteria component, were identified in various other studies. Therefore, only a brief description is given. The hydrocarbon-like organic aerosol (HOA) is dominated by signals characteristic for the decomposition of aliphatic compounds (C_xH_y) and shows a low oxygen-to-carbon elemental ratio (O/C = 0.09) (Docherty et al., 2011; Chirico et al., 2010). The diurnal behavior of this component is governed by the main traffic hours in Zurich at about 07:00−8:00 (local time) and 19:00−20:00. Compared to HOA, the cooking organic aerosol (COA) factor profile has higher signals at m/z 41, m/z 55 and a lower m/z 57 consistent with previous studies in the laboratory (He et al., 2010; Allan et al., 2010; Mohr et al., 2009; Sun et al., 2011) and in ambient air (Mohr et al., 2012; Sun et al., 2011). Highest contributions to organic aerosol appeared at usual meal time hours at noon (11:00−12:00) and in the evening (around 20:00). Low volatility and semi-volatile oxygenated organic aerosol components (SVOOA, LVOOA) have substantial (88% and 99%, respectively) contributions from the CO_2^+ ion at m/z 44 and the $C_2H_3O^+$ ion at m/z 43 which result from the decomposition of oxygenated species such as organic acids, for example (Ng et al., 2010; Duplissy et al., 2011). In general, LVOOA tends to have a higher CO_2^+ contribution and a higher oxygen-to-carbon ratio (O/C = 0.61 for LVOOA and O/C = 0.23 for SVOOA) than SVOOA indicating a less volatile and more oxygenated component (Jimenez et al., 2009). Oxygenated components dominated the

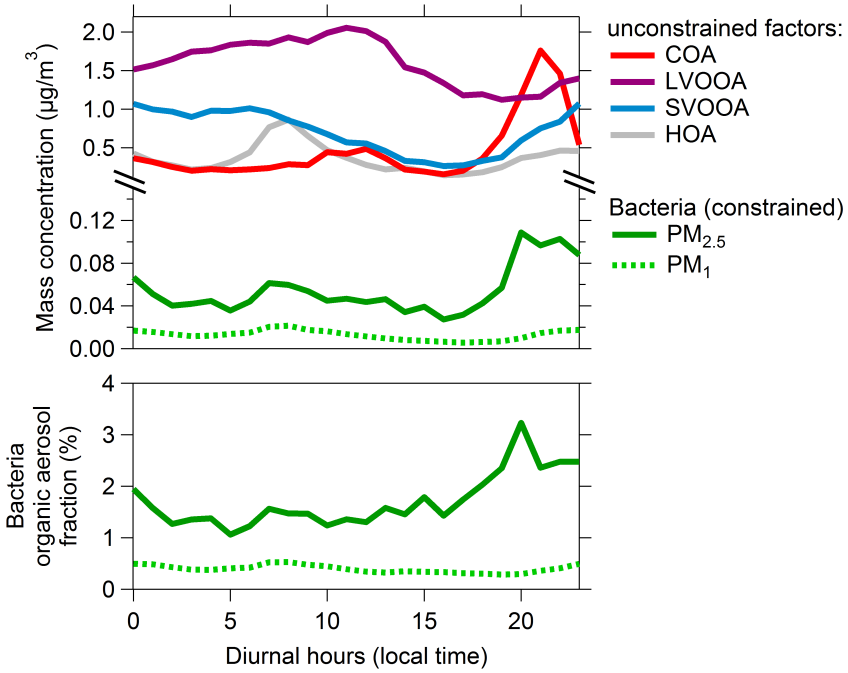

Figure 4.2.: Diurnal behavior of the identified factors in $PM_{2.5}$ at the Zurich Kaserne site from 07.04.2011 until 19.04.2011.

aerosol composition and comprised $\approx 71\%$ of the total non-refractory aerosol mass. A mass fraction of 15.1% in $PM_{2.5}$ and 12.3% in PM_1 is influenced by cooking processes. Perhaps, this remarkable fraction of COA is a consequence of the proximity (about $20\,m$) of the site to a nearby restaurant (figure 4.3). Comparable fractions of HOA and COA have also been

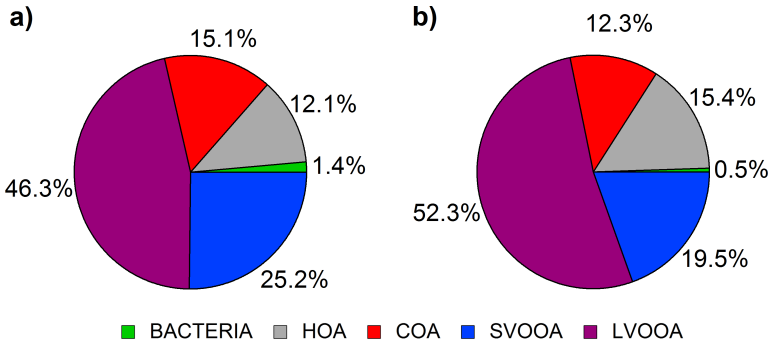

Figure 4.3.: Relative source contribution to non-refractory organic mass in **a)** $PM_{2.5}$ and **b)** PM_1 from 07.04.2011 until 19.04.2011.

quantified using an ACSM at the same site in winter 2011 (Canonaco et al., 2013). Slightly higher contributions from SVOOA in $PM_{2.5}$ are consistent with higher nitrate concentrations in this size range as the SVOOA component is typically correlated with particulate nitrate (Lanz et al., 2007). PToF mode data integrated over particle size revealed a nitrate fraction of the total non-refractory aerosol of 39.2% for particles sizes from $100\,nm$ to $2.5\,\mu m$ in contrast to 32.2% from $100\,nm$ to $1000\,nm$.

Bacteria component

The constrained bacteria organic aerosol factor ("Bacteria") displays characteristic signals that originate from the decomposition of reduced nitrogen-containing species ($C_xH_yN_1$ at m/z 27, m/z 30 and m/z 42) which are characteristic for bacteria mass spectra (Wolf et al., 2015). Since only selected nitrogen-containing signals that are present in the pure bacteria mass spectra can also be fitted unambiguously in the ambient data set, the nitrogen-to-carbon ratio (N/C = 0.056) of the bacteria factor is lower than the ratio determined in the laboratory (N/C = 0.086). The major part of the total AMS nitrogen mass is attributed to both SVOOA and LVOOA (together 77%) whereas 11% are attributed to the bacteria component.

In the time period from 07.04.2011 until 20.04.2011, the average organic mass fraction of airborne bacteria-like particles is higher in $PM_{2.5}$ (1.71%) than in PM_1 (0.52%) which is an expected consequence of a higher transmission efficiency for bacterial cells with aerodynamic diameters of around $1\,\mu m$ (Wolf et al., 2015). In the second part of the campaign ($21.04.2011 - 25.04.2011$), the two co-located HR-ToF-AMS were both operated with the standard PM_1 inlet. During this time period, the average bacteria contributions as measured by both instruments was 0.82% and 0.93%, respectively. A summary of the average and maximum bacteria concentrations and their corresponding organic mass fractions can be found in table B.1.

At the Zurich Kaserne site, averaged diurnal concentrations range between $0.03\,\mu g\,m^{-3}$ and $0.11\,\mu g\,m^{-3}$ in $PM_{2.5}$. These values are in the order of previously reported bacteria concentrations over land. For example, assuming a typical cell density of microorganisms of $1.3\,g\,cm^{-3}$ (Bakken and Olsen, 1983), a spherical particle shape and an average particle diameter of $1\,\mu m$ these mass concentrations correspond to number concentrations of about $0.44 - 1.5 \times 10^5\,\text{cells}\,m^{-3}$. Consequently, the estimated number concentrations for bacteria-like particles are within the wide range for observed surface-near bacteria concentrations ($1 \times 10^5 - 1 \times 10^6\,\text{cells}\,m^{-3}$) and modeled concentrations over most continental regions ($2.5 \times 10^4\,\text{cells}\,m^{-3}$) (Bowers et al., 2011; Spracklen and Heald, 2014).

During the measurements, the estimated concentration of bacteria-like particles did not correlate with relative humidity (linear correlation coefficient R=-0.01), temperature (R=-0.02) or rainfall (figure 4.4). Furthermore, there is no apparent dependency of the estimated bacteria concentration on the gusts of wind (R=-0.04) or the wind direction which could be related to a local source (figure B.5). Figure 4.2 displays a maximum of the mass concentration of bacteria-like particles in the evening and in the early morning hours. Such behavior provides further indication for the validity of the bacteria estimation with the ME-2 method since it is consistent with the diurnal trends for culturable bacteria that has been reported in several studies (Lighthart and Kirilenko, 1998; Tong, 1999; Lindemann and Upper, 1985). Following the argumentation of these studies, it can be hypothesized that a daily maximum for upward bacteria fluxes in rural areas is reached during the warmest hours of the day at noontime (Hirano and Upper, 2000) when plant leaves are dry and winds speeds exceed about $1\,m\,s^{-1}$ (Lindemann and Upper, 1985). The increase in concentration over night could be a combined effect of the transport of air masses with accumulated airborne bacteria levels from these rural source areas and the lower boundary layer height.

A size-resolved analysis of particle time-of-flight data shows that the organic signal at m/z 70 (Org_{70}) and the corresponding organic fraction f_{70} are elevated at aerodynamic diameters

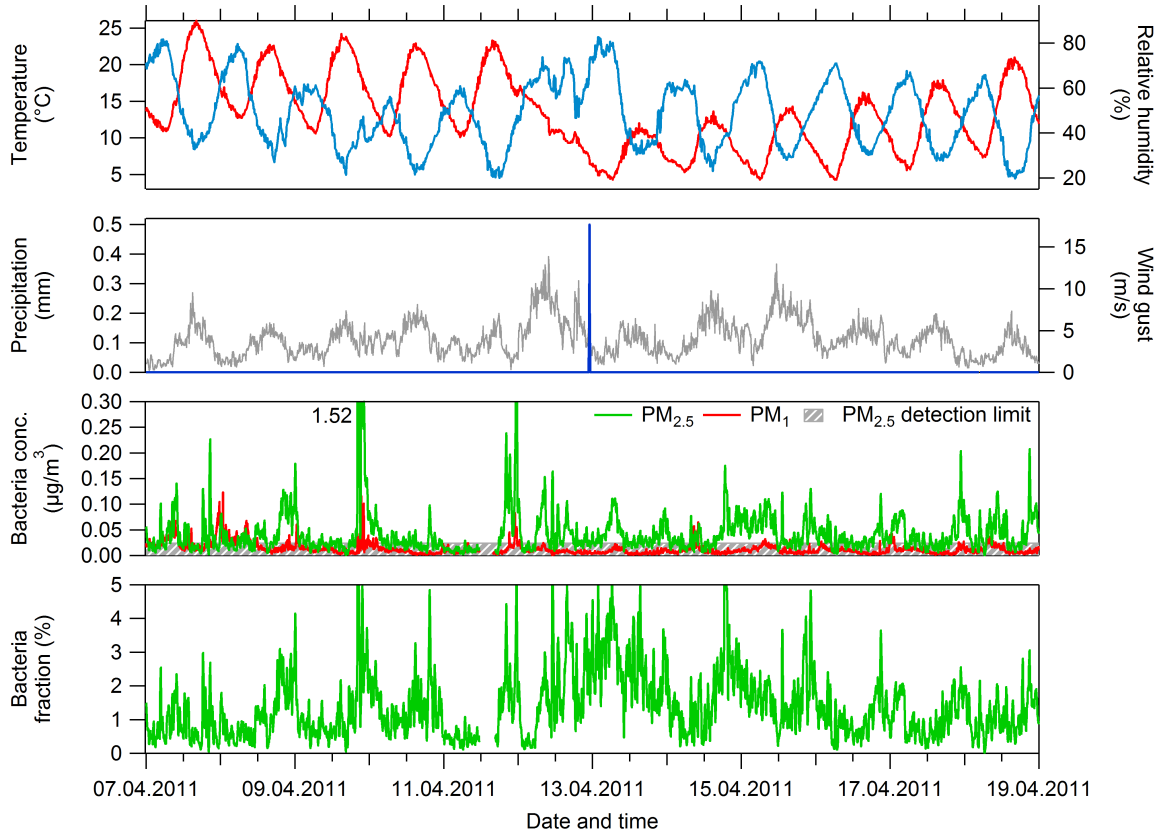

Figure 4.4.: Bacteria concentration time series and meteorological factors for the two co-located AMS with $PM_{2.5}$ and PM_1 inlet. A moving average ($20\,min$) boxcar smoothing for AMS data ($PM_{2.5}$ and PM_1) was applied.

larger than $800\,nm$ (figure B.4). This provides an indication for a possibly increased fraction of airborne bacteria in this particular size range (figure B.4). Higher values for f_{70} were observed at vacuum diameters smaller than $300\,nm$ which may be related to an increased fraction of hydrocarbon-like organic aerosol from traffic emissions because f_{70} is also abundant in the HOA mass spectrum.

4.3.2. Payerne, Switzerland

The methodology for the quantification of bacteria was further applied to a data set acquired in Payerne in summer 2012. Four factors could be distinguished: SVOOA, LVOOA, HOA and the bacteria component when constrained in a ME-2 approach. These aerosol components are similar to the factors as described by Lanz et al., 2010 who deployed a quadrupole-AMS at the same site in June 2006. In Payerne, concentrations of bacteria-like particles in $PM_{2.5}$ (campaign average: $0.11\,\mu g\,m^{-3}$) were higher than at the Zurich Kaserne site (campaign average: $0.06\,\mu g\,m^{-3}$). This is in accordance with findings of higher total bacteria concentrations in summer than in spring (Tong and Lighthart, 2000; Fang et al., 2007; Harrison et al., 2005). Additionally, a distinct correlation between the rainfall events and the estimated bacteria concentration as well as the bacteria marker in unit mass resolution at m/z 70 (f_{70}) was found

(figure 4.5, figure B.8 and figure B.7). The f_{70} marker size distribution shows a maximum around one micrometer in vacuum aerodynamic diameter. Figure B.6 gives further evidence for a release of bacteria cells during this time period. Compared to the total campaign aver-

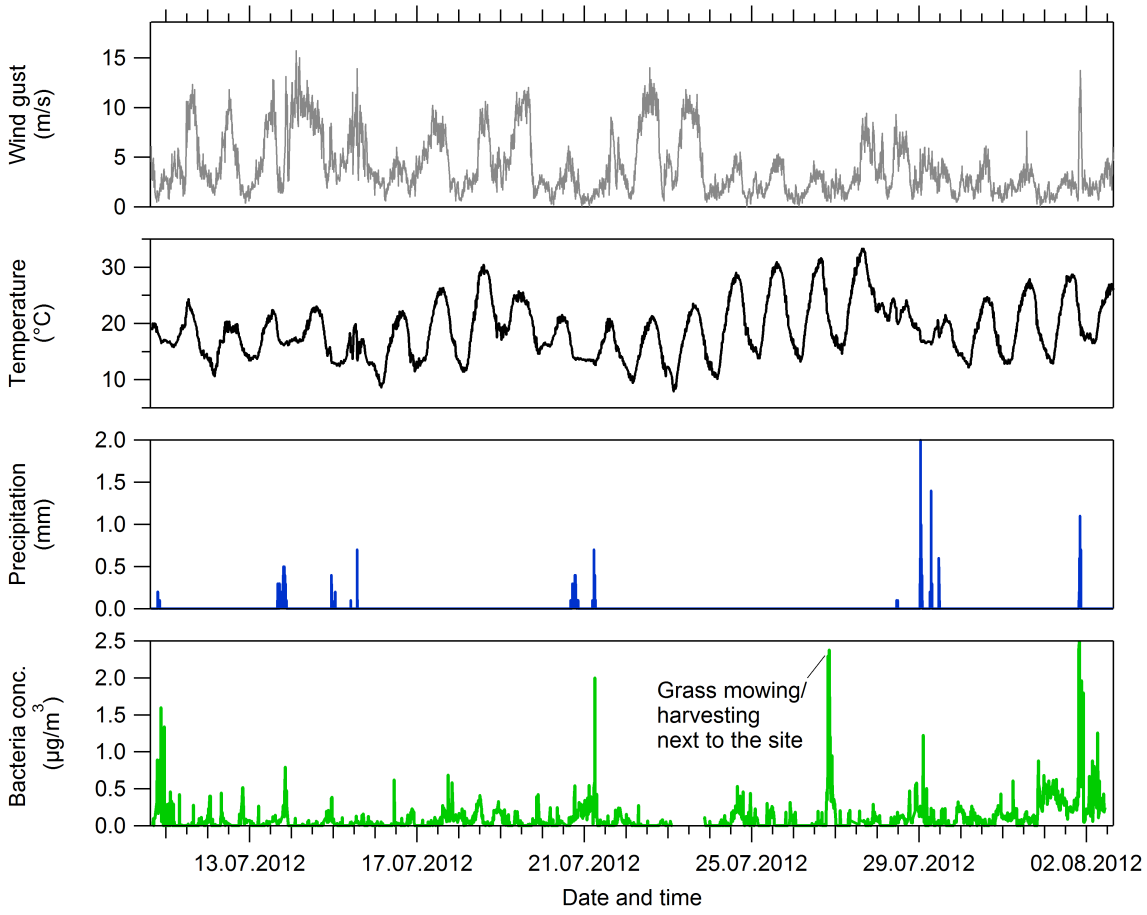

Figure 4.5.: Time series of the estimated bacteria concentration during measurements with a $PM_{2.5}$-HR-ToF-AMS in Payerne from 11.07.2012 until 02.08.2012. Time series of wind gust, temperature ($2\,m$ above ground) and precipitation are provided by the nearby NABEL measurement site.

age, bacteria concentrations were increased by about 24% including a time period of $30\,min$ after the precipitation. A similarly rapid dispersal of culturable airborne bacteria leading to an up to 25-fold increase in concentration has been described by Lindemann and Upper, 1985; Constantinidou et al., 1990; Graham et al., 1977; Huffman et al., 2013. Impacting rain drops on leaf surfaces as well as evaporating or fracturing rain drops may propel residing biological particles into the air and result in a sharp concentration increase during the rain (Butterworth and McCartney, 1991; Madden, 1997; Huber et al., 1998). No apparent correlation with ambient air temperature is observed near the precipitation events which evidences a negligible interference between the bacteria component and the SVOOA component which is anti-correlated with temperature. Another pronounced increase in concentration was observed in the evening on the 26.07.2012. This particular event may be related to the cutting of grass or harvesting directly around the measurement site as this was observed during instrument

maintenance the next day. The cutting of grass could have locally increased concentrations of airborne bacteria similarly to harvesting activities (Lighthart, 1984).

For a further validation of the ME-2 calculation results, a quantitative analysis of the single particle mass spectra as obtained in the LSSP-mode was conducted. The resulting average bacteria ensemble mass spectrum is shown in figure 4.6. The characteristic signals of the pure

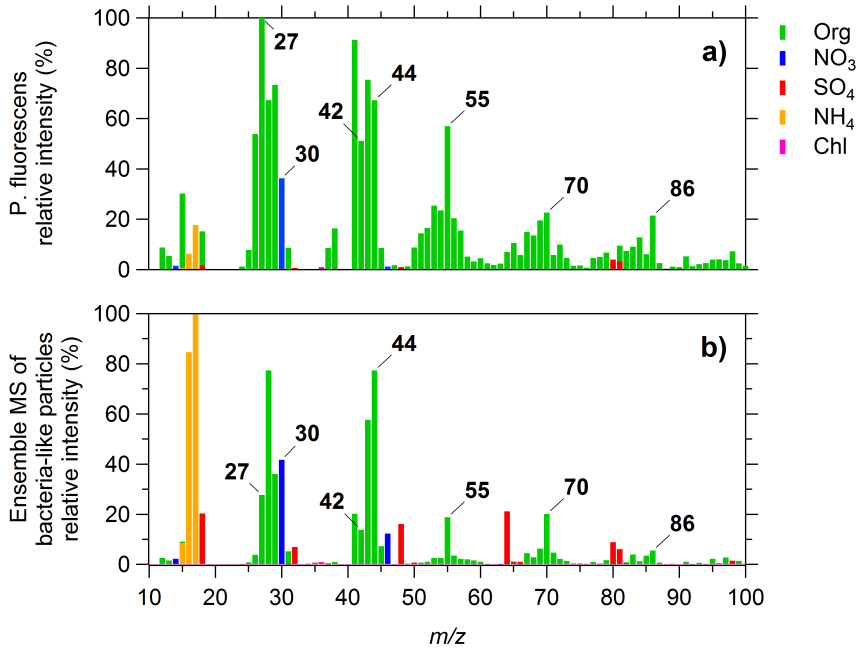

Figure 4.6.: **a)** Unit mass resolution mass spectrum of the pure *Pseudomonas fluorescens* bacteria from laboratory studies (Wolf et al., 2015) and **b)** average mass spectrum of all single particle mass spectra classified as bacteria-like from 12.07.12 until 02.08.12.

bacteria at m/z 27, m/z 30, m/z 42, m/z 70 and m/z 86 are retained in the average spectrum although only m/z 57 and m/z 70 were used as a constraint to classify the single particle mass spectra. A classification of cooking-like particles using single particle mass spectra was not performed as a specific marker m/z in unit mass resolution for COA is currently not available.

Diurnal variations for the ME-2 solution and the light scattering results are displayed in figure 4.7. Only diurnal trends of the single particle method are presented since the number of particles that are classified as bacteria-like is too low (several hundreds of particles per day) for a reasonable comparison with the bacteria component from the ME-2 method. The insufficient counting statistics do not allow for a comparison even for events with high bacteria concentrations derived from the ME-2 method. The mass concentrations (in $\mu g\, m^{-3}$) were converted from number concentrations using equation 4.4. Absolute mass and number concentrations (figure 4.7a) from the light-scattering data do not show a pronounced diurnal cycle whereas the ME-2 solution indicates a doubling of concentration during nighttime. Discrepancies between both estimates are likely within the measurement uncertainties of both techniques. Number concentrations determined by equation 4.3 range between 3.0×10^5 particles m^{-3} and

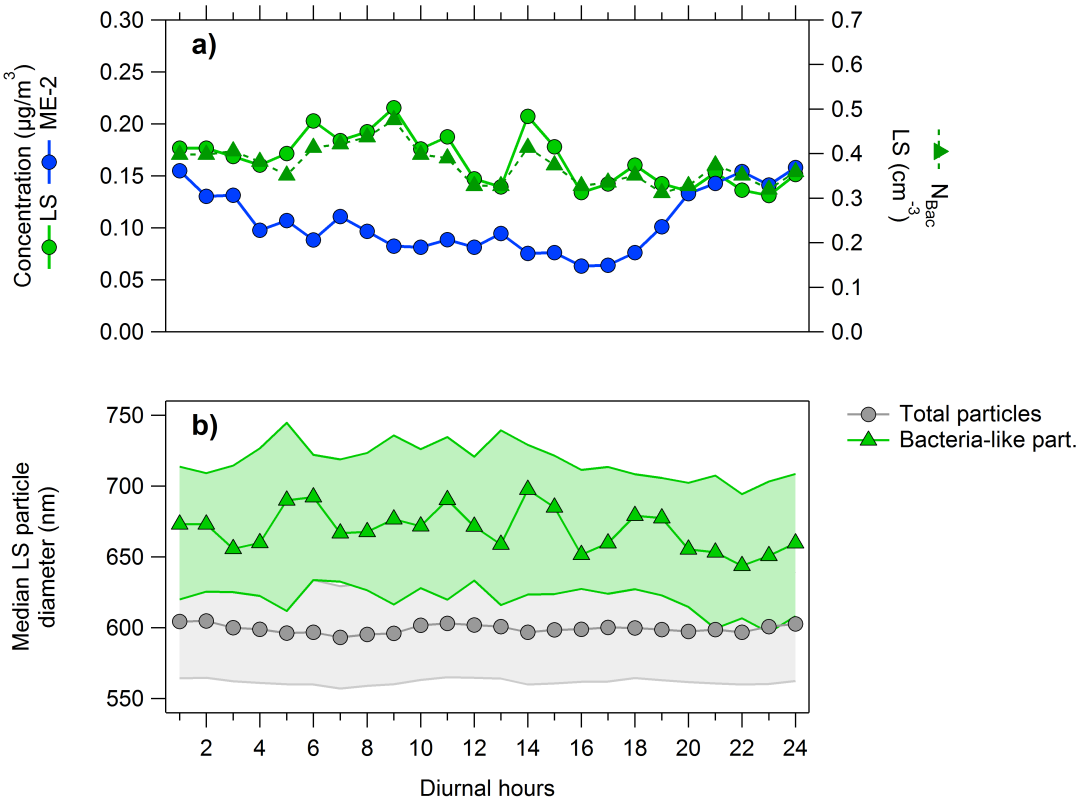

Figure 4.7.: **a)** Diurnal cycle of bacteria-like particle concentrations calculated with the ME-2 technique and via single particle analysis. **b)** Ratio between particles classified as bacteria-like and the total ensemble of detected particles and **c)** the respective median aerodynamic diameters obtained from single particle analysis. Uncertainties are given as Q_{25} and Q_{75} percentiles.

4.7×10^5 particles m^{-3}. The concentration of bacteria-like particles calculated from the single particle method are in the range of observed ambient bacteria number concentrations over grassland and shrub (Spracklen and Heald, 2014).

The diurnal behavior of the median diameter of bacteria-like particles and all counted particles is presented in figure 4.7c. It is evident that the particles with a bacteria-like mass spectrum on average have larger diameters (around 660 nm) than the total ensemble of particles. This may serve as a further evidence for the validity of the classification of single particles since previous studies report a typical single bacteria cell diameter of roughly one micrometer. A deviation from this value might be explained by the asymmetric shape of bacteria particles or the false-positive classification of smaller particles as bacteria-like particles. However, even smaller particles of biological origin have been observed in ambient studies.

4.4. Conclusions

ME-2 calculations with a bacteria input mass spectrum using the a-value method were applied to ambient aerosol mass spectrometer (AMS) data sets to estimate the fraction of airborne particles with a bacteria-like mass spectrum in $PM_{2.5}$. Sensitivity tests on the statistical parameter a show that the estimated contribution of such bacteria-like particles is above the minimum detectable concentration with this approach. Indication exists that the presented method may be appropriate for the time-resolved estimation of bacteria particles in general when using an high-resolution time-of-flight (HR-ToF-AMS) equipped with a $PM_{2.5}$. Viable and non-viable bacteria cannot be distinguished. Furthermore, elevated mass concentrations of the bacteria-like component were captured during precipitation events which is consistent with previous studies that reported increased bioaerosol concentrations during rain. The bacteria-like component appears to constitute only a minor source of organic aerosol in the measured size range with a relative contribution up to 3 mass % and a maximum concentration of $\approx 0.2\,\mu g\,m^{-3}$. The estimated mass concentrations are within the range of previously reported values determined with various methods. The presented method demands for further validation, for example regarding possible cross-sensitivities with other biological materials which currently remain uncertain. In future studies, this could be accomplished by an accompanying analysis of aerosol filters with microscopic, polymerase chain reaction or fluorescence techniques in prospective campaigns. Results of this work can be directly applied to forthcoming advances of AMS analysis tools such as a standard analysis mode for single particles as well as the possibility for off-line filter analysis which may widen the application of the Aerodyne AMS to bioaerosol particles in the future.

Acknowledgement

The authors gratefully acknowledge the financial support by the PEGASOS EU project. Help from EMPA (C. Hüglin) for providing the data from the NABEL network is acknowledged. The authors also thank Aerodyne Research especially L.R. Williams for providing the second generation prototype of the $PM_{2.5}$ lens. J. G. S. acknowledges support from the Swiss National Science Foundation (SNF) through the AMBIZIONE program.

5

Marine and urban influences on summertime $PM_{2.5}$ aerosol in the Po basin using mobile measurements

R. Wolf[1], I. El Haddad[1], M. Crippa[1,*], S. Decesari[2], J.G. Slowik[1], L. Poulain[3], S. Gilardoni[2], M. Rinaldi[2], S. Carbone[4,], F. Canonaco[1], R.-J. Huang[1], U. Baltensperger[1] and A.S.H. Prévôt[1]**

[1] *Laboratory of Atmospheric Chemistry, Paul Scherrer Institute, 5232, Villigen PSI, Switzerland*

[2] *Institute of Atmospheric Sciences and Climate (ISAC), Italian National Research Council (CNR), 40129, Bologna, Italy*

[3] *Leibniz Institute for Tropospheric Research (TROPOS), 04103, Leipzig, Germany*

[4] *Atmospheric Composition Research, Finnish Meteorological Institute, 00101, Helsinki, Finland*

[*] *now at: European Commission, Joint Research Centre (JRC), Institute for Environment and Sustainability, 21027, Ispra, Italy*

[*] *now at: Institute of Physics, University of São Paulo, 05508-060, São Paulo, Brazil*

Published in Atmospheric Environment, 120, 447-454, 2015

Abstract

We report ambient measurements using a high-resolution time-of-flight aerosol mass spectrometer (HR-ToF-AMS) on a mobile platform in the southeast Po Valley (Italy) in summer 2012. During the PEGASOS southbound campaign measurements of non-refractory aerosol were performed in urban and rural environments as well as near the coast of the Adriatic Sea. Organic source apportionment analysis of the aerosol mass spectrometer data was carried out using positive matrix factorization and multilinear engine (ME-2) receptor modelling. Five major organic aerosol components were identified: hydrocarbon-like organic aerosol (HOA), semi-volatile oxygenated organic aerosol (SVOOA), low volatility oxygenated organic aerosol (LVOOA), cooking organic aerosol (COA) and a regionally influenced highly oxygenated organic aerosol (HOOA). Essential changes in both aerosol composition and concentration were induced by the ventilation and recirculation of air masses in the East-West direction of the valley (land/sea breeze system) and via the Apennine mountain range (mountain/valley wind system). An urban increment of the non-refractory aerosol mass concentration in Bologna of about $1.6 - 2.3\ \mu g/m^3$ compared to the surrounding regions was quantified which can be explained by the sum of local contributions from cooking activities and from hydrocarbon-like aerosol related to traffic emissions.

5.1. Introduction

The Po Valley is a large-scale densely populated area with more than 16 million inhabitants. It is a plain with frequent severe air pollution events with respect to the concentrations of aerosols, nitrogen oxides (NO_x), ozone (O_3) and ammonia (NH_3) (Wichink Kruit et al., 2012) as a consequence of intense anthropogenic emissions from industry, agriculture and traffic as well as high photochemical activity in summertime. The basin-like topography facilitates the accumulation of pollutants in stagnant air masses and favours frequent fog events in wintertime (Wobrock et al., 1992). Therefore, the Po Valley is regarded as an air pollution hot spot in Europe with aerosol concentration levels comparable to other metropolitan areas or megacities. In order to establish future mitigation measures an improved knowledge about the composition and the sources of atmospheric aerosol is necessary.

Aerosol composition in the Po Valley is governed by a complex array of emission sources, seasonal effects, and meteorological processes. Using proton nuclear magnetic resonance spectroscopy (H-NMR) analysis of the water soluble-fraction of organic aerosol (OA), Decesari et al., 2001 demonstrated a strong seasonal variation in the composition of fine mode aerosol ($< 1.5\,\mu m$) at the rural San Pietro Capofiume (SPC) site. During measurements in the framework of the EUCAARI project in spring 2008, biomass burning, marine sources and amines were identified as contributors to the water soluble fraction of organic carbon at SPC (Paglione et al., 2014b). Oxygenated organic aerosol constituted the dominant fraction (61%) of non-refractory fine mode aerosol according to aerosol mass spectrometer measurements during the same period (Saarikoski et al., 2012). Crosier et al., 2007 related the sub-micron aerosol composition to air mass trajectories by means of aircraft measurements. Organic matter and sulfate dominated during easterly flow and large ammonium nitrate concentrations were found during westerly flow. Modeling studies indicate that NO_x, CO and particulate matter concentration levels may be more frequently affected by the venting of the valley with air from the Adriatic Sea in summer than in winter (Sofiev et al., 2011).

Besides boundary layer dynamics (Saarikoski et al., 2012; Vecchi et al., 2007), the exchange of air masses with trans-alpine regions (Decesari et al., 2014) and mesoscale air circulations can affect atmospheric dispersion of pollutants and their evolution within the valley. In summertime, thermally induced pressure gradients between the plain area and the Alps as well as the Apennines mountain ridge can drive diurnal mountain wind circulations which may be superimposed by the land-sea breeze system close to the Adriatic Sea (Decesari et al., 2014).

The Po Valley was chosen as a designated investigation area by the PEGASOS (pan-European gas-aerosols-climate interaction study) project during summer 2012. This study aimed at a comprehensive *in situ* analysis of gas and aerosol composition by means of measurements with a zeppelin, ground-based mobile laboratories, multiple ground sites and accompanying modelling studies across Europe. Here, we present spatially and temporally resolved measurements of non-refractory $PM_{2.5}$ aerosol using a high-resolution aerosol mass spectrometer on a ground based mobile platform in the southeast Po Valley in summer 2012. The main objective was the investigation of regional and local differences in aerosol composition and corresponding sources in this region, with a special focus on the urban area of Bologna and the influence of the sea breeze system near the Adriatic Sea.

5.2. Material and methods

5.2.1. Mobile laboratory

The PSI (Paul Scherrer Institute) mobile laboratory was deployed during the southbound campaign of the PEGASOS project in the Po Valley. Figure C.1 in the Supplementary Material depicts the setup of the mobile laboratory during the measurements from June 8 through July 11 in 2012. The mobile platform was equipped with a main sampling line on the top of the roof with an air sampling speed of about $13\,m/s$ to provide steady sampling conditions at different driving speeds (Bukowiecki et al., 2002). Air is drawn into two racks equipped with various instruments for gas and particle analysis. For aerosol measurements, the sampled air is dried (relative humidity RH $< 30\%$) using a Permapure Nafion® membrane gas dryer to prevent changes in aerosol mass spectrometer (AMS) collection efficiency due to varying particle phase at different RH. The residence times in the sampling lines are less than $5\,s$ (Mohr et al., 2011) prior to detection by the instruments. Size-dependent particle losses were modelled for the two racks using the particle loss calculator tool (von der Weiden et al., 2009) and are shown in figure C.2. Calculated losses for particles with aerodynamic diameters between $50\,nm$ to $1200\,nm$ are below 1% for both racks. In the size range of interest for the AMS (rack 2) from about $50\,nm$ to $2500\,nm$ the size-dependent particle losses are smaller than 5%. A high-resolution time of flight aerosol mass spectrometer (HR-ToF-AMS) (DeCarlo et al., 2006) equipped with a $PM_{2.5}$ inlet was used to investigate size and chemical composition of non-refractory aerosol. The $PM_{2.5}$ inlet is a second generation prototype provided by Aerodyne Research Inc. (Billerica, MA, US) including a high-pressure aerodynamic lens (serial number SN13) and a relaxation tube to reduce particle losses due to impaction behind the $100\,\mu m$ critical orifice at the inlet of the AMS (Williams et al., 2013). It should be noted that the experimentally determined upper limit of the particle transmission of $PM_{2.5}$ lens prototypes may differ from the definition of a 50% cut-off at an aerodynamic diameter of

2.5 μm. For example, this particular lens has been tested under laboratory conditions with a 100% transmission at 3 μm. Sampling modes alternated between measuring ensemble mass spectra (15 s), measuring size-resolved mass spectra (15 s) and light scattering single particle mode (15 s). High-resolution AMS data were processed with SQUIRREL (SeQUential Igor data RetRiEvaL) v1.52F and PIKA (Peak Integration by Key Analysis) v1.11G using the IGOR Pro software package (Wavemetrics, Inc., Portland, OR, USA). O/C, H/C and N/C elemental ratios were calculated as described by (Aiken et al., 2007). A cavity ring down spectroscopy analyser (Picarro, Model G2401) was employed for measurements of carbon dioxide, carbon monoxide, methane and water vapour at a time resolution of 2 s and a multi-angle absorption photometer (MAAP, Thermo Scientific™ 5012) was used for equivalent black carbon (EBC) measurements at a time resolution of 1 s.

5.2.2. Driving routes

When possible, secondary roads with low traffic density were used to minimize the bias by sampling directly behind the tailpipe of a moving vehicle. Exceptions to this were sampling drives in the Bologna city centre. The measurement strategy employed herein was to map pollutant concentrations under similar meteorological conditions in repeated driving patterns in order to retrieve local sources and gradients in aerosol composition within the Po Valley.

On days with expected wind from the east, the Adriatic Sea route was chosen to investigate the influence of the sea breeze on aerosol characteristics near the coast. This route was repeated two to three times during the course of the day starting in the morning (around 9 am local time, LT) and ending in the evening (around 6 pm, LT). The maximum distance between the coastline and the inland within the repeated circle around Ravenna was approximately 25 km. On days with negligible wind, drives in the city centre of Bologna and the designated background route were performed to investigate urban aerosol sources and the urban increment of the aerosol mass concentration in the area of Bologna. In the city centre, loops on the inner street circle (7.8 km, approximately 30 min per loop) were repeated during the course of the day and each 2 h alternated with a background route (12.8 km, approximately 40 min per loop) in an elevated (about 100 m above the Bologna city centre) and partially forested area. Overnight the PSI mobile laboratory measured continuously connected to an external power supply at the San Pietro Capofiume (44°30'N, 11°22'E, 11 m a.s.l.) rural measurement site.

5.2.3. Positive matrix factorization

Positive matrix factorization (PMF), described in detail by Paatero and Tapper, 1994, is a bilinear model widely used in receptor-based source apportionment modelling. Here we use the multilinear engine implementation (Paatero, 1999), which allows for full rotational control and thus improved source resolution. In this model, a two-dimensional matrix of measurement data (X) is represented as a linear combination of source/process related factors with static composition and their time-dependent contributions (i.e. time series), respectively expressed as the matrices F and G. The model can be expressed as:

$$x_{ij} = \sum_{k=1}^{p} g_{ik} \times f_{kj} + e_{ij} \tag{5.1}$$

where x_{ij}, g_{ik}, f_{kj} are the matrix elements of X, G, F, and e_{ij} are the model residuals. The indices i, j, and k denote time, the mass fragment measured by the AMS, and factor identity, respectively, while p denotes the number of resolved factors. PMF minimizes the objective function Q (Equation 2) using a least squares optimization.

$$Q = \sum_{i=1}^{m} \sum_{j=1}^{n} \left(\frac{e_{ij}}{\sigma_{ij}} \right)^2 \tag{5.2}$$

In this equation, σ_{ij} represents the measurement uncertainties. The solutions of the PMF algorithm possess rotational ambiguity, i.e. the solutions GF and $G'F'$ are mathematically equally valid, where $G' = GT$ and $F' = T^{-1}F$ given the transformation matrix T and its inverse T^{-1}. A method that allows for a reduced degree of rotational ambiguity is the multilinear engine (ME-2) algorithm in which a priori information about the factor profiles can be added as an input in the calculations (Paatero, 1999; Paatero and Hopke, 2009). In this study, an a-value approach is used:

$$f_j(solution) = f_j(input) \pm a \times f_j(input) \tag{5.3}$$

In this approach, the solution mass spectrum $f_j(solution)$ is required to fall within a predefined range defined by an input mass spectrum $f_j(input)$ and the scalar a. This method has been shown to yield an improved separation of organic aerosol sources in rural or background sites compared to unconstrained positive matrix factorization calculations (Lanz et al., 2008; Crippa et al., 2014). As a user-frontend for the ME-2 input and the visualization of the solution we used the SoFi (Source Finder) toolkit version 4.4 (Canonaco et al., 2013).

The source apportionment of non-refractory organic aerosol data from the HR-ToF-AMS was carried out independently on two data sets. The first represented data collected during the entire campaign and the second represented only data from drives in the urban area of Bologna in order to resolve specific, local sources which may be underrepresented in the entire data set. In accordance with the source apportionment protocol suggested by Crippa et al., 2014 unconstrained positive matrix factorization calculations were performed for both data sets. A hydrocarbon-like organic aerosol (HOA) source profile was then constrained in ME-2 calculations using the a-value approach. An analysis of the sensitivity of the results to the parameter was investigated. A summary of the discussed source apportionment calculations (table C.1) and the preparation of the data matrices can be found in the supplementary.

5.3. Results and Discussion

5.3.1. Non-refractory $PM_{2.5}$ aerosol composition for all combined measurements

Figure 5.1a shows the time series of organic matter, nitrate, sulfate, ammonium and chloride species in $PM_{2.5}$ derived from AMS measurements using a composition-dependent collection efficiency model developed by Middlebrook et al., 2012. The average campaign mass

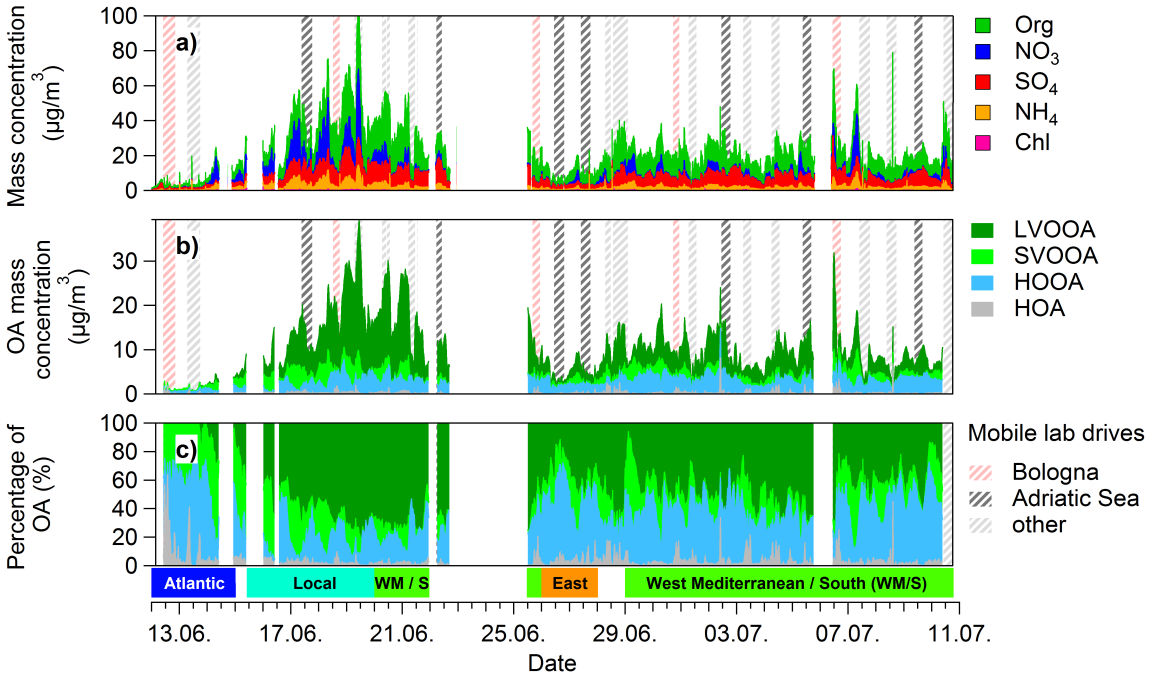

Figure 5.1.: **a)** Temporal behavior of non-refractory organic matter (Org), sulfate (SO_4), nitrate (NO_3), ammonium (NH_4), and chloride (Chl) as measured by the AMS during the entire campaign. **b)** Time series of mass concentrations and **c)** relative contributions of components of organic aerosol. Source apportionment results exclude data obtained from outside the Po Valley. Hashed areas denote data acquired during the drives of the mobile laboratory. Classified air masses are shown as coloured sections on the time axis depending on their origin.

concentration of non-refractory $PM_{2.5}$ (denoted as $nrPM_{2.5}$) as measured by the HR-ToF-AMS was 21.1 $\mu g\, m^{-3}$ and was dominated by organic matter (49.7%). Lower contributions were detected from sulfate (27.1%), nitrate (12.7%), ammonium (9.9%) and chloride (0.5%). Long-range transported air masses originated from the Atlantic region (denoted as "Atlantic"), central-east Europe ("East") as well as the western and southern Mediterranean area ("West Mediterranean/South") during the time period of the measurements. This classification was based on the origin of transported air masses by back trajectory analysis using the NOAA HYSPLIT model (http://ready.arl.noaa.gov/HYSPLIT.php). The trajectories were calculated four times per day (at 00, 06, 12 and 18 UTC), for a 48 h transport time, and an arrival point at 1500 m above SPC. The trajectories are representative for the regional-scale

circulation (average length $\approx 900\,km$).

A pronounced diurnal cycle is observed for the organic aerosol (OA), ammonium and nitrate components during the period denoted as "local" in which anti-cyclonic conditions over the Po Valley induced stagnant air masses and a weak mesoscale circulation governed by the sea breeze system. As shown in figure C.3 the total mean $nrPM_{2.5}$ concentration at the SPC site is significantly higher during westerly winds at night and in the early morning ($44.0\,\mu g\,m^{-3}$) than during the day with wind from the East ($25.0\,\mu g\,m^{-3}$). Figure 5.2 illustrates the diurnal

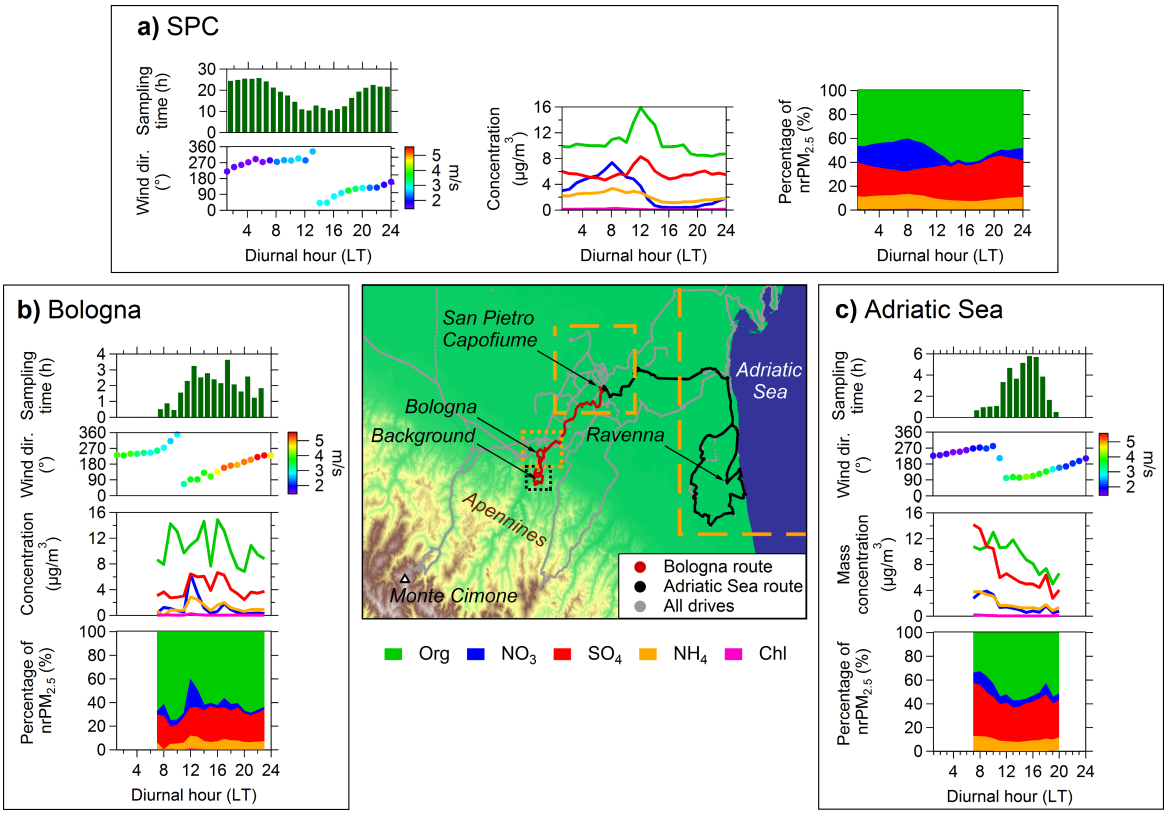

Figure 5.2.: Diurnal contributions (median values) to $nrPM_{2.5}$ **a)** around San Pietro Capofiume, **b)** in the urban area of Bologna (excluding background route) and **c)** close to the Adriatic Sea averaged over all drives in the relevant zone marked in orange. Sampling time histograms indicate sampling times in the different zones. Hourly wind direction and speed data (Bologna: Torre Asinelli, Ravenna: city center, San Pietro Capofiume: rural measurement site) were averaged over the entire measurement period (June 08, 2012 – July 11, 2012).

trends of $nrPM_{2.5}$ chemical composition in three selected zones: SPC (rural, 44°36'N−44°48'N, 11°24'E−11°48'E), Bologna (urban, 44°28'N−44°32'N, 11°15'E−11°26'E) and close to the Adriatic Sea (44°17'N−45°60'N, 12°00'E−12°35'E). Note that the near coast area at the Adriatic Sea (AS) encloses parts of the urban area of Ravenna and the port of Ravenna which is embedded in an industrial area. Since winds from the East dominated during the driving time in the AS zone and thus imposed a negligible bias by these industrial areas on the zonal average, the corresponding data points were not removed from the averaging procedure. The $nrPM_{2.5}$ concentration and composition in the SPC zone and the AS zone is influenced by the

ventilation and recirculation of Po Valley air in East–West direction. At the onset of the sea breeze circulation around 11 : 00 (LT), concentration levels begin to decrease. Simultaneously, the relative fraction of sulfate increases slightly ($9 - 10\%$ in both the AS and the SPC zone) until about 20 : 00 (LT). A peak of the sulfate concentration which coincides with a peak of organic matter at noontime could be associated with a change in wind direction at that time. The daily nitrate cycle is determined by the volatilization of particulate ammonium nitrate with rising temperatures and decreasing RH during the day. Diurnal trends in the Bologna zone show a higher fraction of organic matter.

5.3.2. Source apportionment of organic aerosol mass

Components of organic aerosol were distinguished according to their mass spectra, time series, diurnal variability and the correlation of their time series with external data. Figure 5.1b and figure 5.1c show their temporal behaviour; figure 5.3 and figure 5.4 show the corresponding mass spectra and diurnal cycles, respectively. In addition, correlations of their time trends with other species measured by the AMS, equivalent black carbon and carbon monoxide are given in figure C.5. A more detailed discussion of the validation of the source apportionment can also be found in the supplementary material. Identified components (factors) comprise HOA (hydrocarbon-like organic aerosol), COA (cooking organic aerosol) and oxygenated organic aerosols: SVOOA (semi-volatile oxygenated organic aerosol), LVOOA (low volatility oxygenated organic aerosol) and HOOA (highly oxygenated organic aerosol). HOA, SVOOA and LVOOA have been described in numerous studies. HOA, a surrogate for fossil fuel combustion (Jimenez et al., 2009), has a typical mass spectral fingerprint similar to aliphatic hydrocarbons. This component has a reasonable correlation with equivalent black carbon ($R = 0.49$) and to a weaker extent with carbon monoxide ($R = 0.31$). SVOOA and LVOOA distinguish oxygenated organic aerosol according to their volatility (Cappa and Jimenez, 2010). SVOOA correlates with particulate nitrate ($R = 0.84$) and shows a characteristic peak due to the condensation of semi-volatile species in the morning around 5:00−9:00 (LT) at lowest ambient temperatures. LVOOA correlates with sulfate (SO_4) ($R = 0.56$) and is characterized by a spectral fingerprint that closely resembles previously reported LVOOA spectra ($R = 0.95$, Docherty et al., 2011). Highest contributions from this component are observed during a time period of low air circulation ("local" period) reflecting the accumulation of regional secondary organic aerosol products. The inclusion of a third component of oxygenated organic aerosol, HOOA, significantly improved the correlation of SVOOA with particulate nitrate from $R = 0.66$ for the four factor solution and enhanced the interpretability of the corresponding mass spectra. The terminology of this component was derived from its high degree of oxygenation (O/C = 0.74) which is in the upper range of reported oxygenated organic aerosol components (Ng et al., 2010). Since HOOA also shows significant correlation with sulfate ($R = 0.70$) it represents a rather regional component of low-volatility organic aerosol which shows similarities to an OOA component found by Paglione et al., 2014a. A COA factor related to cooking activities was identified in the Bologna data set consistent with previous studies in urban areas (Canonaco et al., 2013; Hayes et al., 2013; Mohr et al., 2012). A description of the separation of the COA from HOA is given in the Bologna urban increment section. Excluding the higher contribution of primary emission in the urban context of Bologna (COA and HOA), oxygenated components show essentially similar trends. In particular, HOOA and SVOOA show similar diurnal behaviour and absolute concentration in all three zones while

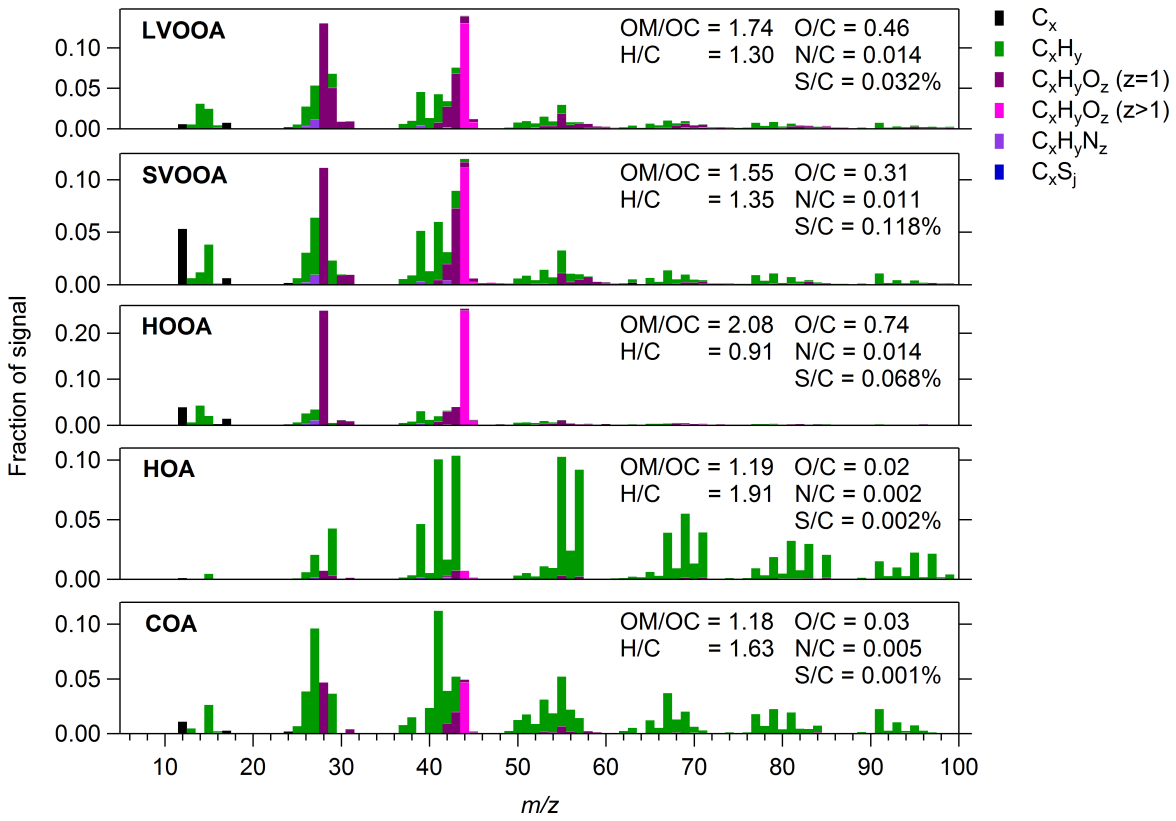

Figure 5.3.: Summary of the factorized mass spectra resulting from ME-2 calculations. The upper four factors were determined in the entire data set using a constrained HOA input mass spectrum ($a = 0.1$) from a study in Barcelona (Mohr et al., 2012). The COA factor was identified only in the urban area of Bologna by constraining the upper four factors from the entire data set in a five factor solution.

the LVOOA contribution is higher at the SPC site. The intrusion of cleaner, more "aged" air masses during the sea breeze is reflected in the higher oxygen-to-carbon (O/C) elemental ratios in this Adriatic Sea zone whereas "fresher" emissions in the urban zone of Bologna yield lower O/C ratios.

5.3.3. Marine influences

Due to the vicinity of the studied area to the marine source areas both terrestrial and marine influences can be expected. Two tracers for a marine influence that can be determined by AMS measurement are methanesulfonic acid (MSA) and the $NaCl^+$ ion. MSA has been reported as a characteristic component of marine secondary organic aerosol (Decesari et al., 2014; Paglione et al., 2014b) which is produced by the decomposition of dimethylsulfide expelled from marine biota (Davis et al., 1998). Therefore, estimated mass concentrations of MSA (MSA_{estim}) were calculated from the sulfur-containing AMS species $CH_2SO_2^+$, $CH_3SO_2^+$ and $CH_4SO_3^+$, which are typical MSA decomposition products (Zorn et al., 2008), and scaled by a factor of 0.147

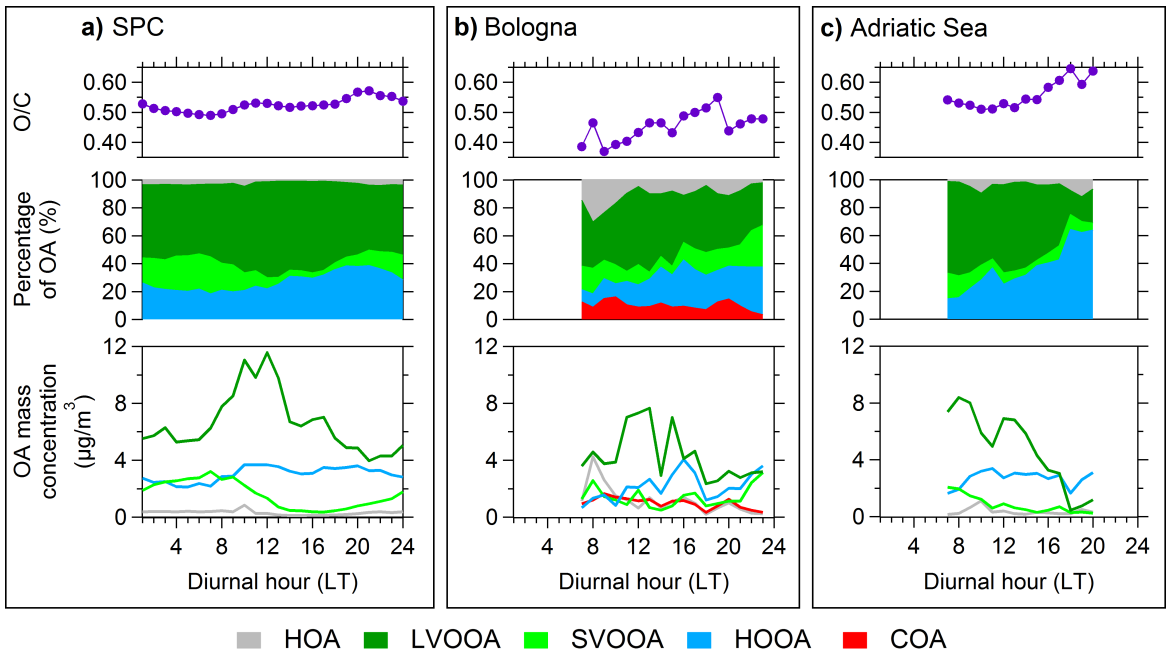

Figure 5.4.: Diurnal trends (median values) of organic aerosol (OA) contributions and O/C elemental ratio **a)** around San Pietro Capofiume, **b)** in the urban area of Bologna (without background route) and **c)** close to the Adriatic Sea averaged over the entire sampling time in the designated zone.

following the recommendations of (Ge et al., 2012):

$$\mathrm{MSA_{estim}} = \frac{\left[\mathrm{CH_2SO_2^+}\right] + \left[\mathrm{CH_3SO_2^+}\right] + \left[\mathrm{CH_4SO_3^+}\right]}{0.147} \tag{5.4}$$

The $NaCl^+$ fragment can also serve as a tracer for primary marine aerosol produced by sea spray (Ovadnevaite et al., 2014; Schmale et al., 2013). It should be noted that the estimated concentration of $NaCl^+$ can only be interpreted qualitatively as this species is considered to be non-volatile under the standard operation conditions of the AMS with a vaporizer temperature of 600°C.

A partial marine influence on the aerosol composition is evident from figure 5.5 which shows a gradient of $\mathrm{MSA_{estim}}$ and $NaCl^+$ within a distance of 25 km orthogonal to the coastline during a particular drive on June 26, 2012 when the sea breeze was weakly developed. A negligible change in absolute concentration for HOOA as a function of distance from sea indicates no significant influence of secondary marine aerosol production on this component and supports its interpretation as a regional background aerosol component. It appears that LVOOA is mainly formed from terrestrial sources within the valley. This is evidenced by the increase in LVOOA during a time period of very low wind speeds ("local" period). Therefore, with increasing distance to the sea LVOOA is less diluted due to the mixing with air masses from the Adriatic Sea. $\mathrm{MSA_{estim}}$ is significantly higher at night and in the early morning than during daytime or directly at the coast (figure C.9). A higher apparent $\mathrm{MSA_{estim}}$ could indicate that other sources of organic sulphur compounds such as organosulfates contributed to the CHSO fragments detected by the AMS (Farmer et al., 2010; Huang et al., 2015). It

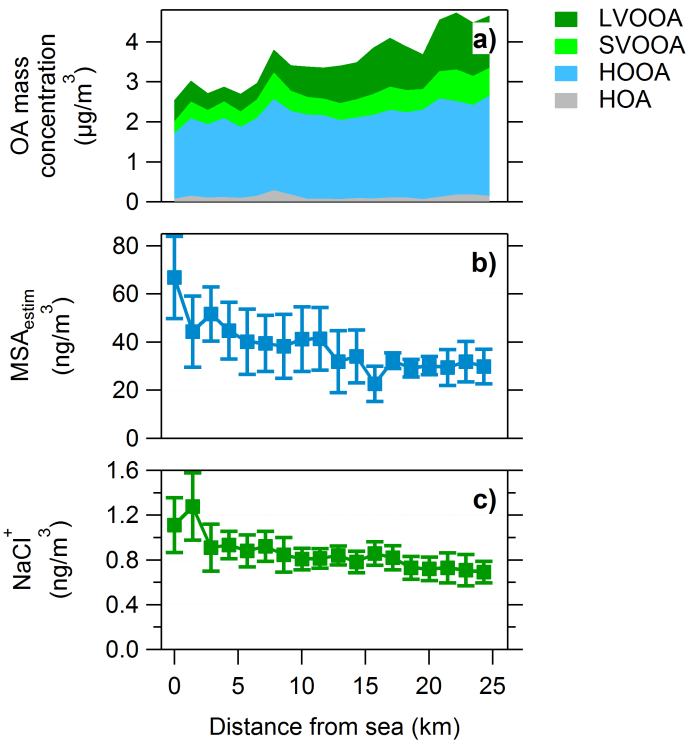

Figure 5.5.: **a)** Gradients of OA components, **b)** estimated MSA (MSA_{estim}, 20 point boxcar moving average) and **c)** $NaCl^+$ ion concentration (20 point boxcar moving average) as function of the distance perpendicular to the coast of the sea during a weakly developed sea breeze on June 26, 2012.

has been shown that numerous biogenic precursors including isoprene and α-pinene can react to form organosulfates (Surratt et al., 2008).

5.3.4. Bologna urban increment

Traffic related emissions (HOA) and emissions from cooking processes (COA) were identified as primary sources in both constrained and unconstrained PMF calculations in the urban zone of Bologna. A detailed description of the source evaluation including mass spectra (figure C.10) and temporal trends (figure C.11 and figure C.12) is given in the supplementary material. The COA mass spectrum contains high signals at m/z 41 and m/z 55 consistent with other published ambient and laboratory cooking experiment mass spectra (Crippa et al., 2013a; He et al., 2010; Mohr et al., 2012) and increases significantly in the city centre of Bologna compared to driving times at the background loop. Discrepancies are apparent in the relative abundance of oxidized ions particularly at m/z 55 and m/z 44. The approach of constrained OOA factors (SVOOA, LVOOA and HOOA) as identified in the entire dataset was preferred as a representative solution since concentrations of the COA component on the background route (elevated area outside of the city centre, 44°24'N−44°28'N, 11°16'E−11°22'E) are low and the correlation with the time trend of the HOA component is the lowest ($R = 0.75$). Significant contributions of COA on the background route as identified with the unconstrained PMF

method indicate a poor deconvolution of this factor. Distinct diurnal profiles are commonly reported for COA in urban areas in the literature (Canonaco et al., 2013; Hayes et al., 2013; Mohr et al., 2012). In averaged drives in the urban zone of Bologna the COA component shows a slight peak around 20 : 00 (LT) consistent with the studies mentioned above. Deviations from a very distinct diurnal pattern likely arise from a combination of statistic and spatial variability of the OA components due to a low sampling time in this zone.

The concept of the local contribution (here: urban increment) as described by Mohr et al., 2011 was applied to HOA, COA, HOOA and organic matter concentrations because sulfate concentration levels change between the area of the background route and the urban city centre route evidencing different air masses or meteorological effects. Local contributions of HOA, COA, HOOA and organic matter concentrations as well as CO and EBC concentrations were averaged in both areas for each day of measurements. The results of the local organic contribution are listed in table C.2. The estimated urban increment for HOOA oscillates around zero (except for drive 5, when the regional background is perturbed by precipitation), consistent with the attribution of this factor to regional SOA. In contrast, the total non-refractory organic aerosol has an urban increment of $1.6 - 2.3\,\mu g\,m^{-3}$, which can be mostly explained by the local contribution of HOA and COA under low wind conditions. This urban increment is slightly lower than combined local emissions of hydrocarbon-like organic aerosol from traffic and cooking processes of about $3\,\mu g\,m^{-3}$ in the Paris metropolitan region, which was found to be surprisingly clean and mainly influenced by long-range transport of air masses (Freutel et al., 2013). The urban increment of HOA is within the range of local HOA contributions ($0.5 - 2.5\,\mu g\,m^{-3}$) found in Zurich in wintertime (Mohr et al., 2011).

5.4. Conclusions

In this study, mobile measurements were used to assess the spatial variability of the non-refractory $PM_{2.5}$ aerosol composition. Both the rather local effect of the urban increment in Bologna as well as the impact of the aerosol transport in a mesoscale sea breeze circulation in the southeast Po Valley could be quantified and characterized in a distance range covered by the mobile laboratory. During anti-cyclonic meteorological conditions, the sea breeze induced measureable changes in aerosol concentration levels and bulk aerosol composition in this part of the valley. A source apportionment analysis with the ME-2/PMF technique revealed that oxygenated components constituted the major fraction of the organic aerosol mass. Besides the common semi-volatile and low-volatility (SVOOA, LVOOA) oxygenated components, a highly oxygenated factor (HOOA) was identified which resembled a regionally influenced organic aerosol component. During daytime, the relative composition of the HOOA and SVOOA components showed similar diurnal behaviour and concentrations within three distinct zones at the Adriatic Sea, in Bologna and in San Pietro Capofiume. The urban increment of the aerosol mass concentration in Bologna in comparison to the surrounding areas was $1.6 - 2.3\,\mu g\,m^{-3}$. It can be attributed to cooking and traffic emissions from the city area.

Acknowledgements

The authors gratefully acknowledge the financial support by the EU project PEGASOS under the Framework Programme 7 (FP7-ENV-2010-265148). Support from G. Bonafe (ARPA) for providing the wind data for Rimini and Bologna is greatly acknowledged. The authors thank the Institute of Atmospheric Sciences and Climate of the Italian National Research Council (ISAC-CNR) as well as Rene Richter for excellent technical support. The project "Supersito" funded by Region Emilia-Romagna (DRG no. 428/10) is also acknowledged.

6

Outlook

Both on-line measurements of the chemical composition in $PM_{2.5}$ and the time-resolved detection of bioaerosols are of interest for future research. In the past, efforts have been spend to develop instruments for the real-time identification of bioaerosols down to the species level in ambient air, for example for civil protection. So far, no method has generally been accepted to meet these criteria. Still, emission estimates for bioaerosols both over the continent and over the sea are poorly constrained.

Within the scope of this thesis, measurements of non-refractory aerosols in an extended size range ($PM_{2.5}$) were performed by using a novel inlet for the Aerodyne aerosol mass spectrometer (AMS). It has been shown that the AMS is capable of detecting airborne bacteria in the laboratory when using the electron ionization technique. Evidence exists that the AMS can also be used to quantify bacteria in general as a fraction of organic aerosol in ambient air.

The Aerodyne AMS has almost become a routine instrument in aerosol research ($>$ 800 publications since 2000). Recent hardware developments and advances in the statistical analysis will widen its application to the PM_{10} size range in the next years. These improvements include the sampling of water extracts from aerosol filters (Dällenbach et al., 2014), a filter inlet for gases and aerosols (Figaero) (Lopez-Hilfiker et al., 2014), a standard sampling mode for single particles or the three dimensional source apportionment technique (Ulbrich et al., 2012). Thus, it may be possible to quantify a broader range of bioaerosols with this instrument. The presented mass spectral features for bacteria and the respective potential marker ions can be useful in the distinction of biogenic material from other atmospheric sources of nitrogen.

Future investigations may be accompanied with more established analytical techniques for the detection of bioaerosols such as microscopic methods, quantitative polymerase chain reaction analysis or fluorescence based techniques. The fraction of larger particles may be enhanced using a counter-flow virtual impactor (CVI) prior to sampling or the source assessment could be focused only on particles within a certain size range using three-dimensional positive matrix factorization (PMF). A size-segregated PMF analysis would be greatly enhanced when employing a newly developed mechanical chopper system for the AMS which allows for a higher transmission of aerosol particles and an improved signal-to-noise ratios. Moreover, an *in-situ* screening of particle fluorescence signals could be achieved by adding an ultraviolet-laser in the AMS assembly.

A more detailed quantification of airborne bacteria may also be carried out close to possible sources, e.g. at a sewage plant or during harvesting to investigate spatial and temporal gradients of their emission source strengths and to provide better estimates for global emission fluxes in general. Furthermore, the loadings of biological aerosol particles on streets, leafs and various other surfaces could be studied by using an active sampling system for the resuspension of coarse mode particles. Future measurements may investigate the complex effects of meteorological factors, e.g. temperature, different wind conditions, rainfall or thunderstorms on concentrations of airborne bacteria.

A

Supplementary information for manuscript: Characterization of ice-nucleating bacteria using on-line electron impact ionization aerosol mass spectrometry

R. Wolf[1], J. G. Slowik[1], C. Schaupp[2], P. Amato[3], H. Saathoff[2], O. Möhler[2], A.S.H Prévôt[1] and U. Baltensperger[1]

[1] *Laboratory of Atmospheric Chemistry, Paul Scherrer Institute, 5232, Villigen PSI, Switzerland*

[2] *Institute for Meteorology and Climate Research, Karlsruhe Institute of Technology, 76021, Karlsruhe, Germany*

[3] *National Center for Scientific Research, Institute of Chemistry of Clermont-Ferrand, 63000, Clermont-Ferrand, France*

Published in Journal of Mass Spectrometry, 50, 662–671, 2015

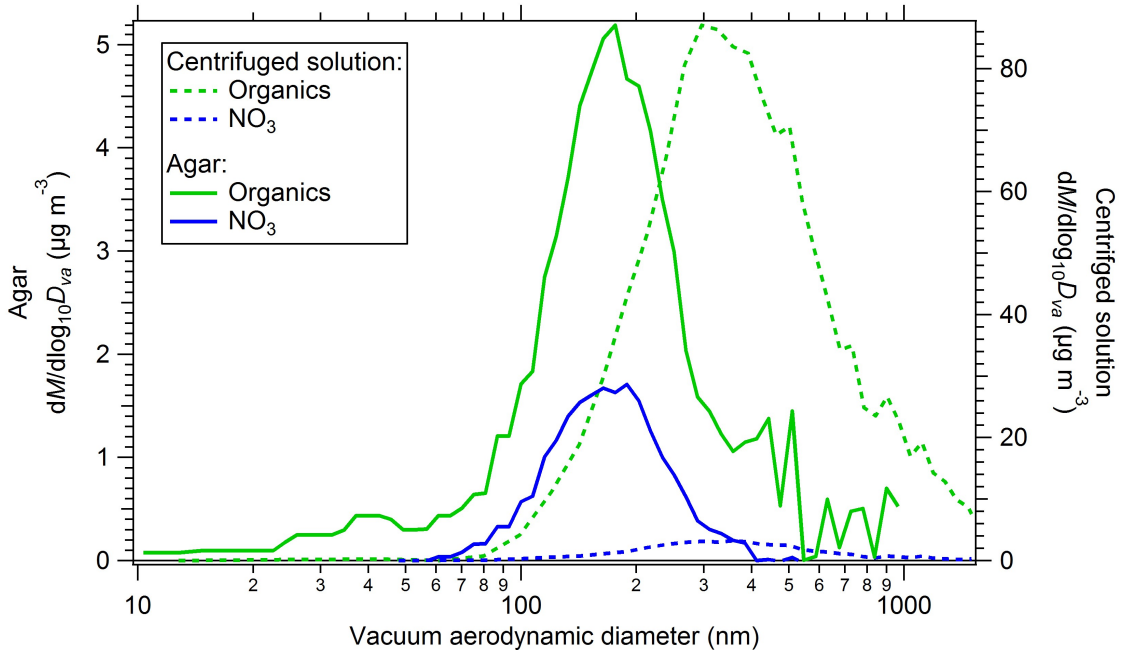

Figure A.1.: Organic and nitrate size distributions of the centrifuged blank and the agar blank experiment at $T_{vap} = 730\,^{\circ}\mathrm{C}$.

Table A.1.: Calculation of the average true agar mass fraction ($\overline{m}_{agar}$) and the average bacteria mass fraction ($\overline{m}^{1stmode}_{bacteria}$) in the first size mode using the f_{70} marker and the ME-2 method. The residual particle mass fraction (m_{res}) is expressed as ratio of the first size mode lognormal fit to the total fit (figure 3.1). $f^{1stmode}_{70}$ and $f^{2ndmode}_{70}$ are the averaged f_{70} mass fractions using pToF data at sufficient organic mass ($dM/dlog_{10}D_{va} > 1\,\mu g\,m^{-3}$). m_{agar} was calculated using equation 3.4. $\overline{m}_{agar}$ is the arithmetic average of m_{agar} calculated with the ME-2 and the f_{70} marker method.

Experiment	**I**	**II**	**III**	**IV**
Residual particle mass (m_{res}) fraction	0.276	0.198	0.098	0.087
$f^{1stmode}_{70}$	0.010	0.016	0.011	0.012
$f^{2ndmode}_{70}$	0.021	0.019	0.022	0.018
$m^{1stmode}_{agar}$(f_{70} marker method)	0.856	0.241	0.808	0.597
m_{agar} (f_{70} marker method)	0.236	0.048	0.079	0.052
m_{agar} (ME-2 method)	0.280	0.034	0.049	0.049
$\overline{m}_{agar}$ (avg. ME-2 and f_{70} marker)	0.258	0.041	0.064	0.050
$\overline{m}^{1stmode}_{agar}$ (avg. ME-2 and f_{70} marker)	0.936	0.207	0.653	0.581
Avg. 1st mode bacteria mass fraction (%)				
($\overline{m}^{1stmode}_{bacteria} = 1 - \overline{m}^{1stmode}_{agar}$)	6.4	79.3	34.7	41.9

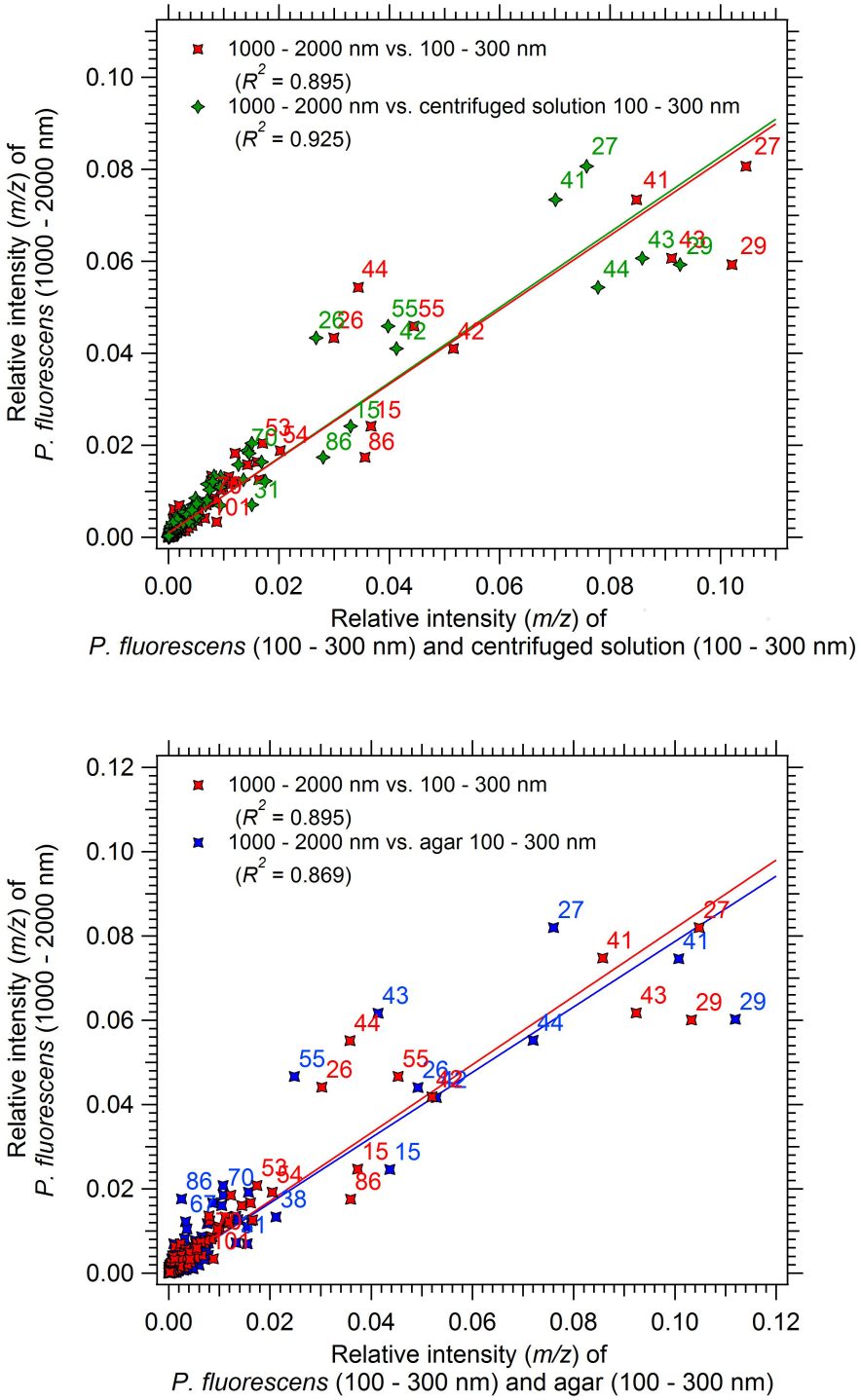

Figure A.2.: Correlation between normalized, size-selected organic mass spectra of bacteria, centrifuged solution and agar blank samples at $T_{vap} = 730\,°C$.

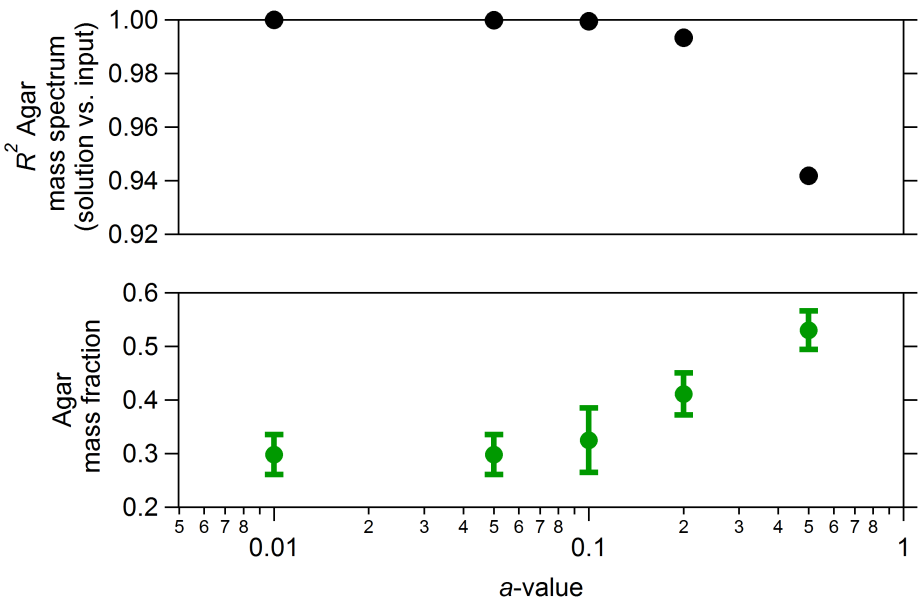

Figure A.3.: Influence of the a-value magnitude on the estimated agar mass fraction for Exp. I (*P. syringae*, $T_{vap} = 600\,°C$) and the similarity between input and solution agar mass spectra. For $a > 0.1$ the bacteria factor mixes with the agar mass spectrum.

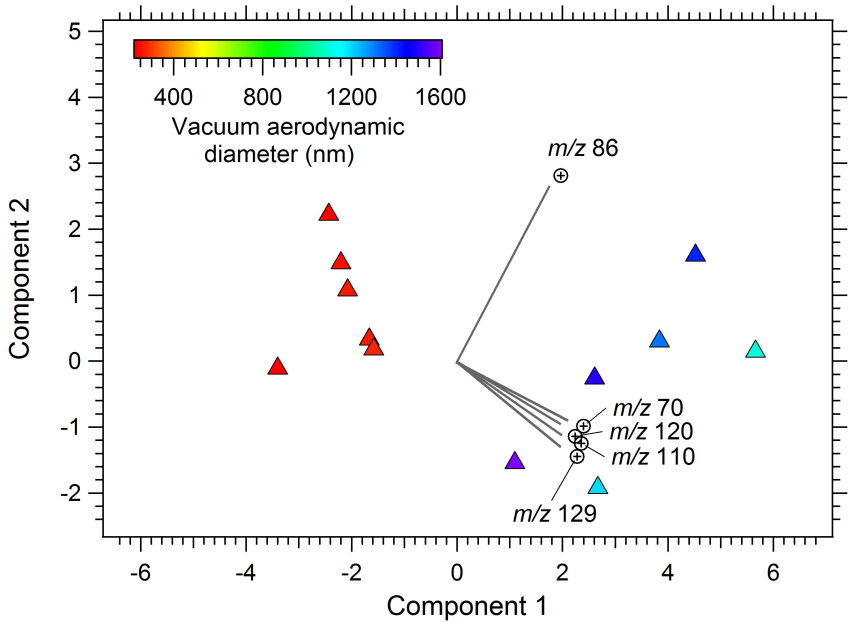

Figure A.4.: Principal component analysis biplot on size-resolved particle time-of-flight (pToF) data of combined *P. fluorescens* experiments at $T_{vap} = 730\,°C$. Selected m/z values are shown in the biplot for clarity. Vacuum aerodynamic diameters larger than $1600\,nm$ are not included in the calculations since they are possibly affected by artifacts due to slow evaporation from the vaporizer surface at $T_{vap} = 730\,°C$.

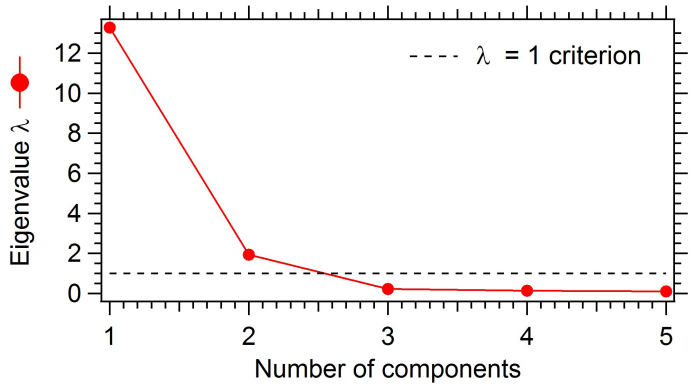

Figure A.5.: Principal component analysis (performed with Statgraphics Centurion XV, StatPoint Technologies, Inc.) eigenvalue plot on size-resolved pToF data of combined *P. fluorescens* experiments at $T_{vap} = 730\,°C$. Selected m/z values ranging from 20 to 130 with a contribution to the total organic mass larger than 0.2% were included in the analysis.

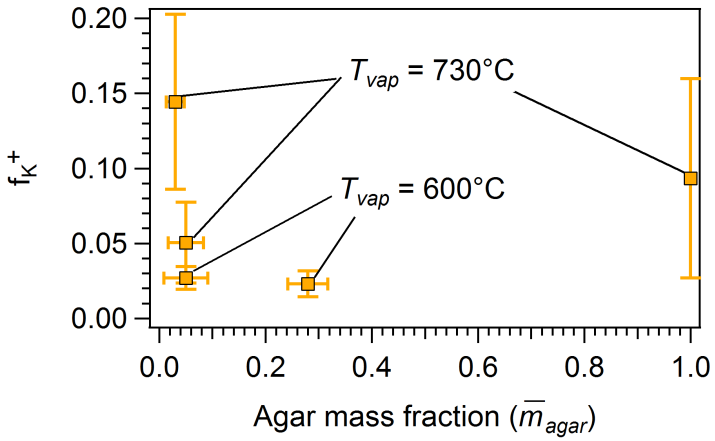

Figure A.6.: Fraction of the total potassium ion signal (f_{K^+}) at m/z 39 and m/z 41 as function of the agar mass fraction ($\overline{m}_{agar}$) for different experiments with P. fluorescens, P. syringae and agar nutritive medium ($\overline{m}_{agar} = 0$). A default relative ionization efficiency of 1 was applied. Elevated levels of potassium in the agar blank experiment may originate from dipotassium hydrogen phosphate (King et al., 1954) and from the peptone constituent of the agar nutrient (Conda, 2014).

B

Supplementary information for manuscript: Contribution of bacteria-like particles to $PM_{2.5}$ aerosol in urban and rural environments

R. Wolf[1], I. El Haddad[1], J. G. Slowik[1], K.R. Dällenbach[1], E. Bruns[1], U. Baltensperger[1] and A.S.H. Prévôt[1]

[1] *Laboratory of Atmospheric Chemistry, Paul Scherrer Institute, 5232, Villigen PSI, Switzerland*

In preparation for Atmospheric Environment

Table B.1.: Summary of the estimated bacteria mass concentrations and the corresponding organic aerosol (OA) mass fractions. The two co-located AMS instruments are labeled as AMS #1 and AMS #2 during the two sampling periods at Zurich Kaserne. Minimum values are below the calculated AMS detection limits ($0.024\,\mu g\,m^{-3}$ for $PM_{2.5}$ and $0.014\,\mu g\,m^{-3}$ for PM_1)

Site	**Time period**	**Inlet**	**Conc. ($\mu g\,m^{-3}$)**		**OA fraction (%)**	
			average	**max.**	**average**	**max.**
Zurich	07.04.11 – 20.04.11	$PM_{2.5}$ (AMS #1)	0.05	1.52[a]	1.71	6.15[a]
	07.04.11 – 20.04.11	PM_1 (AMS #2)	0.02	0.11	0.52	1.06
	21.04.11 – 25.04.11	PM_1 (AMS #1)	0.04	0.16	0.93	1.63
	21.04.11 – 25.04.11	PM_1 (AMS #2)	0.04	0.27	0.82	2.17
Payerne	10.07.12 – 02.08.12	$PM_{2.5}$	0.11	2.51[b]	2.06	24.30[b]

[a] Possible artifact due to very high organic mass concentration peak

[b] After rain

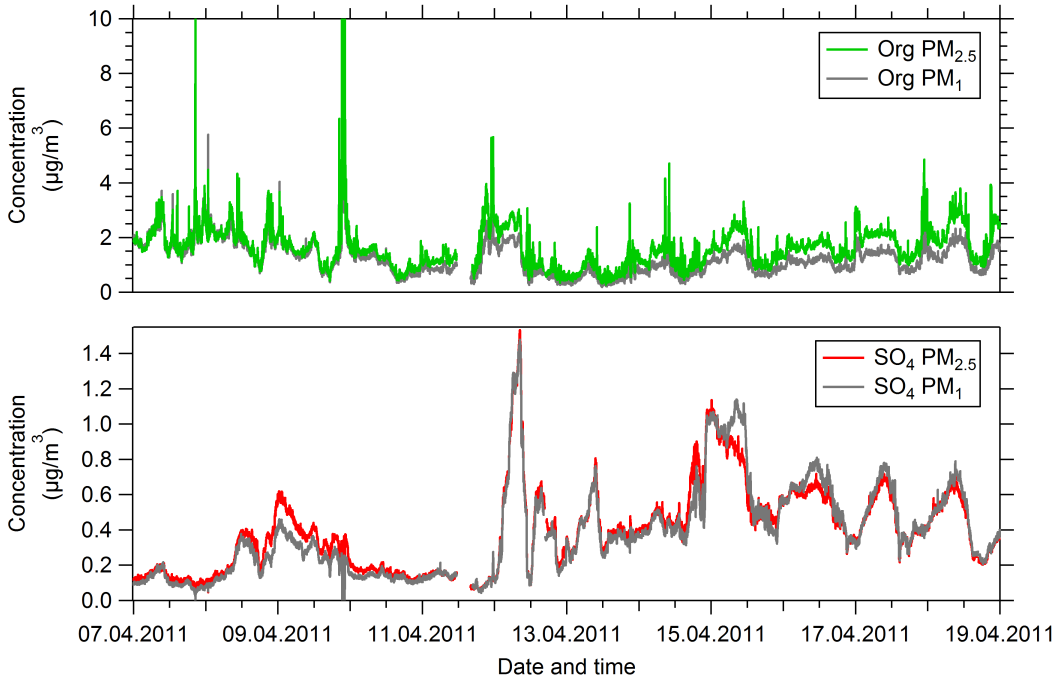

Figure B.1.: Time series of non-refractory organics and sulfate as measured by the two co-located AMS with $PM_{2.5}$ and PM_1 inlet from 07.04.2011 until 21.04.2011.

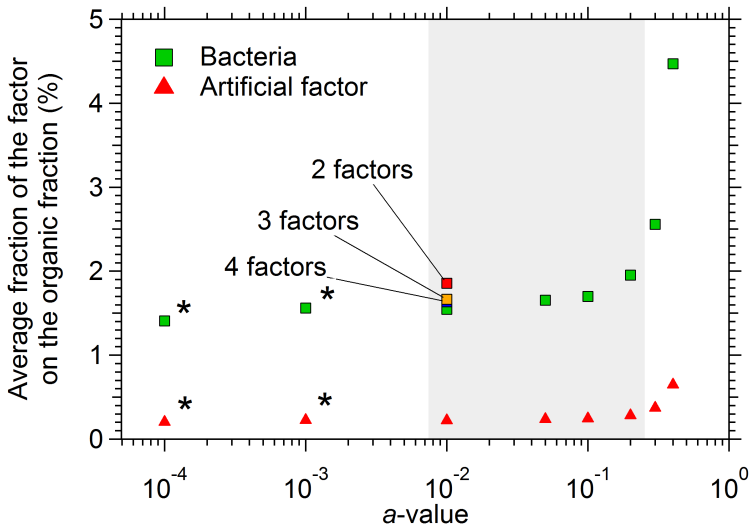

Figure B.2.: Relative contribution of the bacteria component and an artificial factor to organic aerosol as a function of the a-value magnitude in $PM_{2.5}$. The fractions are arithmetic averages of five runs with different pseudo random starting points for a five factor solution. Uncertainties due to the different pseudo random starting points are negligible (standard deviation, $\sigma < 1\%$). The average bacteria fractions for solutions with two, three and four factors are shown for $a = 0.01$ as a reference. At a-values larger than 0.4 the bacteria spectrum resembles an HOA mass spectrum. Stars indicate lower convergence criteria used in the SoFi software.

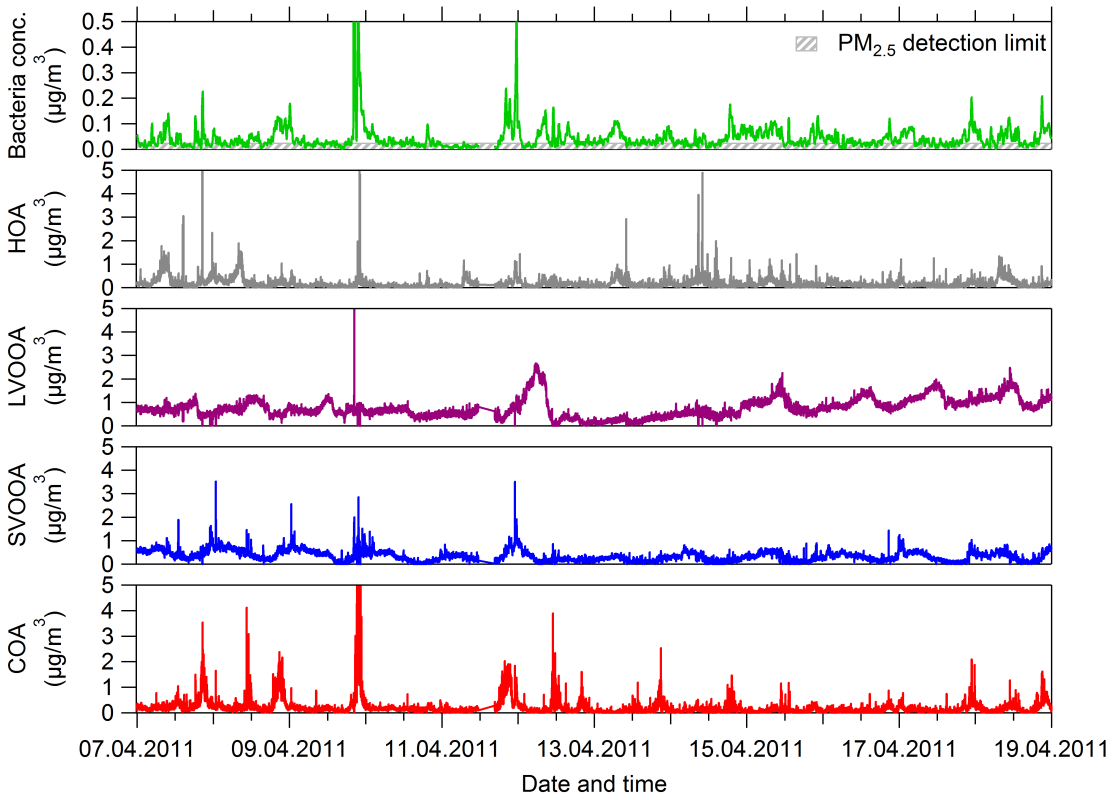

Figure B.3.: Time series of the identified factors in $PM_{2.5}$ at the Zurich Kaserne site from 07.04.2011 until 19.04.2011. The bacteria component was constrained by the a-value approach whereas the other components were unconstrained. A moving average (20 min) boxcar smoothing for the bacteria factor was applied for better visual comparison.

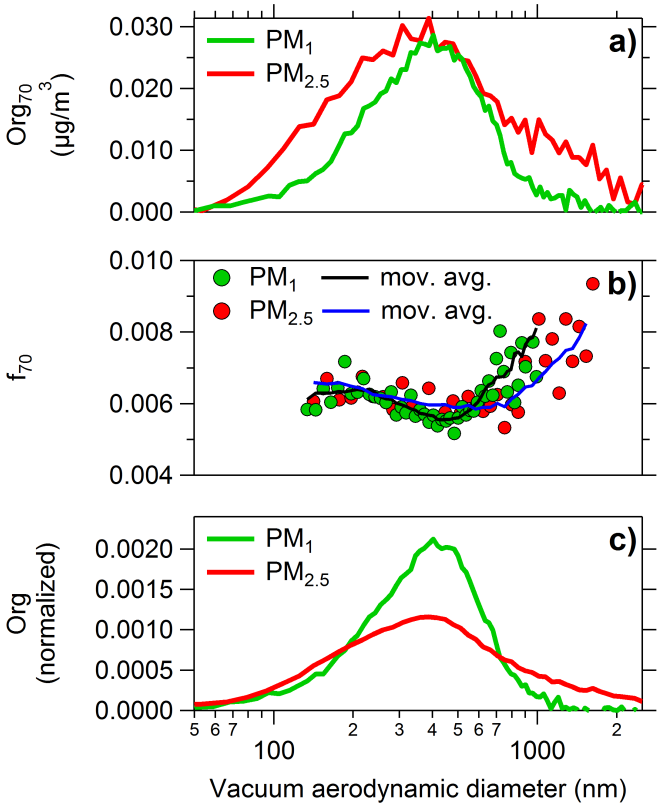

Figure B.4.: **a)** Size distribution of the characteristic fragment for bacteria (Org_{70}), **b)** the respective organic fraction ($f_{70} = Org_{70}/Org$) and **c)** the total organic size distribution during a period of continuous sampling of the two AMS equipped with PM_1 and $PM_{2.5}$ aerosol inlets at Zurich Kaserne from 07.04.2011 until 19.04.2011. Only f_{70} values at sufficient organic mass ($> 10\%$ compared to the size distribution maximum) are shown. Discrepancies of the moving averages (5-point boxcar) probably result from the slower evaporation of larger particles at the AMS vaporizer surface.

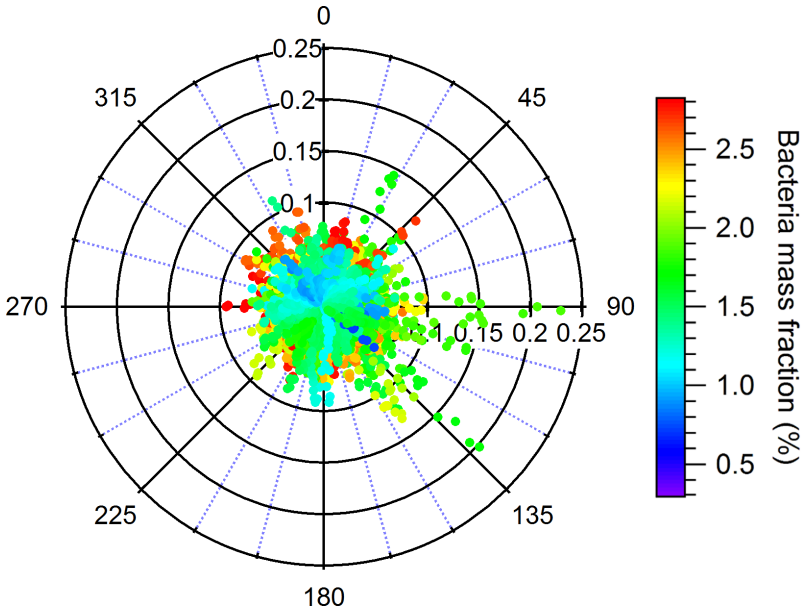

Figure B.5.: Wind rose plot for the bacteria component at Zurich Kaserne. The radial axis scales with the absolute concentration (in $\mu g\, m^{-3}$) of the factor. The color scale represents the relative contribution to non-refractory $PM_{2.5}$.

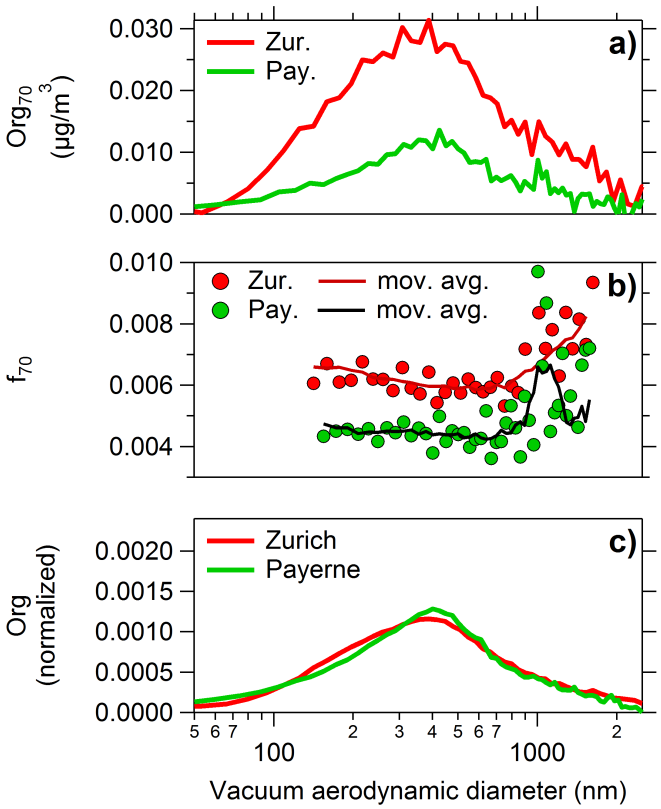

Figure B.6.: **a)** Size distribution of the characteristic fragment for bacteria (Org_{70}), **b)** the respective organic fraction ($f_{70} = Org_{70}/Org$) and **c)** the total organic size distribution compared for measurements with the $PM_{2.5}$ inlet in Zurich (07.04.2011 – 19.04.2011) and during high bacteria contribution in Payerne (01.08.2012, 00:00-02.08.2012, 00:00). The moving average (5-point boxcar) of f_{70} indicates that aerodynamic diameters of the bacteria are around 1 μm during the rainfall event.

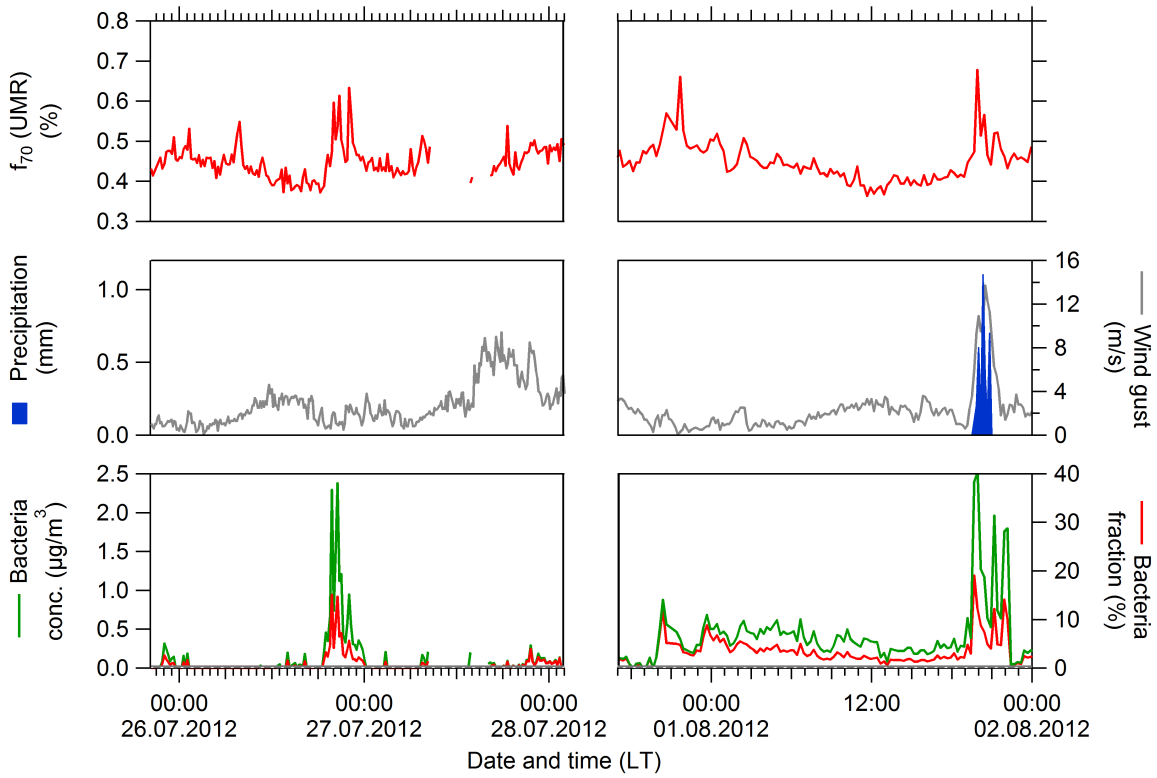

Figure B.7.: Time series of the organic mass fraction f_{70} at m/z 70, precipitation as well as the estimated bacteria concentration and the respective organic mass fraction for the two highest peaks in concentration during the campaign.

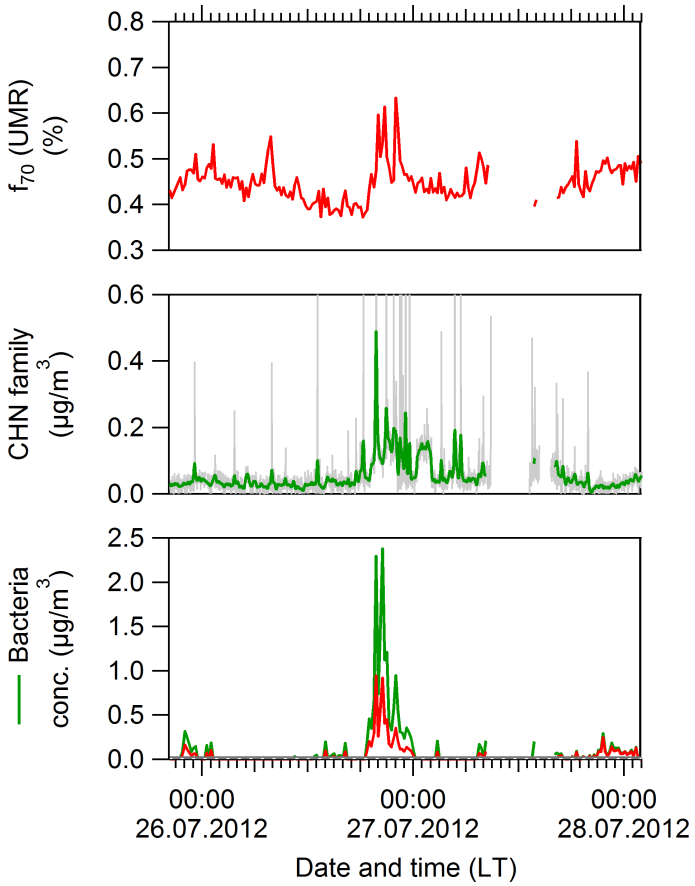

Figure B.8.: Time series of the organic mass fraction f_{70} at m/z 70, CHN family ions as well as the estimated bacteria concentration and the respective organic mass fraction for the highest peak in concentration during the campaign.

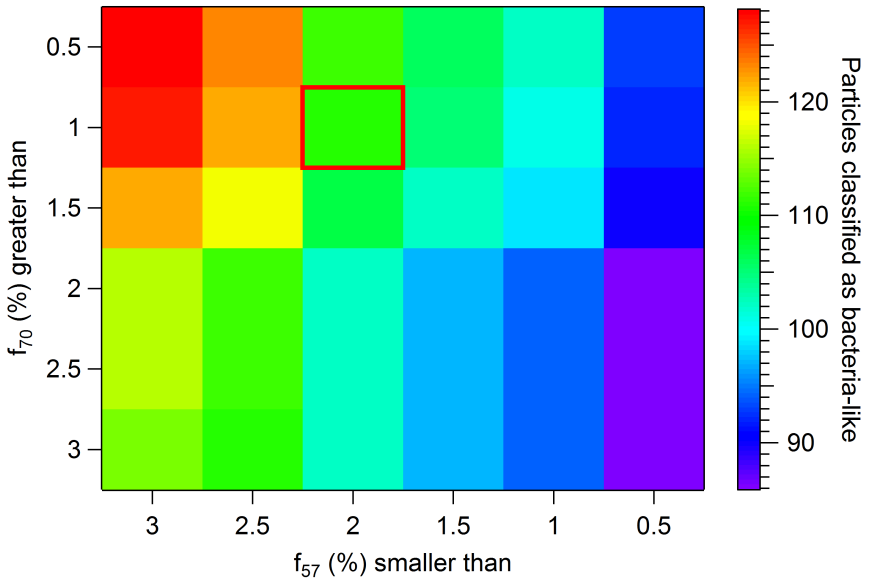

Figure B.9.: Number of single particle mass spectra that are classified as bacteria-like as a function of the selection criteria (f_{57} and f_{70}) in an exemplary time period from the 21.07.2012 until the 22.07.2012. The rectangle displays the chosen criteria.

C

Supplementary information for manuscript: Marine and urban influences on summertime $PM_{2.5}$ aerosol in the Po basin using mobile measurements

R. Wolf[1], I. El Haddad[1], M. Crippa[1,*], S. Decesari[2], J.G. Slowik[1], L. Poulain[3], S. Gilardoni[2], M. Rinaldi[2], S. Carbone[4,], F. Canonaco[1], R.-J. Huang[1], U. Baltensperger[1] and A.S.H. Prévôt[1]**

[1] *Laboratory of Atmospheric Chemistry, Paul Scherrer Institute, 5232, Villigen PSI, Switzerland*

[2] *Institute of Atmospheric Sciences and Climate (ISAC), Italian National Research Council (CNR), 40129, Bologna, Italy*

[3] *Leibniz Institute for Tropospheric Research (TROPOS), 04103, Leipzig, Germany*

[4] *Atmospheric Composition Research, Finnish Meteorological Institute, 00101, Helsinki, Finland*

[*] *now at: European Commission, Joint Research Centre (JRC), Institute for Environment and Sustainability, 21027, Ispra, Italy*

[*] *now at: Institute of Physics, University of São Paulo, 05508-060, São Paulo, Brazil*

Published in Atmospheric Environment, 120, 447-454, 2015

Preparation of data matrices

The high-resolution organic aerosol data matrix (X) of measured ions ranging from mass-to-charge ratio m/z 12 to m/z 100 and the corresponding matrix of measurement uncertainties were prepared following the method of Ulbrich et al., 2009. A minimum counting error corresponding to the measurement of a single ion was applied. Ions with a signal-to-noise ratio ($SNR_i = \sqrt{\frac{\sum_{j=1}^{m} x_{ij}}{\sum_{j=1}^{m} \sigma_{ij}}}$) between $0.2 < SNR_i < 2$ were downweighted by a factor of 2 and ions with a $SNR_i < 0.2$ were downweighted by a factor of 10 following the recommendations of Paatero and Hopke, 2009. Ions calculated as a constant fraction of the CO_2^+ signal (Allan et al., 2004) were downweighted such that they exert approximately the correct weight on the ME-2 solution. Isotopes which are calculated as a constant fraction from parent ions were removed prior to analysis.

Validation of the source apportionment

All discussed source apportionment calculations are summarized in table C.1. The interpretation of the unconstrained PMF calculations (figure C.6) is particularly challenging as more than 90% of organic nr$PM_{2.5}$ are attributed to oxygenated components and the primary aerosols are often detected far from their sources. This is supported by a previous study at SPC (Saarikoski et al., 2012) which reported a HOA mass spectrum with the highest oxygen content within the recent high-resolution AMS database (Ulbrich et al., 2009) as well as three representations of oxygenated aerosol components. Following the recommendations for a standardized source apportionment (Crippa et al., 2014) a suitable representation of a HOA mass spectrum derived from a previous study in Barcelona (Mohr et al., 2012) was constrained to allow for an improved separation between different aerosol components. This input mass spectrum satisfies conditions for a well separated HOA component: 1) low degree of oxygenation (O/C = 0.03 and thus also low signal at m/z 44) 2) reasonable separation from other primary aerosols (COA and BBOA) and 3) high similarity to other exhaust pipe studies (signal at m/z 57 higher than signal at m/z 55) (Canagaratna et al., 2004). Figure C.7 shows the influence of the number of chosen factors on the relative factor contribution to the OA mass.

A sensitivity test of the a-value parameter for a four factor solution is presented in figure C.8. As the a-value has only a minor effect on the contribution of the major factors consistent with Canonaco et al., 2013 a value of $a = 0.1$ has been chosen for the constrained HOA mass spectrum.

A wood burning influence could not be identified with solutions containing up to five factors which contrasts with findings using a more sensitive NMR analysis of levoglucosan from filter samples (S. Decesari, pers. communication). Since the characteristic signal for BBOA at m/z 60 resulting from the biomass burning tracer levoglucosan (Simoneit et al., 1999) is very low it can be speculated that parts of the BBOA component volatilize under the high temperature ambient conditions (Oja and Suuberg, 1999; Grieshop et al., 2009).

For the entire data set, a four factor solution was chosen as a recombination from a five factor ME-2 calculation with a HOA input mass spectrum from a study in Barcelona applying an a-value of 0.1 since diurnal patterns for the LVOOA and the SVOOA component were

more distinct in the five factor solution facilitating an enhanced separation. In addition, an improved separation of the HOA component increased the correlation with equivalent black carbon measurement from $R = 0.36$ to $R = 0.49$. Simultaneously, the normalized quantity Q/Q_{exp} (Canonaco et al., 2013) remains almost the same between the constrained an unconstrained calculations at the same number of factors indicating only a small perturbation of the total solution.

The source apportionment results were essentially the same for the Bologna data set. In contrast to the entire data set, two distinct factors with a higher contribution within the city area of Bologna than on the background route appear above a number of three factors in both unconstrained PMF and ME-2 calculations. These factors were interpreted as the HOA and the COA component according to the similarity of their mass spectral features to previously published HOA and COA factors.

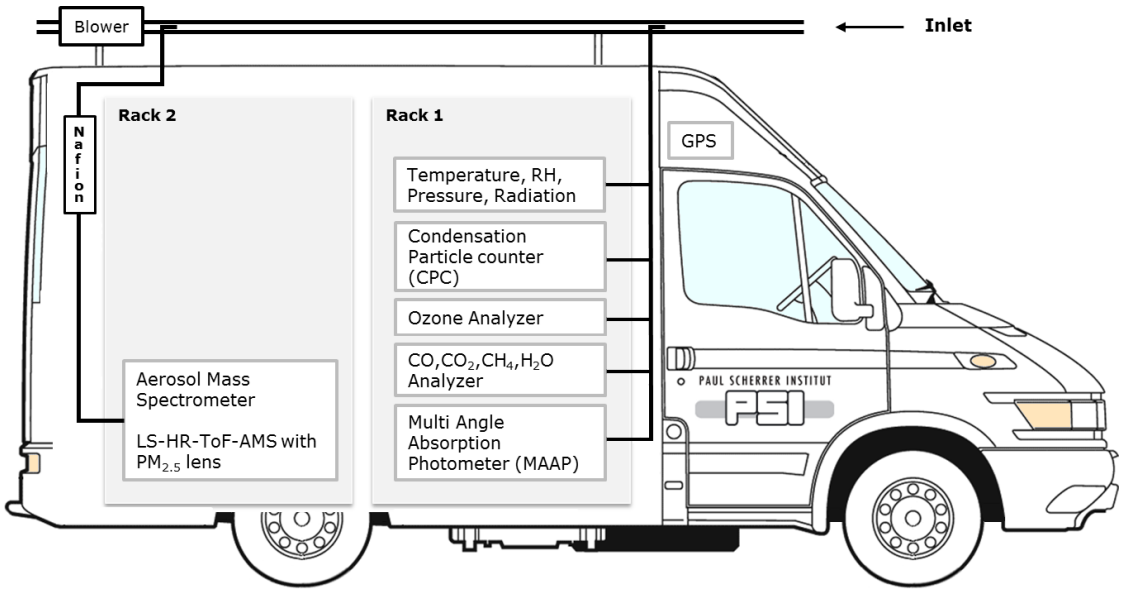

Figure C.1.: PSI mobile laboratory (MOSQUITA: Measurements Of Spatial Quantitative Imissions of Trace gases and Aerosols) instrument set up during the PEGASOS southbound campaign in Italy in summer 2012. Figure adapted from http://carblueprints.info/eng/view/iveco/iveco-daily-2008 (last access May 21, 2015).

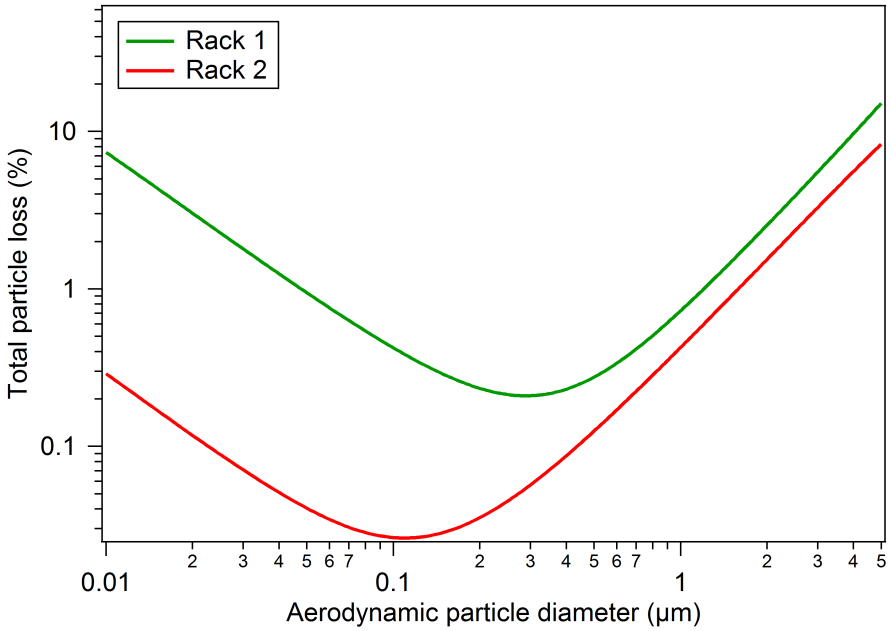

Figure C.2.: Calculation of total particle losses for the inlets of rack one and rack two based on diffusion, sedimentation and inertial deposition particle loss mechanisms using the particle loss calculator tool (von der Weiden et al., 2009).

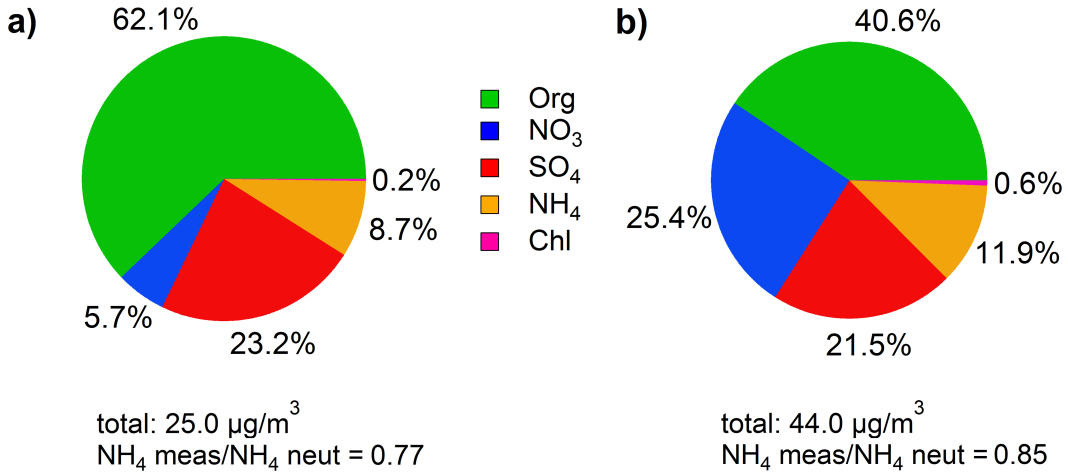

Figure C.3.: Relative contributions to non-refractory $PM_{2.5}$ aerosol during **a)** sea breeze influence (11:00−20:00) and during **b)** westerly winds from the valley at night (21:00−10:00) at the SPC site excluding mobile laboratory drives. Results including the total $nrPM_{2.5}$ mass concentration and the ammonium balance ($\frac{NH_{4\,meas}}{NH_{4\,neut}}$, according to Zhang et al., 2007) are given as arithmetic mean during the "local" period. Relative ionization efficiencies of nitrate and sulfate were $RIE(NO_3)$= 4.3 and $RIE(SO_4)$= 1.12.

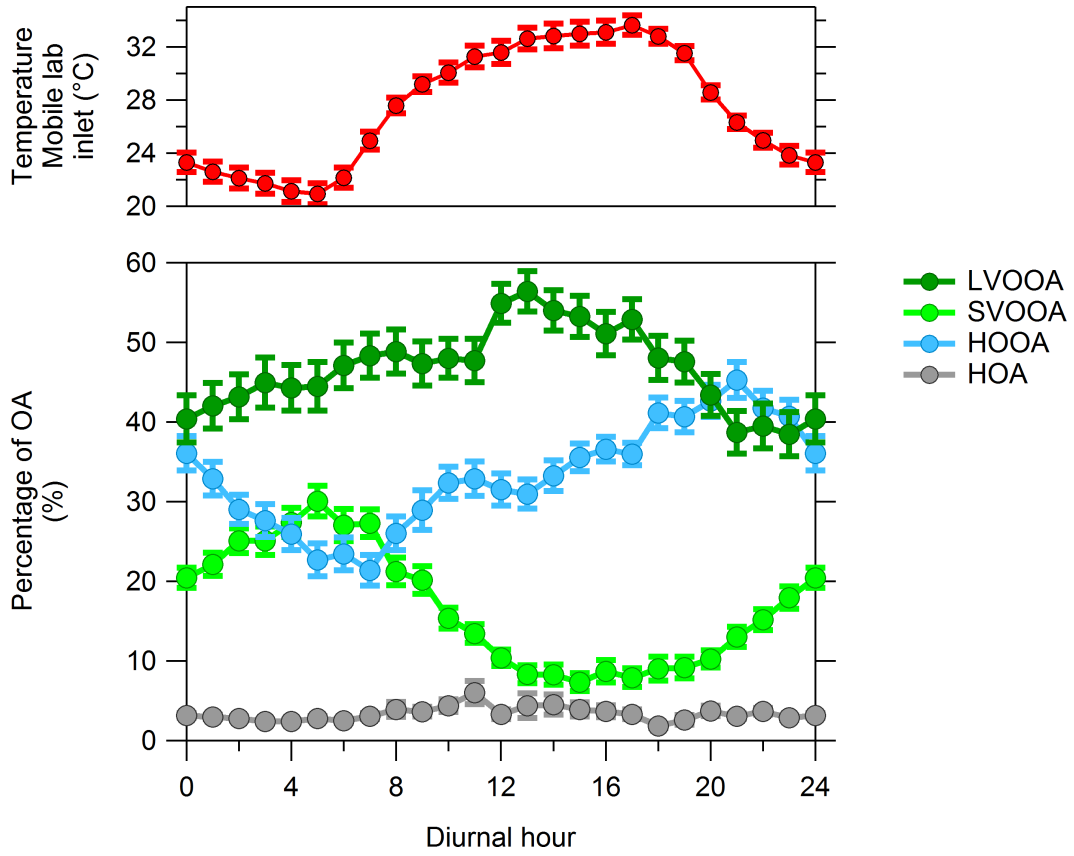

Figure C.4.: Diurnal behaviour of the identified organic aerosol components resulting from ME-2 calculations for all measurements within the valley (June 10, 2012 - July 10, 2012) including stationary measurements at SPC.

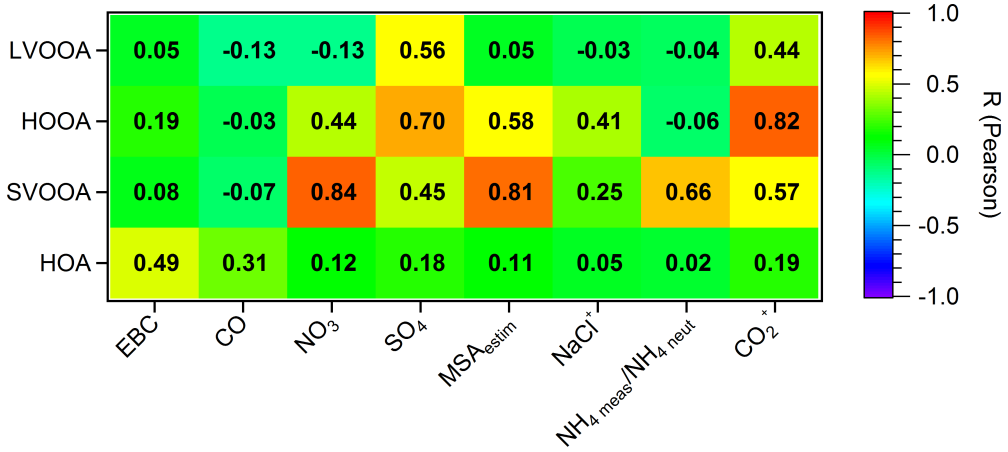

Figure C.5.: Correlation of identified factor mass spectra with additional gas- and particle phase data. EBC: equivalent black carbon, MSA_{estim}: estimated MSA concentration from AMS measurements, $\frac{NH_{4\,meas}}{NH_{4\,neut}}$: ammonium balance, CO_2^+: AMS particulate phase CO_2^+ ion, $NaCl^+$: non-conventional AMS $NaCl^+$ ion.

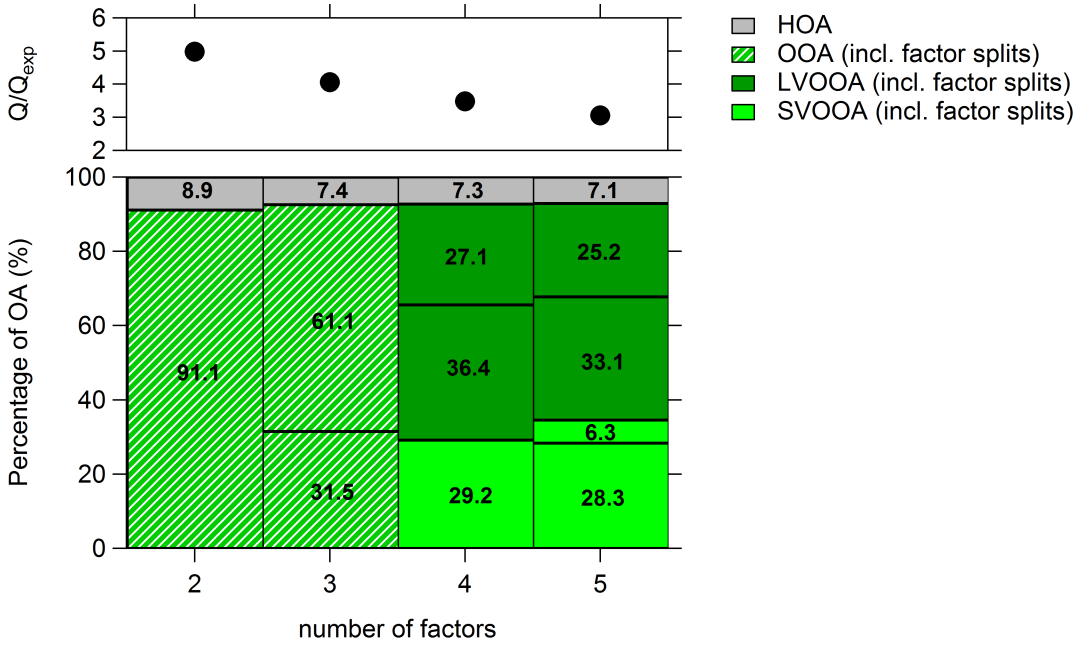

Figure C.6.: Contribution of factors in unconstrained PMF calculations depending on the number of chosen factors. Note that the nomenclature of the factors is only indicative and mainly based on mass spectral features as diurnal cycles are not very pronounced for distinguishing SVOOA and LVOOA factors.

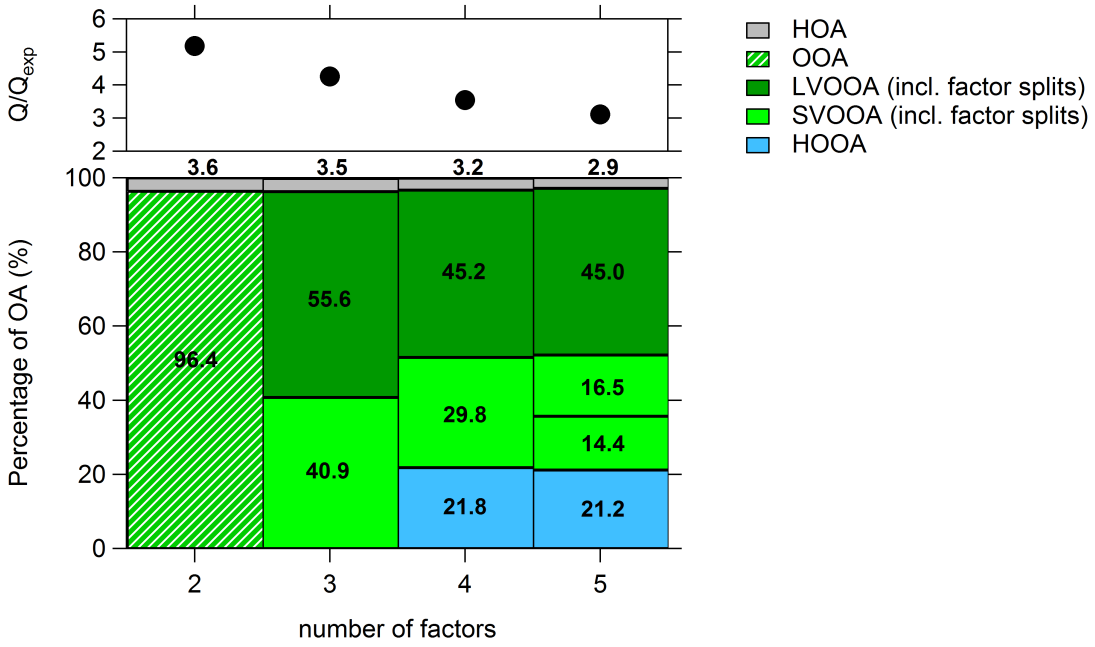

Figure C.7.: Factor contribution of the ME-2 calculations depending on the number of chosen factors for a constrained HOA mass spectrum with an a-value of 0.1. As discussed in the main text, we selected the 5-factor solution for detailed analysis, and recombined the split SVOOA factors into a single SVOOA.

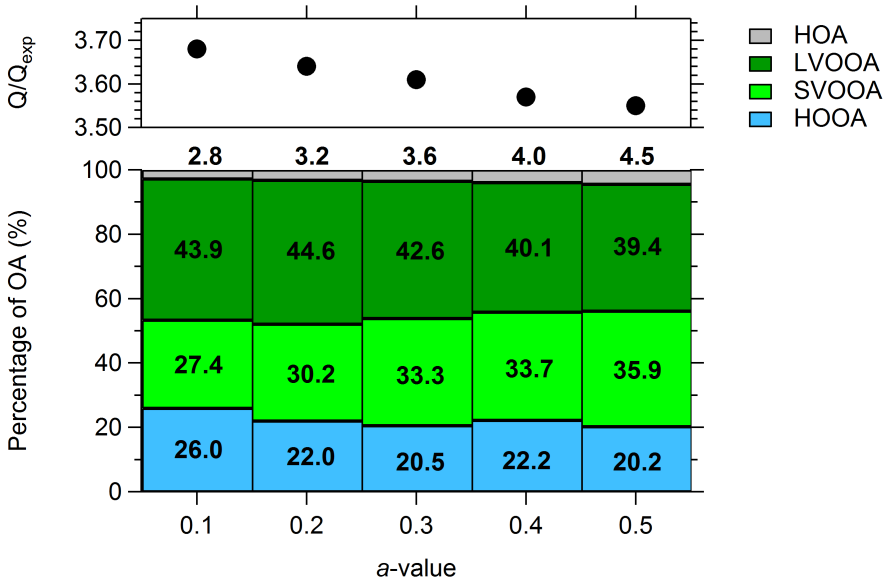

Figure C.8.: Factor contribution of the ME-2 calculations with a constrained HOA mass spectrum as a function of the HOA a-value constraint for the recombined 4-factor solution.

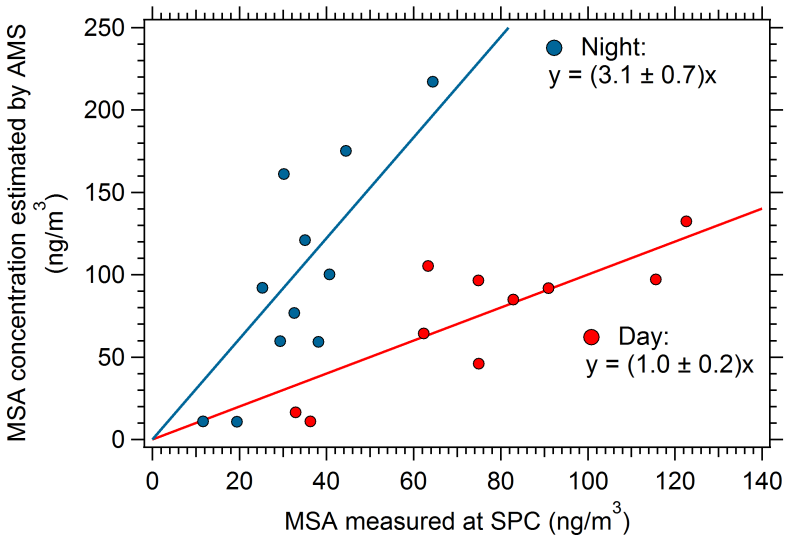

Figure C.9.: Estimated MSA concentrations (MSA_{estim}) as measured by the AMS and MSA determined by ion-chromatography on impactor samples (12 h sampling time) at SPC. Points are divided into samples taken during day (9:00−20:30) and during night (21:00−8:30).

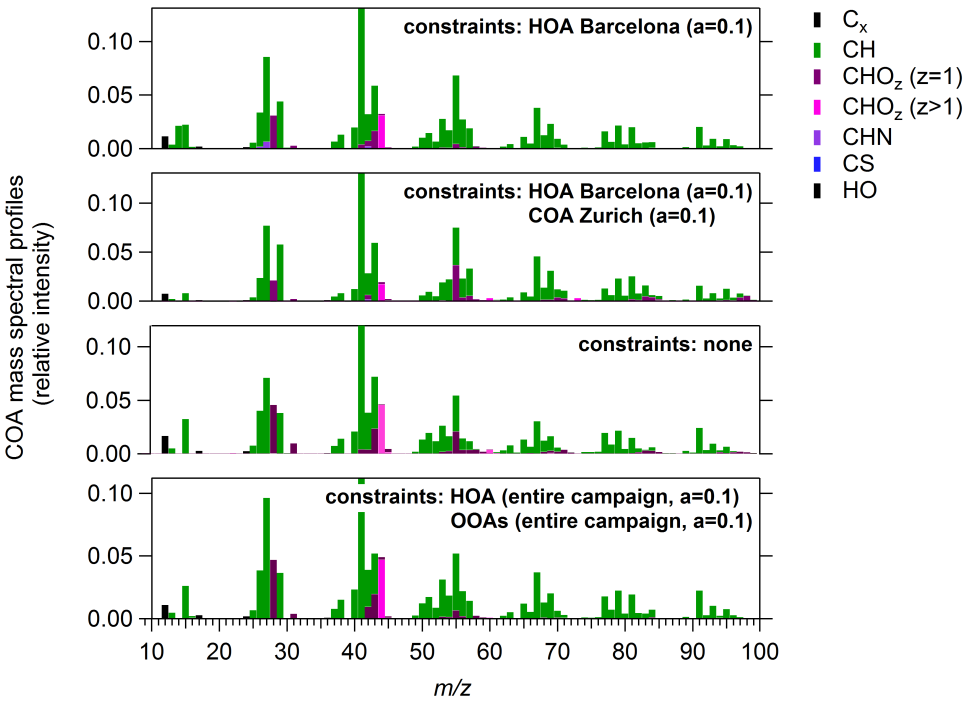

Figure C.10.: High-resolution mass spectra of the COA factors retrieved from different constrained ME-2 solutions (in each case 4 factors) and the unconstrained PMF solution (5 factors) in the urban context of Bologna. Text labels denote the constraints applied in the different ME-2 solutions.

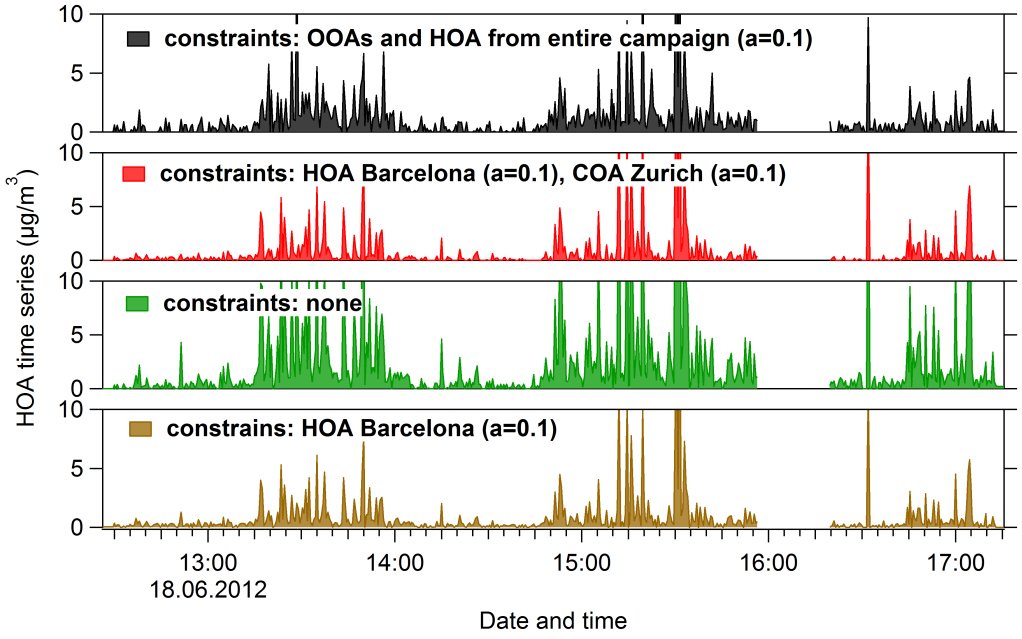

Figure C.11.: Example time series of the HOA component for the unconstrained PMF solution (5 factors) and different constrained ME-2 solutions (in each case 4 factor solution) for the Bologna route on June 18, 2012. Text labels denote the constraints applied in the different ME-2 solutions.

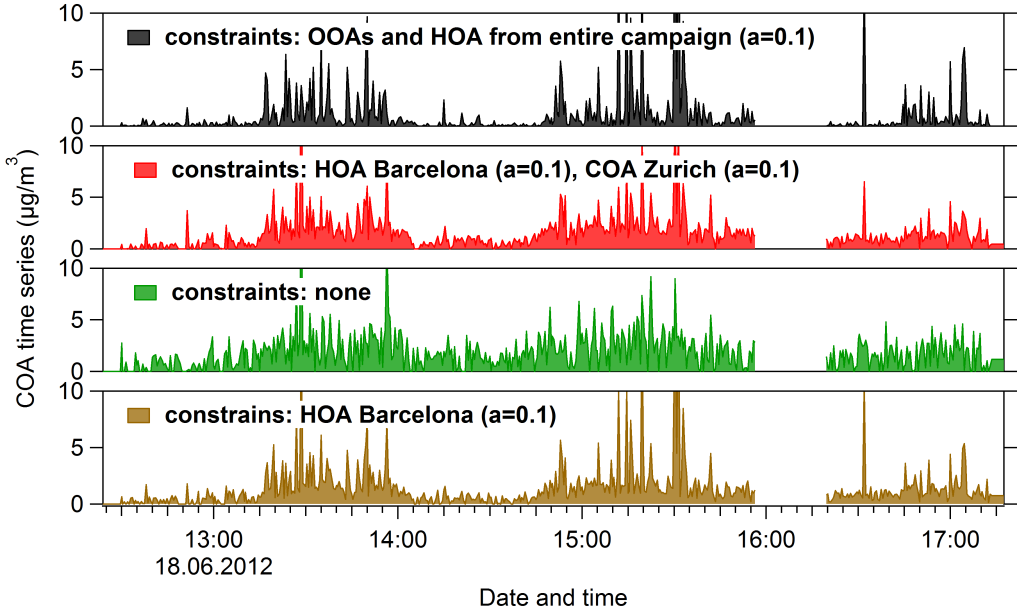

Figure C.12.: Example time series of the COA component for the unconstrained PMF solution (5 factors) and different constrained ME-2 solutions (in each case 4 factors) for the Bologna route on June 18, 2012. Text labels denote the constraints applied in the different ME-2 solutions.

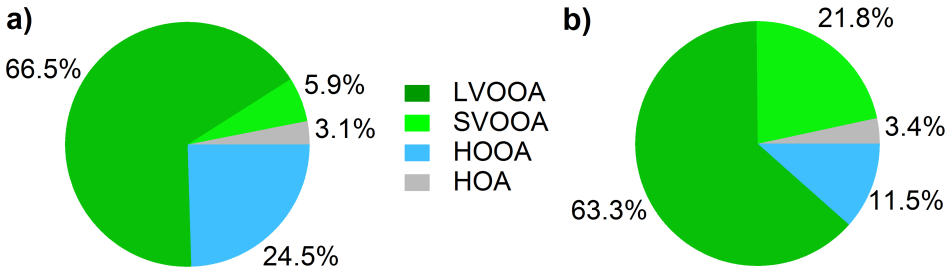

Figure C.13.: Relative contributions organic aerosol components during local mesoscale circulation at the SPC site excluding mobile laboratory drives. **a)** Sea breeze influence (11:00−20:00 LT) and **b)** during westerly winds from the Valley at night (21:00−10:00 LT). Results are given as arithmetic mean during the "local" period from June 15, 2012 (9:00 LT) until June 20, 2012 (00:00 LT).

Table C.1.: Summary of the unconstrained PMF and the constrained ME-2 calculations. Combined drives on the Adriatic Sea route yielded similar results compared to the entire campaign data set and are not presented separately. Highlighted rows show the selected final solutions (for the entire campaign data set an a-value of 0.1 was used). AMS data were averaged to a time step of 15 min to maintain a reasonable computational speed for the entire campaign dataset. Data from combined mobile laboratory drives in the different contexts retained their native time resolution of 30 s.

Data set	**Model**	**Constraints**	***a*-value**
Entire campaign	PMF		
	ME-2	HOA Barcelona (Mohr et al., 2012)	$0.1 - 0.5$
Combined drives in Bologna	PMF		
	ME-2	HOA Barcelona (Mohr et al., 2012)	$0.1 - 0.3$
	ME-2	HOA Barcelona (Mohr et al., 2012), COA Zurich (unpublished mass spectrum)	0.1 each
	ME-2	OOA factors + HOA factor (as identified from the entire campaign)	0.1 each

Table C.2.: Summary of the urban increment of Bologna on five different days. Local contributions S_{local} of the selected species were estimated using $S_{local} = S_{meas} - \frac{SO_{4,\ meas}}{SO_{4,\ backgnd}} \times S_{backgnd}$ as described by Mohr et al., 2011. Average wind speeds were rather low (maximum $8\,m/s$) during the drives.

Drive	**Date**	**Driving time**	$\mathbf{Org_{local}}$ $(\boldsymbol{\mu g\, m^{-3}})$	$\mathbf{BC_{local}}$ $(\boldsymbol{\mu g\, m^{-3}})$	$\mathbf{CO_{local}}$ $(\boldsymbol{ppb})$
1	18.06.12	12 : 30 – 18 : 00 (Mo)	1.79	6.8	596
2	25.06.12	16 : 30 – 22 : 30 (Mo)	1.61	4.4	384
3	28.06.12	7 : 30 – 11 : 30 (Th)	1.64	10.7	680
4	30.06.12	17 : 30 – 22 : 30 (Sa)	2.30	5.3	564
5	06.07.12[a]	11 : 00 – 18 : 00 (Fr)	0.37	8.5	539

[a] Precipitation in Bologna during driving

Drive	$\mathbf{HOA_{local}}$ $(\boldsymbol{\mu g\, m^{-3}})$	$\mathbf{COA_{local}}$ $(\boldsymbol{\mu g\, m^{-3}})$	$\mathbf{HOOA_{local}}$ $(\boldsymbol{\mu g\, m^{-3}})$
1	0.68	1.06	0.30
2	0.38	0.60	0.32
3	0.92	1.05	-0.57
4	0.44	0.82	0.35
5	0.79	0.99	-2.13

[a] Precipitation in Bologna during driving

List of Tables

List of Figures

Bibliography

I. Agranovski: *Aerosols – Science and Technology*. Wiley, New York, 2012.

V. Agranovski and Z. D. Ristovski: Real-time monitoring of viable bioaerosols: capability of the UVAPS to predict the amount of individual microorganisms in aerosol particles. *J. Aerosol. Sci.*, 36(5-6), 665–676, 2005.

A. C. Aiken, P. F. DeCarlo and J. L. Jimenez: Elemental analysis of organic species with electron ionization high-resolution mass spectrometry. *Anal. Chem.*, 79(21), 8350–8358, 2007.

A. C. Aiken, D. Salcedo, M. J. Cubison, J. A. Huffman, P. F. DeCarlo, I. M. Ulbrich, K. S. Docherty, D. Sueper, J. R. Kimmel, D. R. Worsnop, A. Trimborn, M. Northway, E. A. Stone, J. J. Schauer, , R. M. Volkamer, E. Fortner, B. de Foy, J. Wang, A. Laskin, V. Shutthanandan, J. Zheng, R. Zhang, J. Gaffney, N. A. Marley, G. Paredes-Miranda, W. P. Arnott, L. T. Molina, G. Sosa and J. L. Jimenez: Mexico city aerosol analysis during MILAGRO using high resolution aerosol mass spectrometry at the urban supersite (t0) - Part 1: Fine particle composition and organic source apportionment. *Atmos. Chem. Phys.*, 9(17), 6633–6653, 2009.

J. D. Allan, M. R. Alfarra, K. N. Bower, P. I. Williams, M. W. Gallagher, J. L. Jimenez, A. G. McDonald, E. Nemitz, M. R. Canagaratna, J. T. Jayne, H. Coe and D. R. Worsnop: Quantitative sampling using an Aerodyne aerosol mass spectrometer: 2. Measurements of fine particulate chemical composition in two UK cities. *J. Geophys. Res.*, 108(D3), 4091, 2003a.

J. D. Allan, A. E. Delia, H. Coe, K. N. Bower, M. R. Alfarra, J. L. Jimenez, A. M. Middlebrook, F. Drewnick, T. B. Onasch, M. R. Canagaratna, J. T. Jayne and D. R. Worsnop: A generalised method for the extraction of chemically resolved mass spectra from Aerodyne aerosol mass spectrometer data. *J. Aerosol. Sci.*, 35(7), 909–922, 2004.

J. D. Allan, J. L. Jimenez, P. I. Williams, M. R. Alfarra, K. N. Bower, J. T. Jayne, H. Coe and D. R. Worsnop: Quantitative sampling using an Aerodyne aerosol mass spectrometer: 1. Techniques of data interpretation and error analysis. *J. Geophys. Res.*, 108(D3), 4090, 2003b.

J. D. Allan, P. I. Williams, W. T. Morgan, C. L. Martin, M. J. Flynn, J. Lee, E. Nemitz, G. J. Phillips, M. W. Gallagher and H. Coe: Contributions from transport, solid fuel burning and cooking to primary organic aerosols in two UK cities. *Atmos. Chem. Phys.*, 10(2), 647–668, 2010.

M. Amann, I. Bertok, R. Cabala, J. Cofala, C. Heyes, F. Gyarfas, Z. Klimont, W. Schöpp and F. Wagner: A final set of scenarios for the Clean Air For Europe (CAFE) programme. Technical report, International Institute for Applied Systems Analysis (IIASA), 2005.

P. Artaxo, M. Willy, S. Hedwig and R. Van Grieken: Aerosol characteristics and sources for the Amazon basin during the wet season. *J. Geophys. Res. Atmos.*, 95(D10), 16971–16985, 1990.

E. Attard, H. Yang, A.-M. Delort, P. Amato, U. Pöschl, C. Glaux, T. Koop and C. E. Morris: Effects of atmospheric conditions on ice nucleation activity of *Pseudomonas*. *Atmos. Chem. Phys.*, 12(4), 10667–10677, 2012.

L. R. Bakken and R. A. Olsen: Buoyant densities and dry-matter contents of microorganisms: conversion of a measured biovolume into biomass. *Appl. Environ. Microbiol.*, 45(4), 1188–1195, 1983.

H. Bauer, M. Claeys, R. Vermeylen, E. Schueller, G. Weinke, A. Berger and H. Puxbaum: Arabitol and mannitol as tracers for the quantification of airborne fungal spores. *Atmos. Environ.*, 42(3), 588–593, 2008.

H. Bauer, H. Giebl, R. Hitzenberger, A. Kasper-Giebl, G. Reischl, F. Zibuschka and H. Puxbaum: Airborne bacteria as cloud condensation nuclei. *J. Geophys. Res.*, 108(D21), 4658, 2003.

H. Bauer, A. Kasper-Giebl, M. Löflund, H. Giebl, R. Hitzenberger, F. Zibuschka and H. Puxbaum: The contribution of bacteria and fungal spores to the organic carbon content of cloud water, precipitation and aerosols. *Atmos. Res.*, 64(1-4), 109–119, 2002.

C. A. Belis, B. R. Larsen, F. Amato, I. El-Haddad, O. Favez, R. M. Harrison, P. K. Hopke, N. S., P. Paatero, A. S. H. Prévôt, U. Quass, R. Vecchi and M. Viana: European guide on air pollution source apportionment with receptor models. Technical report, JRC Reference Reports, 2014.

K. Biemann, J. Seibl and F. Gapp: Mass spectra of organic molecules. I. Ethyl esters of amino acids. *J. Am. Chem. Soc.*, 83(18), 3795–3804, 1961.

B. Bjorksten, D. Dumitrascu, T. Foucard, N. Khetsuriani, R. Khaitov, M. Leja, G. Lis, J. Pekkanen, A. Priftanji and M. A. Riikjarv: Prevalence of childhood asthma, rhinitis and eczema in Scandinavia and Eastern Europe. *Eur. Respir. J.*, 12(2), 432–437, 1998.

I. R. Booth and P. Louis: Managing hypoosmotic stress: Aquaporins and mediano-sensitive channels in *Escherichia coli*. *Curr. Opin. Microbiol.*, 2(2), 166–169, 1999.

A. Bovallius, B. Bucht, R. Roffey and P. Anas: Three-year investigation of the natural airborne bacterial flora at four localities in Sweden. *Appl. Environ. Microb.*, 35(5), 847, 1978.

R. M. Bowers, S. McLetchie, R. Knight and N. Fierer: Spatial variability in airborne bacterial communities across land-use types and their relationship to the bacterial communities of potential source environments. *ISME J.*, 5(4), 601–612, 2011.

N. Bukowiecki, J. Dommen, A. S. H. Prévôt, R. Richter, E. Weingartner and U. Baltensperger: A mobile pollutant measurement laboratory-measuring gas phase and aerosol

ambient concentrations with high spatial and temporal resolution. *Atmos. Environ.*, 36(36-37), 5569–5579, 2002.

H. A. Burge and C. A. Rogers: Outdoor allergens. *Environ. Health. Persp.*, 108, 653, 2000.

S. M. Burrows, T. Butler, P. Jöckel, H. Tost, A. Kerkweg, U. Pöschl and M. G. Lawrence: Bacteria in the global atmosphere–Part 2: Modeling of emissions and transport between different ecosystems. *Atmos. Chem. Phys.*, 9(23), 9281–9297, 2009.

I. Bussmann, B. Philipp and B. Schink: Factors influencing the cultivability of lake water bacteria. *J. Microbiol. Meth.*, 47(1), 41–50, 2001.

J. Butterworth and H. A. McCartney: The dispersal of bacteria from leaf surfaces by water splash. *J. Appl. Bacteriol.*, 71(6), 484–496, 1991.

M. R. Canagaratna, J. T. Jayne, D. A. Ghertner, S. Herndon, Q. Shi, J. L. Jimenez, P. J. Silva, P. Williams, T. Lanni, F. Drewnick, K. L. Demerjian, C. E. Kolb and D. R. Worsnop: Chase studies of particulate emissions from in-use New York City vehicles. *Aerosol. Sci. Tech.*, 38(6), 555–573, 2004.

F. Canonaco, M. Crippa, J. G. Slowik, U. Baltensperger and A. S. H. Prévôt: SoFi, an Igor based interface for the efficient use of the generalized multilinear engine (ME-2) for source apportionment: application to aerosol mass spectrometer data. *Atmos. Meas. Tech.*, 6(4), 3649–3661, 2013.

C. D. Cappa and J. L. Jimenez: Quantitative estimates of the volatility of ambient organic aerosol. *Atmos. Chem. Phys.*, 10, 5409–5424, 2010.

A. Celenza, J. Fothergill, E. Kupek and R. J. Shaw: Thunderstorm associated asthma: a detailed analysis of environmental factors. *The BMJ*, 312(7031), 604–607, 1996.

R. Chirico, P. F. DeCarlo, M. F. Heringa, T. Tritscher, R. Richter, A. S. H. Prévôt, J. Dommen, E. Weingartner, G. Wehrle, M. Gysel, M. Laborde and U. Baltensperger: Impact of aftertreatment devices on primary emissions and secondary organic aerosol formation potential from in-use diesel vehicles: results from smog chamber experiments. *Atmos. Chem. Phys.*, 10(23), 11545–11563, 2010.

B. C. Christner, C. E. Morris, C. M. Foreman, R. Cai and D. C. Sands: Ubiquity of biological ice nucleators in snowfall. *Science*, 319(5867), 1214, 2008.

T. H. Chrzanowski and M. Kyle: Ratios of carbon, nitrogen and phosphorus in *Pseudomonas fluorescens* as a model for bacterial element ratios and nutrient regeneration. *Aquat. Microb. Ecol.*, 10(2), 115–122, 1996.

H. Constantinidou, S. S. Hirano, L. S. Baker and C. D. Upper: Atmospheric dispersal of ice nucleation-active bacteria: the role of rain. *Phytopathology*, 80(10), 934–937, 1990.

S. T. Costa, L. T. F. Gonçalves, A. M. Yamasoe, A. J. Martins and C. E. Morris: Bacterial ice nuclei impact cloud lifetime and radiative properties and reduce atmospheric heat loss in the BRAMS simulation model. *Environ. Res. Lett.*, 9, 1–11, 2014.

C. S. Cox and C. M. Wathes: *Bioaerosols Handbook*. CRC Press, 1995.

M. Crippa, F. Canonaco, V. A. Lanz, M. Äijälä, J. D. Allan, S. Carbone, G. Capes, M. Dall'Osto, D. A. Day, P. F. DeCarlo, M. Ehn, A. Eriksson, E. Freney, L. Hildebrandt Ruiz, R. Hillamo, J. L. Jimenez, H. Junninen, A. Kiendler-Scharr, A.-M. Kortelainen, M. Kulmala, A. A. Mensah, C. Mohr, E. Nemitz, C. O'Dowd, J. Ovadnevaite, S. Pandis, T. Petäjä, L. Poulain, S. Saarikoski, K. Sellegri, E. Swietlicki, P. Tiitta, D. R. Worsnop, U. Baltensperger and A. S. H. Prèvôt: Organic aerosol components derived from 25 AMS data sets across Europe using a consistent ME-2 based source apportionment approach. *Atmos. Chem. Phys.*, 14(12), 6159–6176, 2014.

M. Crippa, F. Canonaco, J. G. Slowik, I. El Haddad, P. F. DeCarlo, C. Mohr, M. F. Heringa, R. Chirico, N. Marchand, B. Temime-Roussel, E. Abidi, L. Poulain, A. Wiedensohler, U. Baltensperger and A. S. H. Prévôt: Primary and secondary organic aerosol origin by combined gas-particle phase source apportionment. *Atmos. Chem. Phys.*, 13(3), 8411–8426, 2013a.

M. Crippa, P. F. DeCarlo, J. G. Slowik, C. Mohr, M. F. Heringa, R. Chirico, L. Poulain, F. Freutel, J. Sciare, J. Cozic, C. F. Di Marco, M. Elsasser, J. B. Nicolas, N. Marchand, E. Abidi, A. Wiedensohler, F. Drewnick, J. Schneider, S. Borrmann, E. Nemitz, R. Zimmermann, J.-L. Jaffrezo, A. S. H. Prévôt and U. Baltensperger: Wintertime aerosol chemical composition and source apportionment of the organic fraction in the metropolitan area of Paris. *Atmos. Chem. Phys.*, 13(2), 961–981, 2013b.

M. Crippa, I. El Haddad, J. G. Slowik, P. F. DeCarlo, C. Mohr, M. F. Heringa, R. Chirico, N. Marchand, J. Sciare, U. Baltensperger and A. S. H. Prévôt: Identification of marine and continental aerosol sources in Paris using high resolution aerosol mass spectrometry. *J. Geophys. Res. Atmos.*, 118, 1950–1963, 2013c.

J. Crosier, J. Allan, H. Coe, K. Bower, P. Formenti and P. Williams: Chemical composition of summertime aerosol in the Po Valley (Italy), northern Adriatic and Black Sea. *Q. J. Roy. Meteor. Soc.*, 133(S1), 61–75, 2007.

E. S. Cross, T. B. Onasch, M. Canagaratna, J. T. Jayne, J. Kimmel, X.-Y. Yu, M. L. Alexander, D. R. Worsnop and P. Davidovits: Single particle characterization using a light scattering module coupled to a time-of-flight aerosol mass spectrometer. *Atmos. Chem. Phys.*, 9, 7769–7793, 2009.

E. S. Cross, J. G. Slowik, P. Davidovits, J. D. Allan, D. R. Worsnop, J. T. Jayne, D. K. Lewis, M. Canagaratna and T. B. Onasch: Laboratory and ambient particle density determinations using light scattering in conjunction with aerosol mass spectrometry. *Aerosol. Sci. Tech.*, 41(4), 343–359, 2007.

G. A. Czerwieniec, S. C. Russell, H. J. Tobias, M. E. Pitesky, D. P. Fergenson, P. Steele, A. Srivastava, J. M. Horn, M. Frank, E. E. Gard and C. B. Lebrilla: Stable isotope labeling of entire *Bacillus atrophaeus* spores and vegetative cells using bioaerosol mass spectrometry. *Anal. Chem.*, 77(4), 1081–1087, 2005.

D. Davis, G. Chen, P. Kasibhatla, A. Jefferson, D. Tanner, F. Eisele, D. Lenschow, W. Neff and H. Berresheim: DMS oxidation in the Antarctic marine boundary layer: Comparison of model simulations and held observations of DMS, DMSO, $DMSO_2$, H_2SO_4 (g), MSA (g), and MSA (p). *J. Geophys. Res. Atmos.*, 103(D1), 1657–1678, 1998.

W. D. Davis: Surface ionization mass spectroscopy of airborne particulates. *J. Vac. Sci. Technol.*, 10(1), 278–278, 1973.

P. DeCarlo, J. G. Slowik, D. R. Worsnop, P. Davidovits and J. L. Jimenez: Particle morphology and density characterization by combined mobility and aerodynamic diameter measurements. Part 1: Theory. *Aerosol. Sci. Tech.*, 38(12), 1185–1205, 2004.

P. F. DeCarlo, J. R. Kimmel, A. Trimborn, M. J. Northway, J. T. Jayne, A. C. Aiken, M. Gonin, K. Fuhrer, T. Horvath, K. S. Docherty, D. R. Worsnop and J. L. Jimenez: Field-deployable, high-resolution, time-of-flight aerosol mass spectrometer. *Anal. Chem.*, 78(24), 8281–8289, 2006.

S. Decesari, J. Allan, C. Plass-Duelmer, B. J. Williams, M. Paglione, M. C. Facchini, C. O'Dowd, R. M. Harrison, J. K. Gietl, H. Coe, L. Giulianelli, G. P. Gobbi, C. Lanconelli, C. Carbone, D. R. Worsnop, A. T. Lambe, A. T. Ahern, F. Moretti, E. Tagliavini, T. Elste, S. Gilde, Y. Zhang and M. Dall'Osto: Measurements of the aerosol chemical composition and mixing state in the Po Valley using multiple spectroscopic techniques. *Atmos. Chem. Phys.*, 14(7), 12109–12132, 2014.

S. Decesari, M. C. Facchini, E. Matta, F. Lettini, M. Mircea, S. Fuzzi, E. Tagliavini and J.-P. Putaud: Chemical features and seasonal variation of fine aerosol water-soluble organic compounds in the Po Valley, Italy. *Atmos. Environ.*, 35(21), 3691–3699, 2001.

N. DeLeon-Rodriguez, T. L. Lathem, L. M. Rodriguez-R, J. M. Barazesh, B. E. Anderson, A. J. Beyersdorf, L. D. Ziemba, M. Bergin, A. Nenes and K. T. Konstantinidis: Microbiome of the upper troposphere: Species composition and prevalence, effects of tropical storms, and atmospheric implications. *P. Natl. Acad. Sci. U.S.A.*, 110(7), 2575–2580, 2013.

P. A. Demirev and C. Fenselau: Mass spectrometry in biodefense. *J. Mass. Spectrom.*, 43(11), 1441–1457, 2008.

V. R. Després, J. A. Huffman, S. M. Burrows, C. Hoose, A. S. Safatov, G. Buryak, J. Fröhlich-Nowoisky, W. Elbert, M. O. Andreae, U. Pöschl and R. Jaenicke: Primary biological aerosol particles in the atmosphere: a review. *Tellus B*, 64(0), 1–58, 2012.

K. R. Dällenbach, C. Bozzetti, A. Krepelová, F. Canonaco, R. Wolf, R.-J. Huang, P. Zotter, M. Crippa, J. G. Slowik, Y. Zhang, S. Szidat, U. Baltensperger, A. S. H. Prévôt and I. El Haddad: Characterization and source apportionment of organic aerosol using offline aerosol mass spectrometry. *Atmos. Meas. Tech.*, in prep., 2014.

K. S. Docherty, A. C. Aiken, J. A. Huffman, I. M. Ulbrich, P. F. DeCarlo, D. Sueper, D. R. Worsnop, D. C. Snyder, R. E. Peltier, R. J. Weber, B. D. Grover, D. J. Eatough, B. J. Williams, A. H. Goldstein, P. J. Ziemann and J. L. Jimenez: The 2005 Study of Organic Aerosols at Riverside (SOAR-1): instrumental intercomparisons and fine particle composition. *Atmos. Chem. Phys.*, 11(23), 12387–12420, 2011.

J. Duplissy, P. F. DeCarlo, J. Dommen, M. R. Alfarra, A. Metzger, I. Barmpadimos, A. S. H. Prévôt, E. Weingartner, T. Tritscher, M. Gysel, A. C. Aiken, J. L. Jimenez, M. R. Canagaratna, D. R. Worsnop, D. R. Collins, J. Tomlinson and U. Baltensperger: Relating hygroscopicity and composition of organic aerosol particulate matter. *Atmos. Chem. Phys.*, 11(3), 1155–1165, 2011.

C. G. Ehrenberg: *Passatstaub und Blutregen. Ein großes organisches unsichtbares Wirken und Leben in der Atmosphäre*. Königliche Akademie der Wissenschaften, 1847.

M. C. Facchini, S. Decesari, M. Rinaldi, C. Carbone, E. Finessi, M. Mircea, S. Fuzzi, F. Moretti, E. Tagliavini, D. Ceburnis and C. O'Dowd: Important source of marine secondary organic aerosol from biogenic amines. *Environ. Sci. Technol.*, 42(24), 9116–9121, 2008.

A. M. Falick, W. M. Hines, K. F. Medzihradszky, M. A. Baldwin and B. W. Gibson: Low-mass ions produced from peptides by high-energy collision-induced dissociation in tandem mass spectrometry. *J. Am. Soc. Mass. Spectr.*, 4(11), 882–893, 1993.

Z. Fang, Z. Ouyang, H. Zheng, X. Wang and L. Hu: Culturable airborne bacteria in outdoor environments in Beijing, China. *Microbial. Ecol.*, 54(3), 487–496, 2007.

D. Farmer, A. Matsunaga, K. Docherty, J. Surratt, J. Seinfeld, P. Ziemann and J. Jimenez: Response of an aerosol mass spectrometer to organonitrates and organosulfates and implications for atmospheric chemistry. *Proc. Natl. Acad. Sci. U.S.A.*, 107(15), 6670–6675, 2010.

D. P. Fergenson, M. E. Pitesky, H. J. Tobias, P. T. Steele, G. A. Czerwieniec, S. C. Russell, C. B. Lebrilla, J. M. Horn, R. Keith, A. Srivastava, S. P. Pillai, M.-T. P. Shih, H. L. Hall, A. J. Ramponi, J. T. Chang, R. G. Langlois, P. L. Estacio, R. T. Hadley, M. Frank and E. E. Gard: Reagentless detection and classification of individual bioaerosol particles in seconds. *Anal. Chem.*, 76(2), 373–378, 2004.

A. Forthomme, A. Joubert, Y. Andrès, X. Simon, P. Duquenne, D. Bemer and L. Le Coq: Microbial aerosol filtration: Growth and release of a bacteria–fungi consortium collected by fibrous filters in different operating conditions. *J. Aerosol. Sci.*, 72, 32–46, 2014.

F. Freutel, J. Schneider, F. Drewnick, S.-L. von der Weiden-Reinmüller, M. Crippa, A. S. H. Prévôt, U. Baltensperger, L. Poulain, A. Wiedensohler, J. Sciare, R. Sarda-Estève, J. F. Burkhart, S. Eckhardt, A. Stohl, V. Gros, A. Colomb, V. Michoud, J. F. Doussin, A. Borbon, M. Haeffelin, Y. Morille, M. Beekmann and S. Borrmann: Aerosol particle measurements at three stationary sites in the megacity of Paris during summer 2009: meteorology and air mass origin dominate aerosol particle composition and size distribution. *Atmos. Chem. Phys.*, 13(2), 933–959, 2013.

T. R. Frieden et al.: CDC health disparities and inequalities report - United States, 2011. *Morbidity and mortality weekly report. Surveillance summaries*, 60, 1, 2011.

R. Fröhlich, M. J. Cubison, J. G. Slowik, N. Bukowiecki, A. S. H. Prévôt, U. Baltensperger, J. Schneider, J. R. Kimmel, M. Gonin, U. Rohner, D. R. Worsnop and J. T. Jayne: The ToF-ACSM: a portable aerosol chemical speciation monitor with TOFMS detection. *Atmos. Meas. Tech.*, 6(11), 3225–3241, 2013.

S. Fuzzi, P. Mandrioli and A. Perfetto: Fog droplets - an atmospheric source of secondary biological aerosol particles. *Atmos. Environ.*, 31(2), 287–290, 1997.

C. García-Aljaro, M. A. Bangar, E. Baldrich, F. J. Muñoz and A. Mulchandani: Conducting polymer nanowire-based chemiresistive biosensor for the detection of bacterial spores. *Biosens. Bioelectron.*, 25(10), 2309–2312, 2010.

X. Ge, Q. Zhang, Y. Sun, C. R. Ruehl and A. Setyan: Effect of aqueous-phase processing on aerosol chemistry and size distributions in fresno, california, during wintertime. *Environmental Chemistry*, 9(3), 221–235, 2012.

R. A. Gieray, P. T. A. Reilly, M. Yang, W. B. Whitten and J. M. Ramsey: Real-time detection of individual airborne bacteria. *J. Microbiol. Meth.*, 29(3), 191–199, 1997.

M. Glikson, S. Rutherford, R. W. Simpson, C. A. Mitchell and A. Yago: Microscopic and submicron components of atmospheric particulate matter during high asthma periods in Brisbane, Queensland, Australia. *Atmos. Environ.*, 29(4), 549–562, 1995.

A. H. Goldstein and I. E. Galbally: Known and unexplored organic constituents in the earth's atmosphere. *Environ. Sci. Technol.*, 41(5), 1514–1521, 2007.

D. C. Graham, C. E. Quinn and L. F. Bradley: Quantitative studies on the generation of aerosols of *Erwinia carotovora var. atroseptica* by simulated raindrop impaction on blackleg-infected potato stems. *J. Appl. Bacteriol.*, 43(3), 413–424, 1977.

A. P. Grieshop, J. M. Logue, N. M. Donahue and A. L. Robinson: Laboratory investigation of photochemical oxidation of organic aerosol from wood fires 1: measurement and simulation of organic aerosol evolution. *Atmos. Chem. Phys.*, 9(4), 1263–1277, 2009.

D. W. Griffin, N. Kubilay, M. Koçak, M. A. Gray, T. C. Borden and E. A. Shinn: Airborne desert dust and aeromicrobiology over the Turkish Mediterranean coastline. *Atmos. Environ.*, 41(19), 4050–4062, 2007.

S. A. Grinshpun: *Aerosols – Science and Technology*. Wiley, New York, 2010.

M. Hallquist, J. C. Wenger, U. Baltensperger, Y. Rudich, D. Simpson, M. Claeys, J. Dommen, N. M. Donahue, C. George, A. H. Goldstein, J. F. Hamilton, H. Herrmann, T. Hoffmann, Y. Iinuma, M. Jang, M. E. Jenkin, J. L. Jimenez, A. Kiendler-Scharr, W. Maenhaut, G. McFiggans, T. F. Mentel, A. Monod, A. S. H. Prévôt, J. H. Seinfeld, J. D. Surratt, R. Szmigielski and J. Wildt: The formation, properties and impact of secondary organic aerosol: current and emerging issues. *Atmos. Chem. Phys.*, 9(14), 5155–5236, 2009.

R. M. Harrison, A. M. Jones, P. D. E. Biggins, N. Pomeroy, C. S. Cox, S. P. Kidd, J. L. Hobman, N. L. Brown and A. Beswick: Climate factors influencing bacterial count in background air samples. *Int. J. Biometeorol.*, 49(3), 167–178, 2005.

P. L. Hayes, A. M. Ortega, M. J. Cubison, K. D. Froyd, Y. Zhao, S. S. Cliff, W. W. Hu, D. W. Toohey, J. H. Flynn, B. L. Lefer, N. Grossberg, S. Alvarez, B. Rappenglück, J. W. Taylor, J. D. Allan, J. S. Holloway, J. B. Gilman, W. C. Kuster, J. A. de Gouw, P. Massoli, X. Zhang, J. Liu, R. J. Weber, A. L. Corrigan, L. M. Russell, G. Isaacman, D. R. Worton, N. M. Kreisberg, A. H. Goldstein, R. Thalman, E. M. Waxman, R. Volkamer, Y. H. Lin, J. D. Surratt, T. E. Kleindienst, J. H. Offenberg, S. Dusanter, S. Griffith, P. S. Stevens, J. Brioude, W. M. Angevine and J. L. Jimenez: Organic aerosol composition and sources in Pasadena, California, during the 2010 CalNex campaign. *J. Geophys. Res. Atmos.*, 118(16), 9233–9257, 2013.

L.-Y. He, Y. Lin, X.-F. Huang, S. Guo, L. Xue, Q. Su, M. Hu, S.-J. Luan and Y.-H. Zhang: Characterization of high-resolution aerosol mass spectra of primary organic

aerosol emissions from Chinese cooking and biomass burning. *Atmos. Chem. Phys.*, 10(23), 11535–11543, 2010.

S. P. Hersey, J. S. Craven, K. A. Schilling, A. R. Metcalf, A. Sorooshian, M. N. Chan, R. C. Flagan and J. H. Seinfeld: The Pasadena Aerosol Characterization Observatory (PACO): chemical and physical analysis of the Western Los Angeles basin aerosol. *Atmos. Chem. Phys.*, 11(15), 7417–7443, 2011.

L. Hildebrandt, E. Kostenidou, V. Lanz, A. S. H. Prévôt, U. Baltensperger, N. Mihalopoulos, A. Laaksonen, N. M. Donahue and S. N. Pandis: Sources and atmospheric processing of organic aerosol in the Mediterranean: insights from aerosol mass spectrometer factor analysis. *Atmos. Chem. Phys.*, 11(12), 499, 2011.

W. C. Hinds: *Aerosol Technology*. Wiley - Interscience, 1999.

K.-P. Hinz, E. Gelhausen, K.-C. Schäfer, Z. Takats and B. Spengler: Characterization of surgical aerosols by the compact single-particle mass spectrometer LAMPAS 3. *Anal. Bioanal. Chem.*, 401(10), 3165–3172, 2011.

S. S. Hirano and C. D. Upper: Bacteria in the leaf ecosystem with emphasis on *Pseudomonas syringae* – a pathogen, ice nucleus, and epiphyte. *Microbiol. Mol. Biol. Rev.*, 64(3), 624–653, 2000.

B. N. Hock: *Massenspektrometrische in-situ Messungen zur Bestimmung der chemischen Zusammensetzung von natürlichem und anthropogenem Aerosol*. Ph.D. thesis, Johannes Gutenberg-Universität, 2005.

C. Hoose, J. E. Kristjánsson and S. M. Burrows: How important is biological ice nucleation in clouds on a global scale? *Environ. Res. Lett.*, 5, 024009, 2010.

D. Hospodsky, N. Yamamoto and J. Peccia: Accuracy, precision, and method detection limits of quantitative PCR for airborne bacteria and fungi. *Appl. Environ. Microb.*, 76(21), 7004–7012, 2010.

D. D. Huang, Y. J. Li, B. P. Lee and C. K. Chan: Analysis of organic sulfur compounds in atmospheric aerosols at the hkust supersite in hong kong using hr-tof-ams. *Environ. Sci. Technol.*, 49(6), 3672–3679, 2015.

L. Huber, L. V. Madden and B. D. L. Fitt: Rain-splash and spore dispersal: a physical perspective. In: *The epidemiology of plant diseases*, pages 348–370, Springer, 1998.

J. A. Huffman, J. T. Jayne, F. Drewnick, A. C. Aiken, T. Onasch, D. R. Worsnop and J. L. Jimenez: Design, modeling, optimization, and experimental tests of a particle beam width probe for the Aerodyne aerosol mass spectrometer. *Aerosol. Sci. Tech.*, 39(12), 1143–1163, 2005.

J. A. Huffman, A. J. Prenni, P. J. DeMott, C. Pöhlker, R. H. Mason, N. H. Robinson, J. Fröhlich-Nowoisky, Y. Tobo, V. R. Després, E. Garcia, D. J. Gochis, E. Harris, I. Müller-Germann, C. Ruzene, B. Schmer, B. Sinha, D. A. Day, M. O. Andreae, J. L. Jimenez, M. Gallagher, S. M. Kreidenweis, A. K. Bertram and U. Pöschl: High concentrations of biological aerosol particles and ice nuclei during and after rain. *Atmos. Chem. Phys.*, 13(13), 6151–6164, 2013.

J. A. Huffman, B. Sinha, R. M. Garland, A. Snee-Pollmann, S. S. Gunthe, P. Artaxo, S. T. Martin, M. O. Andreae and U. Pöschl: Size distributions and temporal variations of biological aerosol particles in the Amazon rainforest characterized by microscopy and real-time UV-APS fluorescence techniques during AMAZE-08. *Atmos. Chem. Phys.*, 12, 11997–12019, 2012.

M. Hussain, P. Madl and A. Khan: Lung deposition predictions of airborne particles and the emergence of contemporary diseases, Part-i. *The Health*, 2, 51–59, 2011.

A. A. Imshenetsky, S. V. Lysenko and G. A. Kazakov: Upper boundary of the biosphere. *Appl. Environ. Microb.*, 35(1), 1–5, 1978.

M. Z. Jacobson and D. G. Streets: Influence of future anthropogenic emissions on climate, natural emissions, and air quality. *J. Geophys. Res.*, 114(D8), D08118, 2009.

R. Jaenicke: Abundance of cellular material and proteins in the atmosphere. *Science*, 308(5718), 73, 2005.

J. T. Jayne, D. C. Leard, X. Zhang, P. Davidovits, K. A. Smith, C. E. Kolb and D. R. Worsnop: Development of an aerosol mass spectrometer for size and composition analysis of submicron particles. *Aerosol. Sci. Tech.*, 33(1), 49–70, 2000.

J. L. Jimenez, M. R. Canagaratna, N. M. Donahue, A. S. H. Prévôt, Q. Zhang, J. H. Kroll, P. F. DeCarlo, J. D. Allan, H. Coe, N. L. Ng, A. C. Aiken, I. M. Docherty, K. S.and Ulbrich, A. P. Grieshop, A. L. Robinson, J. Duplissy, J. D. Smith, K. R. Wilson, V. A. Lanz, C. Hueglin, Y. L. Sun, J. Tian, A. Laaksonen, T. Raatikainen, J. Rautiainen, P. Vaattovaara, M. Ehn, M. Kulmala, J. M. Tomlinson, D. R. Collins, M. J. Cubison, E. J. Dunlea, J. A. Huffman, T. B. Onasch, M. R. Alfarra, P. I. Williams, K. Bower, Y. Kondo, J. Schneider, F. Drewnick, S. Borrmann, S. Weimer, K. Demerjian, D. Salcedo, L. Cottrell, R. Griffin, A. Takami, T. Miyoshi, S. Hatakeyama, A. Shimono, J. Y. Sun, Y. M. Zhang, K. Dzepina, J. R. Kimmel, D. Sueper, J. T. Jayne, S. C. Herndon, A. M. Trimborn, L. R. Williams, E. C. Wood, A. M. Middlebrook, C. E. Kolb, U. Baltensperger and D. R. Worsnop: Evolution of organic aerosols in the atmosphere. *Science*, 326(5959), 1525–1529, 2009.

J. L. Jimenez, J. T. Jayne, Q. Shi, C. E. Kolb, D. R. Worsnop, I. Yourshaw, J. H. Seinfeld, R. C. Flagan, X. Zhang, K. A. Smith, J. W. Morris and P. Davidovits: Ambient aerosol sampling using the Aerodyne aerosol mass spectrometer. *J. Geophys. Res.*, 108(D7), 8425, 2003.

D. L. Johnson: The effect of phosphate buffer on aerosol size distribution of nebulized *Bacillus subtilis* and *Pseudomonas fluorescens* bacteria. *Aerosol. Sci. Tech.*, 30(2), 202–210, 1999.

M. Joly, E. Attard, M. Sancelme, L. Deguillaume, C. Guilbaud, C. E. Morris, P. Amato and A.-M. Delort: Ice nucleation activity of bacteria isolated from cloud water. *Atmos. Environ.*, 70, 392–400, 2013.

A. M. Jones and R. M. Harrison: The effects of meteorological factors on atmospheric bioaerosol concentrations – a review. *Sci. Total. Environ.*, 326(1), 151–180, 2004.

E. O. King, M. K. Ward and D. E. Raney: Two simple media for the demonstration of pyocyanin and fluorescin. *J. Lab. Clin. Med.*, 44(2), 301–307, 1954.

I. Kleefsman, M. A. Stowers, P. J. T. Verheijen, A. L. Wuijckhuijse, C. E. Kientz and J. Marijnissen: Bioaerosol analysis by single particle mass spectrometry. *Part. Part. Syst. Charact.*, 24(2), 85–90, 2007.

C. R. Kuske: Current and emerging technologies for the study of bacteria in the outdoor air. *Curr. Opin. Biotech.*, 17(3), 291–296, 2006.

Laboratorios Conda web page: http://www.condalab.com/pdf/1607.pdf, last access: 6 Jan. 2015.

F. Laden, J. Schwartz, F. E. Speizer and D. W. Dockery: Reduction in fine particulate air pollution and mortality: extended follow-up of the Harvard Six Cities study. *Am. J. Respir. Crit. Care Med.*, 173(6), 667–672, 2006.

V. A. Lanz, M. R. Alfarra, U. Baltensperger, B. Buchmann, C. Hueglin and A. S. H. Prévôt: Source apportionment of submicron organic aerosols at an urban site by factor analytical modelling of aerosol mass spectra. *Atmos. Chem. Phys.*, 7(6), 1503–1522, 2007.

V. A. Lanz, M. R. Alfarra, U. Baltensperger, B. Buchmann, C. Hueglin, S. Szidat, M. N. Wehrli, L. Wacker, S. Weimer, A. Caseiro, H. Puxbaum and A. S. H. Prévôt: Source attribution of submicron organic aerosols during wintertime inversions by advanced factor analysis of aerosol mass spectra. *Environ. Sci. Technol.*, 42(1), 214–220, 2008.

V. A. Lanz, A. S. H. Prévôt, M. R. Alfarra, C. Mohr, P. F. De-Carlo, S. Weimer, M. F. D. Gianini, C. Hueglin, J. Schneider, O. Favez, B. D'Anna, C. George and U. Baltensperger: Characterization of aerosol chemical composition by aerosol mass spectrometry in Central Europe: an overview. *Atmos. Chem. Phys.*, 10(6), 10453–10471, 2010.

B. Lighthart: Microbial aerosols: estimated contribution of combine harvesting to an airshed. *Appl. Environ. Microb.*, 47(2), 430–432, 1984.

B. Lighthart: The ecology of bacteria in the alfresco atmosphere. *Fems. Microbiol. Ecol.*, 23(4), 263–274, 1997.

B. Lighthart and A. Kirilenko: Simulation of summer-time diurnal bacterial dynamics in the atmospheric surface layer. *Atmos. Environ.*, 32(14), 2491–2496, 1998.

J. Lindemann and C. D. Upper: Aerial dispersal of epiphytic bacteria over bean plants. *Appl. Environ. Microbiol.*, 50(5), 1229–1232, 1985.

P. S. K. Liu, R. Deng, K. A. Smith, L. R. Williams, J. T. Jayne, M. R. Canagaratna, K. Moore, T. B. Onasch, D. R. Worsnop and T. Deshler: Transmission efficiency of an aerodynamic focusing lens system: Comparison of model calculations and laboratory measurements for the Aerodyne aerosol mass spectrometer. *Aerosol. Sci. Tech.*, 41(8), 721–733, 2007.

F. D. Lopez-Hilfiker, C. Mohr, M. Ehn, F. Rubach, E. Kleist, J. Wildt, T. F. Mentel, A. Lutz, M. Hallquist, D. Worsnop and J. A. Thornton: A novel method for online analysis of gas and particle composition: description and evaluation of a filter inlet for gases and aerosols (FIGAERO). *Atmos. Meas. Tech.*, 7(4), 983–1001, 2014.

L. V. Madden: Effects of rain on splash dispersal of fungal pathogens. *Can. J. Plant Pathol.*, 19(2), 225–230, 1997.

T. Maki, S. Susuki, F. Kobayashi, M. Kakikawa, Y. Tobo, M. Yamada, T. Higashi, A. Matsuki, C. Hong, H. Hasegawa and Y. Iwasaka: Phylogenetic analysis of atmospheric halotolerant bacterial communities at high altitude in an Asian dust (KOSA) arrival region, Suzu City. *Sci. Total. Environ.*, 408(20), 4556–4562, 2010.

S. M. R. H. Marafie and L. Ashkanani: Airborne bacteria in Kuwait (1986–1988). *Grana*, 30(2), 472–476, 1991.

S. Matthias-Maser, M. Kramer, J. Brinkmann and W. Schneider: A contribution of primary biological aerosol particles as insoluble component to the atmospheric aerosol over the South Atlantic Ocean. *J. Aerosol. Sci.*, 28(1001), 3–4, 1997.

P. J. McKeown, M. V. Johnston and D. M. Murphy: On-line single-particle analysis by laser desorption mass spectrometry. *Anal. Chem.*, 63(18), 2069–2073, 1991.

M. Meselson, J. Guillemin, M. Hugh-Jones, A. Langmuir, I. Popova, A. Shelokov and O. Yampolskaya: The Sverdlovsk anthrax outbreak of 1979. *Science*, 266(5188), 1202–1208, 1994.

A. M. Middlebrook, R. Bahreini, J. L. Jimenez and M. R. Canagaratna: Evaluation of composition-dependent collection efficiencies for the Aerodyne aerosol mass spectrometer using field data. *Aerosol. Sci. Tech.*, 46, 258–271, 2012.

P. J. Milne and R. G. Zika: Amino acid nitrogen in atmospheric aerosols: Occurrence, sources and photochemical modification. *J. Atmos. Chem.*, 16(4), 361–398, 1993.

P. Miquel: *Les organismes vivants de l'atmosphere*. Gauthier-Villars, 1883.

O. Möhler, S. Benz, H. Saathoff, M. Schnaiter, R. Wagner, J. Schneider, S. Walter, V. Ebert and S. Wagner: The effect of organic coating on the heterogeneous ice nucleation efficiency of mineral dust aerosols. *Environ. Res. Lett.*, 3(2), 025007, 2008a.

O. Möhler, P. J. DeMott, G. Vali and Z. Levin: Microbiology and atmospheric processes: the role of biological particles in cloud physics. *Biogeosciences*, 4(4), 1059–1071, 2007.

O. Möhler, D. G. Georgakopoulos, C. E. Morris, S. Benz, V. Ebert, S. Hunsmann, H. Saathoff, M. Schnaiter and R. Wagner: Heterogeneous ice nucleation activity of bacteria: new laboratory experiments at simulated cloud conditions. *Biogeosciences*, 5(2), 1425–1435, 2008b.

C. Mohr, P. F. DeCarlo, M. F. Heringa, R. Chirico, J. G. Slowik, R. Richter, C. Reche, A. Alastuey, X. Querol, R. Seco, J. Peñuelas, J. L. Jiménez, M. Crippa, R. Zimmermann, U. Baltensperger and A. S. H. Prévôt: Identification and quantification of organic aerosol from cooking and other sources in Barcelona using aerosol mass spectrometer data. *Atmos. Chem. Phys.*, 12(4), 1649–1665, 2012.

C. Mohr, J. Huffman, M. Cubison, A. Aiken, K. Docherty, J. Kimmel, I. Ulbrich, M. Hannigan and J. Jimenez: Characterization of primary organic aerosol emissions from meat cooking, trash burning, and motor vehicles with high-resolution aerosol mass spectrometry and comparison with ambient and chamber observations. *Environ. Sci. Technol.*, 43(7), 2443–2449, 2009.

C. Mohr, R. Richter, P. F. DeCarlo, A. S. H. Prévôt and U. Baltensperger: Spatial variation of chemical composition and sources of submicron aerosol in Zurich during

wintertime using mobile aerosol mass spectrometer data. *Atmos. Chem. Phys.*, 11(15), 7465–7482, 2011.

S. M. Murphy, A. Sorooshian, J. H. Kroll, N. L. Ng, P. Chhabra, C. Tong, J. D. Surratt, E. Knipping, R. C. Flagan and J. H. Seinfeld: Secondary aerosol formation from atmospheric reactions of aliphatic amines. *Atmos. Chem. Phys.*, 7(9), 2313–2337, 2007.

R. L. Myers and W. L. Fite: Electrical detection of airborne particulates using surface ionization techniques. *Environ. Sci. Technol.*, 9(4), 334–336, 1975.

N. L. Ng, M. R. Canagaratna, Q. Zhang, J. L. Jimenez, J. Tian, I. M. Ulbrich, J. H. Kroll, K. S. Docherty, P. S. Chhabra, R. Bahreini, S. M. Murphy, J. H. Seinfeld, L. Hildebrandt, N. M. Donahue, P. F. DeCarlo, V. A. Lanz, A. S. H. Prévôt, E. Dinar, Y. Rudich and D. R. Worsnop: Organic aerosol components observed in northern hemispheric datasets from aerosol mass spectrometry. *Atmos. Chem. Phys.*, 10(10), 4625–4641, 2010.

N. L. Ng, S. C. Herndon, A. Trimborn, M. R. Canagaratna, P. L. Croteau, T. B. Onasch, D. Sueper, D. R. Worsnop, Q. Zhang, Y. L. Sun and J. T. Jayne: An aerosol chemical speciation monitor (ACSM) for routine monitoring of the composition and mass concentrations of ambient aerosol. *Aerosol. Sci. Tech.*, 45(7), 780–794, 2011.

C. A. Noble and K. A. Prather: Real-time measurement of correlated size and composition profiles of individual atmospheric aerosol particles. *Environ. Sci. Technol.*, 30(9), 2667–2680, 1996.

V. Oja and E. M. Suuberg: Vapor pressures and enthalpies of sublimation of D-glucose, D-xylose, cellobiose, and levoglucosan. *J. Chem. Eng. Data*, 44(1), 26–29, 1999.

J. Ovadnevaite, D. Ceburnis, S. Leinert, M. Dall'Osto, M. Canagaratna, S. O'Doherty, H. Berresheim and C. O'Dowd: Submicron NE atlantic marine aerosol chemical composition and abundance: Seasonal trends and air mass categorization. *J. Geophys. Res. Atmos.*, 119, 1–14, 2014.

P. Paatero: The multilinear engine - a table-driven, least squares program for solving multilinear problems, including the n-way parallel factor analysis model. *J. Comput. Graph. Stat.*, 8(4), 854–888, 1999.

P. Paatero, S. Eberly, S. G. Brown and G. A. Norris: Methods for estimating uncertainty in factor analytic solutions. *Atmos. Meas. Tech.*, 7(3), 781–797, 2014.

P. Paatero and P. Hopke: Rotational tools for factor analytic models. *J. Chemometr.*, 23(2), 91–100, 2009.

P. Paatero and U. Tapper: Positive matrix factorization: A non-negative factor model with optimal utilization of error estimates of data values. *Environmetrics*, 5(2), 111–126, 1994.

M. Paglione, A. Kiendler-Scharr, A. A. Mensah, E. Finessi, L. Giulianelli, S. Sandrini, M. C. Facchini, S. Fuzzi, P. Schlag, A. Piazzalunga, E. Tagliavini, J. S. Henzing and S. Decesari: Identification of humic-like substances (HULIS) in oxygenated organic aerosols using NMR and AMS factor analyses and liquid chromatographic techniques. *Atmos. Chem. Phys.*, 14(1), 25–45, 2014a.

M. Paglione, S. Saarikoski, S. Carbone, R. Hillamo, M. C. Facchini, E. Finessi, L. Giulianelli, C. Carbone, S. Fuzzi, F. Moretti, E. Tagliavini, E. Swietlicki, K. E. Stenström, A. S. H. Prévôt, P. Massoli, M. Canaragatna, D. Worsnop and S. Decesari: Primary and secondary biomass burning aerosols determined by proton nuclear magnetic resonance (^{1}H-NMR) spectroscopy during the 2008 EUCAARI campaign in the Po Valley (Italy). *Atmos. Chem. Phys.*, 14(10), 5089–5110, 2014b.

L. Pasteur: *Mémoire sur les corpuscles organises qui existent dans l'atmosphere.* Annales de Chimie, 1862.

J. Peccia and M. Hernandez: Incorporating polymerase chain reaction-based identification, population characterization, and quantification of microorganisms into aerosol science: A review. *Atmos. Environ.*, 40(21), 3941–3961, 2006.

B. W. Peterson, P. K. Sharma, H. C. van der Mei and H. J. Busscher: Bacterial cell surface damage due to centrifugal compaction. *Appl. Environ. Microb.*, 78(1), 120–125, 2012.

V. T. J. Phillips, C. Andronache, B. Christner, C. E. Morris, D. C. Sands, A. Bansemer, A. Lauer, C. McNaughton and C. Seman: Potential impacts from biological aerosols on ensembles of continental clouds simulated numerically. *Biogeosciences*, 6(6), 987–1014, 2009.

R. G. Pinnick, S. C. Hill, P. Nachman, J. D. Pendleton, G. L. Fernandez, M. W. Mayo and J. G. Bruno: Fluorescence particle counter for detecting airborne bacteria and other biological particles. *Aerosol. Sci. Tech.*, 23(4), 653–664, 1995.

C. Pöhlker, K. T. Wiedemann, B. Sinha, M. Shiraiwa, S. S. Gunthe, M. Smith, H. Su, P. Artaxo, Q. Chen, Y. Cheng, W. Elbert, M. K. Gilles, A. L. D. Kilcoyne, R. C. Moffet, M. Weigand, S. T. Martin, U. Pöschl and M. O. Andreae: Biogenic potassium salt particles as seeds for secondary organic aerosol in the Amazon. *Science*, 337(6098), 1075–1078, 2012.

C. A. Pope, B. Young and D. W. Dockery: Health effects of fine particulate air pollution: lines that connect. *J. Air. Waste. Manage.*, 56(6), 709–742, 2006.

K. A. Prather, T. Nordmeyer and K. Salt: Real-time characterization of individual aerosol particles using time-of-flight mass spectrometry. *Anal. Chem.*, 66(9), 1403–1407, 1994.

K. A. Pratt, P. J. DeMott, J. R. French, Z. Wang, D. L. Westphal, A. J. Heymsfield, C. H. Twohy, A. J. Prenni and K. A. Prather: In situ detection of biological particles in cloud ice-crystals. *Nat. Geosci.*, 2(6), 398–401, 2009.

U. Pöschl, S. T. Martin, B. Sinha, Q. Chen, S. S. Gunthe, J. A. Huffman, S. Borrmann, D. K. Farmer, R. M. Garland, G. Helas, J. L. Jimenez, S. M. King, A. Manzi, E. Mikhailov, T. Pauliquevis, M. D. Petters, A. J. Prenni, P. Roldin, D. Rose, J. Schneider, H. Su, S. R. Zorn, P. Artaxo and M. O. Andreae: Rainforest aerosols as biogenic nuclei of clouds and precipitation in the Amazon. *Science*, 329(5998), 1513–1516, 2010.

M. Pösfai, J. Li, J. R. Anderson and P. R. Buseck: Aerosol bacteria over the Southern Ocean during ACE-1. *Atmos. Res.*, 66(4), 231–240, 2003.

J. P. Putaud, F. Raes, R. Van Dingenen, E. Bruggemann, M. C. Facchini, S. Decesari, S. Fuzzi, R. Gehrig, C. Hüglin, P. Laj, G. Lorbeer, W. Maenhaut, N. Mihalopoulos, K. Müller, X. Querol, S. Rodriguez, J. Schneider, G. Spindler, H. ten Brink, K. Torseth and A. Wiedensohler: A European aerosol phenomenology–2: chemical characteristics of particulate matter at kerbside, urban, rural and background sites in Europe. *Atmos. Environ.*, 38(16), 2579–2595, 2004.

N. Ramírez, A. Cuadras, E. Rovira, R. M. Marcé and F. Borrull: Risk assessment related to atmospheric polycyclic aromatic hydrocarbons in gas and particle phases near industrial sites. *Environ. Health. Perspect.*, 119(8), 1110, 2011.

T. Reponen, K. Willeke, S. Grinshpun and A. Nevalainen: *Aerosol Measurement – Principles, Techniques and Applications*. Wiley - Interscience, 2001.

X. Rodó, R. Curcoll, M. Robinson, J. Ballester, J. C. Burns, D. R. Cayan, W. I. Lipkin, B. L. Williams, M. Couto-Rodriguez, Y. Nakamura, R. Uehara, H. Tanimoto and J.-A. Morguí: Tropospheric winds from northeastern China carry the etiologic agent of Kawasaki disease from its source to Japan. *P. Natl. Acad. Sci. U.S.A.*, 111(22), 7952–7957, 2014.

S. Saarikoski, S. Carbone, S. Decesari, L. Giulianelli, F. Angelini, M. Canagaratna, N. L. Ng, A. Trimborn, M. C. Facchini, S. Fuzzi, R. Hillamo and D. R. Worsnop: Chemical characterization of springtime submicrometer aerosol in Po Valley, Italy. *Atmos. Chem. Phys.*, 12, 8401–8421, 2012.

D. Sarantaridis, C. Hennig and D. J. Caruana: Bioaerosol detection using potentiometric tomography in flames. *Chem. Sci.*, 3(7), 2210–2216, 2012.

B. Sattler, H. Puxbaum and R. Psenner: Bacterial growth in supercooled cloud droplets. *Geophys. Res. Lett.*, 28(2), 239–242, 2001.

J. Schmale, J. Schneider, E. Nemitz, Y. S. Tang, U. Dragosits, T. D. Blackall, P. N. Trathan, G. J. Phillips, M. Sutton and C. F. Braban: Sub-Antarctic marine aerosol: dominant contributions from biogenic sources. *Atmos. Chem. Phys.*, 13(17), 8669–8694, 2013.

J. Schneider, F. Freutel, S. R. Zorn, Q. Chen, D. K. Farmer, J. L. Jimenez, S. T. Martin, P. Artaxo, A. Wiedensohler and S. Borrmann: Mass-spectrometric identification of primary biological particle markers and application to pristine submicron aerosol measurements in Amazonia. *Atmos. Chem. Phys.*, 11, 11415–11429, 2011.

A. Sesartic, U. Lohmann and T. Storelvmo: Bacteria in the ECHAM 5-HAM global climate model. *Atmos. Chem. Phys.*, 12(1), 8645–8661, 2012.

P. J. Silva and K. A. Prather: Interpretation of mass spectra from organic compounds in aerosol time-of-flight mass spectrometry. *Anal. Chem.*, 72(15), 3553–3562, 2000.

B. R. T. Simoneit, J. J. Schauer, C. G. Nolte, D. R. Oros, V. O. Elias, M. P. Fraser, W. F. Rogge and G. R. Cass: Levoglucosan, a tracer for cellulose in biomass burning and atmospheric particles. *Atmos. Environ.*, 33(2), 173–182, 1999.

J. G. Slowik, A. Vlasenko, M. McGuire, G. J. Evans and J. P. D. Abbatt: Simultaneous factor analysis of organic particle and gas mass spectra: AMS and PTR-MS measurements at an urban site. *Atmos. Chem. Phys.*, 10(4), 1969–1988, 2010.

M. Sofiev, M. Prank and A. Baklanov: MEGAPOLI scientific report 11-12 influence of regional scale emissions on megacity air quality. Technical report, Helsinki-Copenhagen, 2011.

D. V. Spracklen and C. L. Heald: The contribution of fungal spores and bacteria to regional and global aerosol number and ice nucleation immersion freezing rates. *Atmos. Chem. Phys.*, 14(17), 9051–9059, 2014.

P. T. Steele, H. J. Tobias, D. P. Fergenson, M. E. Pitesky, J. M. Horn, G. A. Czerwieniec, S. C. Russell, C. B. Lebrilla, E. E. Gard and M. Frank: Laser power dependence of mass spectral signatures from individual bacterial spores in bioaerosol mass spectrometry. *Anal. Chem.*, 75(20), 5480–5487, 2003.

S. L. Stewart, S. A. Grinshpun, K. Willeke, S. Terzieva, V. Ulevicius and J. Donnelly: Effect of impact stress on microbial recovery on an agar surface. *Appl. Environ. Microb.*, 61(4), 1232–1239, 1995.

T. F. Stocker, D. Qin, G.-K. Plattner, M. Tignor, S. K. Allen, J. Boschung, A. Nauels, Y. Xia, V. Bex and P. M. Midgley (eds.): *IPCC: Climate Change 2013: The Physical Science Basis. Working Group I Contribution to the Fifth Assessment Report of the Intergovernmental Panel on Climate Change*. Cambridge University Press, 2014.

R. C. Sullivan and K. A. Prather: Recent advances in our understanding of atmospheric chemistry and climate made possible by on-line aerosol analysis instrumentation. *Anal. Chem.*, 77(12), 3861, 2005.

Y.-L. Sun, Q. Zhang, J. J. Schwab, K. L. Demerjian, W.-N. Chen, M.-S. Bae, H.-M. Hung, O. Hogrefe, B. Frank, O. V. Rattigan and Y.-C. Lin: Characterization of the sources and processes of organic and inorganic aerosols in New York city with a high-resolution time-of-flight aerosol mass apectrometer. *Atmos. Chem. Phys.*, 11(4), 1581–1602, 2011.

J. D. Surratt, Y. Gómez-González, A. W. Chan, R. Vermeylen, M. Shahgholi, T. E. Kleindienst, E. O. Edney, J. H. Offenberg, M. Lewandowski, M. Jaoui et al.: Organosulfate formation in biogenic secondary organic aerosol. *J. Phys. Chem. A*, 112(36), 8345–8378, 2008.

C. A. Suttle: Viruses in the sea. *Nature*, 437(7057), 356–361, 2005.

W. Szyrmer and I. Zawadzki: Biogenic and anthropogenic sources of ice-forming nuclei: A review. *B. Am. Meteorol. Soc.*, 78(2), 209–228, 1997.

Y. Tong: Diurnal distribution of total and culturable atmospheric bacteria at a rural site. *Aerosol. Sci. Technol.*, 30(2), 246–254, 1999.

Y. Tong and B. Lighthart: The annual bacterial particle concentration and size distribution in the ambient atmosphere in a rural area of the Willamette Valley, Oregon. *Aerosol. Sci. Tech.*, 32(5), 393–403, 2000.

E. Toprak and M. Schnaiter: Fluorescent biological aerosol particles measured with the Waveband Integrated Bioaerosol Sensor WIBS-4: laboratory tests combined with a one year field study. *Atmos. Chem. Phys.*, 13(1), 225–243, 2013.

I. M. Ulbrich, M. R. Canagaratna, M. J. Cubison, Q. Zhang, N. L. Ng, A. C. Aiken and J. L. Jimenez: Three-dimensional factorization of size-resolved organic aerosol mass spectra from Mexico City. *Atmos. Meas. Tech.*, 5(4), 195–224, 2012.

I. M. Ulbrich, M. R. Canagaratna, Q. Zhang, D. R. Worsnop and J. L. Jimenez: Interpretation of organic components from Positive Matrix Factorization of aerosol mass spectrometric data. *Atmos. Chem. Phys.*, 9(9), 2891–2918, 2009.

M. Vaïtilingom, E. Attard, N. Gaiani, M. Sancelme, L. Deguillaume, A. I. Flossmann, P. Amato and A.-M. Delort: Long-term features of cloud microbiology at the Puy de Dôme (France). *Atmos. Environ.*, 56, 88–100, 2012.

L. Van Vaeck, J. Bennett, W. Lauwers, A. Vertes and R. Gijbels: Laser microprobe mass spectrometry: possibilities and limitations. *Microchim. Acta.*, 102(4-6), 283–303, 1990.

R. Vecchi, G. Marcazzan and G. Valli: A study on nighttime–daytime PM10 concentration and elemental composition in relation to atmospheric dispersion in the urban area of Milan (Italy). *Atmos. Environ.*, 41(10), 2136–2144, 2007.

M. Viana, T. A. J. Kuhlbusch, X. Querol, A. Alastuey, R. M. Harrison, P. K. Hopke, W. Winiwarter, M. Vallius, S. Szidat, A. S. H. Prévôt, C. Hueglin, H. Bloemen, P. Wåhlin, R. Vecchi, A. I. Miranda, A. Kasper-Giebl, W. Maenhaut and R. Hitzenberger: Source apportionment of particulate matter in Europe: a review of methods and results. *J. Aerosol. Sci.*, 39(10), 827–849, 2008.

S. L. von der Weiden, F. Drewnick and S. Borrmann: Particle loss calculator – a new software tool for the assessment of the performance of aerosol inlet systems. *Atmos. Meas. Tech.*, 2, 479–494, 2009.

T. Vrede: Elemental composition (C:N:P) and growth rates of bacteria and Rhodomonas grazed by *Daphnia*. *J. Plankton. Res.*, 20(3), 455–470, 1998.

K. L. Wahl, H. A. Colburn, D. S. Wunschel, C. E. Petersen, K. H. Jarman and N. B. Valentine: Residual agar determination in bacterial spores by electrospray ionization mass spectrometry. *Anal. Chem.*, 82(4), 1200–1206, 2010.

A. E. D. Wardman, D. Stefani and J. C. MacDonald: Thunderstorm-associated asthma or shortness of breath epidemic: a Canadian case report. *Can. Resp. J.*, 9(4), 267–270, 2002.

J. D. Watson, T. A. Baker, S. P. Bell, A. A. F. Gann, M. Levine and R. M. Losick: *Molecular biology of the gene*. Benjamin Cummings, 2007.

R. J. Wichink Kruit, M. Schaap, F. J. Sauter, M. C. van Zanten and W. A. J. van Pul: Modeling the distribution of ammonia across Europe including bi-directional surface-atmosphere exchange. *Biogeosciences*, 9(12), 5261–5277, 2012.

L. R. Williams: What is my vaporizer temperature? Technical report, AMS Users Meeting, Hyytiala, Finland, 2010.

L. R. Williams, L. A. Gonzalez, J. Peck, D. Trimborn, J. McInnis, M. R. Farrar, K. D. Moore, J. T. Jayne, W. A. Robinson, D. K. Lewis, T. B. Onasch, M. R. Canagaratna,

A. Trimborn, M. T. Timko, G. Magoon, R. Deng, D. Tang, E. de la Rosa Blanco, A. S. H. Prévôt, K. A. Smith and D. R. Worsnop: Characterization of an aerodynamic lens for transmitting particles $>$ 1 micrometer in diameter into the Aerodyne aerosol mass spectrometer. *Atmos. Meas. Tech.*, 6, 3271–3280, 2013.

W. Wobrock, D. Schell, R. Maser, M. Kessel, W. Jaeschke, S. Fuzzi, M. C. Facchini, G. Orsi, A. Marzorati, P. Winkler, B. G. Arends and J. Bendix: Meteorological characteristics of the Po Valley fog. *Tellus B*, 44(5), 469–488, 1992.

R. Wolf, J. G. Slowik, C. Schaupp, P. Amato, H. Saathoff, O. Möhler, A. S. H. Prévôt and U. Baltensperger: Characterization of ice-nucleating bacteria using aerosol mass spectrometry. *J. Mass. Spectrom.*, 50, 662–671, 2015.

T. O. Womiloju, J. D. Miller, P. M. Mayer and J. R. Brook: Methods to determine the biological composition of particulate matter collected from outdoor air. *Atmos. Environ.*, 37(31), 4335–4344, 2003.

Q. Zhang, M. R. Alfarra, D. R. Worsnop, J. D. Allan, H. Coe, M. R. Canagaratna and J. L. Jimenez: Deconvolution and quantification of hydrocarbon-like and oxygenated organic aerosols based on aerosol mass spectrometry. *Environ. Sci. Technol.*, 39(13), 4938–4952, 2005.

Q. Zhang, J. L. Jimenez, M. R. Canagaratna, I. M. Ulbrich, N. L. Ng, D. R. Worsnop and Y. Sun: Understanding atmospheric organic aerosols via factor analysis of aerosol mass spectrometry: a review. *Anal. Bioanal. Chem.*, 401, 1–23, 2011.

Q. Zhang, J. L. Jimenez, D. R. Worsnop and M. Canagaratna: A case study of urban particle acidity and its influence on secondary organic aerosol. *Environ. Sci. Technol.*, 41(9), 3213–3219, 2007.

S. R. Zorn, F. Drewnick, M. Schott, T. Hoffmann and S. Borrmann: Characterization of the South Atlantic marine boundary layer aerosol using an Aerodyne aerosol mass spectrometer. *Atmos. Chem. Phys.*, 8(16), 4711–4728, 2008.

Acknowledgement

I would like to thank many people who contributed to this thesis:

- My supervisor Prof. Dr. Urs Baltensperger for his both pragmatic and constructive advices during meetings and seminars.
- Prof. Dr. Alexander Wokaun for being the co-referent during my PhD studies and for reviewing the thesis.
- Prof. Dr. Yinon Rudich for reading and commenting on the PhD thesis and for finding the time to come to Switzerland as a co-examiner.
- Dr. André Prévôt for his countless ideas for further analysis and possible experiments. Thanks also for coming to Italy in the beginning of the southbound PEGASOS campaign and for driving around with the mobile lab.
- All the colleagues that shared the OFLB/002 ("AMS") office over time, i.e. Imad, Lisa, Stephen, Monica, Francesco, Simone, Claudia and Maarten for a great atmosphere at work.
- To all the colleagues from the LAC. It has truly been a pleasure to work in such a multicultural environment and I enjoyed to be part of the social events of this lab very much.
- Thanks to the Mosquita crew: Monica and René. Rene, I thank you for excellent technical assistance in all questions concerning the mobile lab and for your help with all kinds of electronics.
- Of course, I also thank the legendary Höhtalstrasse community in Ennetbaden (i.e. Emanuel, Alice, Imad, Marie, Federico, Giancarlo, Ricardo, Carla, Jun, Francesco, Peter) for the BBQs, parties and the fun time.
- Special thanks to Jay. Your knowledge in any field that is somehow related to the AMS or to the IGOR analysis software was priceless for the quality of the data.
- Thanks to Miriam for being my greatest supporter and all the time with you.
- Most of all, I want to thank my parents and grandparents even thought I showed up at home much less than they wanted me to.